AuPt nano-alloys as reduction promoters for Co/TiO_2 Fischer-Tropsch catalysts

Avela Kunene

BSc Chemistry (Honours), University of Cape Town, South Africa

Thesis presented to the University of Cape Town in
fulfilment of the requirements
for the degree of

Master of Science in Engineering

Centre of Catalysis Research

Department of Chemical Engineering

University of Cape Town

South Africa

August 2014

DECLARATION

I, Avela Kunene certify that this submission is my own, unaided work, except for the information obtained from literature sources and my prescribed supervisors. All sources of information have been adequately acknowledged and referenced. I have not received assistance from any other source in completing this submission.

Signature:…… Date:……..

Acknowledgements

I would like to give a heartfelt gratitude to my Heavenly Father, the Almighty God for sustaining and strengthening me throughout my academic life. I would also like to thank my mom for being there for when I needed her and for the support and encouragement that she has been giving me. Special thank you to my supervisors Prof Eric van Steen and Prof Michael Claeys for their assistance, advice and support that contributed beyond measure to this study. Special thank you to Mintek and Duitkiewicz for the financial support.

Abstract:

Cobalt-based catalysts for the Fischer-Tropsch synthesis are typically promoted with noble metals to achieve a more facile reduction of Co_3O_4 to the catalytically active metal, Co^0. Hydrogen spillover is thought to be the dominant mechanism for the functioning of noble metals during the reduction process. Platinum is a well-known reduction promoter and its functioning as a reduction promoter is thought to occur via H_2- spillover mechanism. This process is switched off during the Fischer-Tropsch synthesis, when platinum is used as a reduction promoter, since platinum has been shown to be catalytically inert under these conditions, due to strong adsorption of CO. Some hydrogen spill-over during the Fischer-Tropsch synthesis might be desired to obtain more stable catalysts (less coking), but this effect has to be balanced against increased methanation activity.

Gold has been shown to be ineffective in hydrogen spillover, due to high dissociation energy of H_2 molecule and low chemisorption energy on Au surface. Therefore, the promotional effects of Au are typically not ascribed to H_2 spillover mechanism. Gold dissociate CO better than platinum, thereby facilitating hydrogenation of CO under Fischer-Tropsch synthesis.

Promotion of cobalt-based catalyst with either Pt or Au on their own has its limitations regarding their application. Platinum-gold alloys may possess a lower strength of adsorption of CO, thereby not only facilitating the reduction of cobalt oxide, but also enhancing the catalyst activity during Fischer-Tropsch synthesis. Furthermore, alloying the Au and Pt noble metals changes the chemical behaviour of Au, as AuPt nano-alloy system stimulate a twofold reduction mechanism (i.e. H_2-spillover and direct Co-noble metal interaction). Larger availability of surface hydrogen results in an increased CO hydrogenation.

18wt.%Co/TiO_2 is promoted with Au , $Au_{30}Pt_{70}$, $Au_{50}Pt_{50}$ and Pt. The reduction behaviour of the promoted catalyst is investigated using Temperature programmed reduction (TPR). Unpromoted Co/TiO_2 is used as a basis for comparison. Furthermore, the catalyst activity of unpromoted and promoted catalyst was investigated using a fixed bed reactor operating at 220 ^{0}C and 20 bar.

The reduction temperature peak of the alloy promoted Co/TiO_2 shifted to lower temperatures compared to the unpromoted Co/TiO_2.

The presence of THPC poisons the catalyst. However, a slight improvement in catalytic activity is observed upon promotion.

Contents

List of Figures

Chapter 2

Chapter 3

Chapter 4

Figure 4.11: TEM-images of the calcined Co/TiO_2 emphasizing poor contrast between Co_3O_4 and TiO_2 support in the catalyst

List of Tables

List of schemes

Nomenclature

AAS	Atomic adsorption spectroscopy
A_i	Area representing component i in the gas chromatogram
ASF	Anderson-Schulz-Flory
BET	Brunauer Emmett Teller
d	diameter (crystallite size)
eV	Electron Volts
fcc	face-centred cube
FID	Flame Ionisation Detector
FTIR	Fourier transform Infrared spectroscopy
FTS	Fischer-Tropsch Synthesis
GC	Gas chromatograph
GTL	gas-to-liquids
HTFT	High temperature Fischer-Tropsch process
LTFT	Low temperature Fischer-Tropsch process
MFC	Mass flow controller
mL	millilitres
n_i	molar flow rate of component i
NTP	Normal temperature and pressure (1 atm and 293K)
p_g	chain growth probability
RF	Response Factor
RPM	Revolutions per minute
TCD	Thermal conductivity detector
TEM	Transmission electron microscope
THPC	Tetrakis(hydroxymethyl) Phosphonium chloride
TPR	Temperature programmed reduction

wt.% weight percent

X_{CO} Carbon monoxide conversion

XRD X-ray diffraction

1 Introduction

1.1. Fischer-Tropsch synthesis

Since the early 1930s Fischer-Tropsch synthesis (FTS) has gained much interest due an increased global energy demand and environmental concerns. In this process, a carbon source, coal, natural gas or biomass is first converted to syngas (H_2/CO mixture) via steam reforming, partial oxidation, auto-thermal reforming or gasification [1]. Coal can be gasified to achieve syngas [2]. Syngas can be converted into long chain hydrocarbons via the Fischer-Tropsch synthesis. These can subsequently be converted upon hydrocracking to fuels [3]. This process can be regarded as a part of gas-to-liquids (GTL) technology (which converts natural gas into high-boiling waxy hydrocarbons) or the coal-to-liquid technology (CTL) and biomass-to liquid (BTL) technology.

1.2. Cobalt catalyst

Low temperature Fischer-Tropsch synthesis (LTFTS) operates between 200-250°C while high temperature Fischer-Tropsch (HTFTS) synthesis operates between 300-350°C. One of the catalysts for the low temperature Fischer-Tropsch synthesis is based on metallic cobalt [4-9]. Cobalt-based catalysts show a high selectivity for the desired linear liquid hydrocarbons, C_{5+} [5]. The high cost of cobalt necessitates high cobalt dispersion [6, 7] to maximize its availability (exposure of the active metal to the gaseous atoms i.e. syngas). This, in conjunction with the required mechanical strength of the catalyst [8], necessitates the use of a support to deposit the catalytically active material. Supported catalysts are typically prepared by impregnation of the oxide support with a cobalt salt (typically cobalt nitrate and/or acetate) [5, 9]. Cobalt is fixated on the support by calcination (typically in air), after which most of the cobalt is present as Co_3O_4. The latter can be reduced in hydrogen via a two-step process, viz. $Co_3O_4 \rightarrow CoO$ and $CoO \rightarrow Co^0$ [10]. Highly dispersed ionic cobalt can interact strongly with the oxidic carrier leading to the formation of species such as cobalt titanate, cobalt silicate or cobalt aluminate which are difficult to reduce to achieve metallic cobalt [11]. This represents a loss of the catalytically

active material since the metallic cobalt is the catalytically active species in the Fischer-Tropsch synthesis. These species could be reduced, but their reduction to metallic cobalt will require thermal conditions which will favour sintering as well [4]. The strength of these interactions increases in the order SiO_2<TiO_2<Al_2O_3 [12].

1.3. Noble metal promoter

The addition of small amounts noble metals such as Pt [11-17] and Au [18] can facilitate the reduction of oxidic cobalt associated with the support. Platinum and gold enable the reduction of oxidic cobalt at relatively low temperatures compared to an unpromoted cobalt catalyst. Therefore, high temperature treatments are not necessary to obtain a catalyst with a high degree of reduction. The major downfall for platinum being used as a reduction promoter is that the facile reduction of the oxidic cobalt comes at a cost of the selectivity (methane selectivity is enhanced). Similarly, gold has been shown to have promotional effects on the reduction behaviour of supported cobalt catalysts [18]. However, at higher loadings the activity of the catalyst, in terms of carbon monoxide conversion decreases. This was ascribed to blockage of active site by gold, hence the decrease in the activity is observed.

1.4. Motivation of the study

The addition of two noble metals may give additional properties which are quite different than the expected properties for the individual components. Platinum-gold alloys may possess a lower strength of CO adsorption which may lead to an improved selectivity towards C_{5+} hydrocarbons relative to the unpromoted and pure Pt- and Au promoted catalysts. AuPt alloys may also result in a dual promotional functioning on the reduction behaviour of the oxidic cobalt species, i.e. H_2-spillover and direct Co-noble metal interaction. In the case of Au, Pt may modify the H_2 dissociative ability for Au such that it can promote via H_2 spillover mechanism.

1.5. Project Overview

In this study *ca*. 2 nm Pt, Au and AuPt alloy nano-particles with narrow particle size distribution will be synthesized. These nano-particles are used to promote a cobalt-based Fischer-Tropsch catalyst. The dispersion of these nano-particles over the Co/TiO_2-catalyst will be controlled by adjustment of the pH of the suspension containing the Co/TiO_2 catalyst prior to the addition of tetrakis(hydromethyl)

phosphonium chloride THPC and NaOH. The effect of Pt/Au alloys as a noble metal reduction promoter on the physical characteristics of a Co/TiO_2 catalyst and its reduction behaviour are investigated. Moreover, the catalytic activity (given by CO conversion) during the Fischer-Tropsch synthesis and the product selectivity are evaluated. The mechanism, by which the reduction of the cobalt species is promoted, may depend on the ratio between Pt and Au. The objective of the study is to investigate the effect of Pt/Au ratio at a constant noble metal/cobalt ratio under Fischer-Tropsch synthesis conditions. The influence of each individual metal on Pt/Au alloy on the Fischer-Tropsch product distribution will be evaluated, with platinum promoted Co/TiO_2 and gold promoted Co/TiO_2 catalysts as basis for comparison.

2 Literature Review

2.1. Fischer-Tropsch synthesis

In 1923 Franz Fischer and Hans Tropsch, after whom the Fischer-Tropsch process is named, discovered that a mixture of CO and H_2 can be converted into liquid hydrocarbons using an iron catalyst [20]. This was a landmark for the synthesis of transport fuels from syngas.

The Fischer-Tropsch synthesis (FTS) is a polymerisation process of CH_x (with x = 0, 1, 2) in the presence of a catalyst affording hydrocarbons with a wide range of carbon chain length [4] (see equation 1), and oxygenates.

$$CO + 2nH_2 \rightarrow \frac{1}{n}(-CH_2-)_n + H_2O \qquad (2.1)$$

The syngas reacts over a catalyst in a stoichiometric ratio of H_2/CO=2 [21]. The mechanism for the formation of Fischer-Tropsch products (hydrocarbons and oxygenates) involves a surface polymerisation of a CH_x (x= 1-3) monomer [4]. Polymerization occurs through: 1) initiation of chains, 2) chain propagation and 3) chain termination steps [4]

The initiation step is the formation of the starter chain which involves adsorption of carbon monoxide on to the active catalyst surface. Carbon monoxide can dissociate in various ways, which include direct (2) and assisted (14) CO dissociation (see Figure 2.1). Direct CO dissociation gives rise to a surface carbon and an oxygen atom. Carbon may undergo hydrogenation yielding methylidyne (4), surface methylene (5) and surface methyl (6) species. On the other hand the hydrogen assisted CO dissociation to form surface methylen-ol (14) either as a chain starter or upon hydrogenation, surface methyl-ol species (15) can be obtained, which undergoes further hydrogenation/dehydration to yield surface methyl species (6).

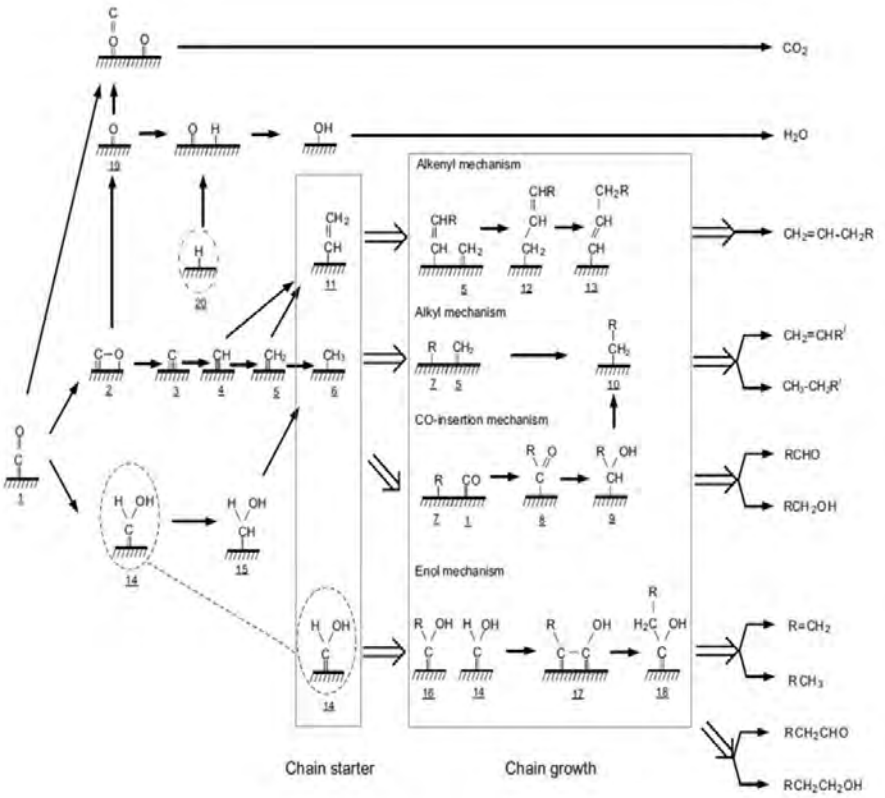

Figure 2.1: Overview of the mechanism Fischer-Tropsch product formation for the Fischer-Tropsch synthesis [adapted from [22]]

The chain starters can grow, polymerise, in various ways and subsequently upon desorption, termination, yield hydrocarbons and oxygenates with an extensive range of functionalities. The different mechanisms of polymerisation that have been discussed include: alkyl, alkenyl, CO- insertion and enol mechanism.

2.1.1. Alkyl mechanism

The alkyl mechanism was first proved by Brady and Pettit [23-24] who observed that there is a reaction between a surface methylene and a surface hydrogen to form a surface methyl, which can act as a chain starter. Chain propagation occurs by successive insertions of alkylene group into the metal-alkyl bond as shown in Figure 2.1 (with R= alkyl group). The alkyl mechanism is the widely accepted mechanism for the formation of hydrocarbons in the Fischer-Tropsch synthesis.

Chain growth termination can take place by either β-hydride elimination to form olefins or reduction by surface hydride to from alkanes. When the surface-chain bond is cleaved by the adsorbed OH group, the alcohols are formed [25].

2.1.2. Alkenyl mechanism

The reaction is instigated by the formation of a surface ethylene from a surface methyne and a surface methylene, both being chain starters [26]. The consequence of this mechanism is that methane is not considered as Fischer-Tropsch process product. The hydrocarbon chain propagates by the reaction of the vinyl species with a surface methylene to form an allyl species ($-CH_2CH=CH_2$). The chain growth occurs by means of successive insertion of the R group. Termination occurs when the surface alkenyl species is reduced by surface hydrogen forming an olefin. Paraffins are thought to be formed in the secondary hydrogenation of olefins.

2.1.3. CO insertion Mechanism

The oxygenated products formed in Fischer-Tropsch synthesis may be formed through carbonyl insertion reaction with the surface alkyl species forming a surface acyl species as shown in Figure 2.2. Upon reduction of the surface acyl species by surface hydrogen alcohol and aldehydes can be obtained. The amount and the type of the oxygenated compounds is catalyst and reaction condition dependent [27].

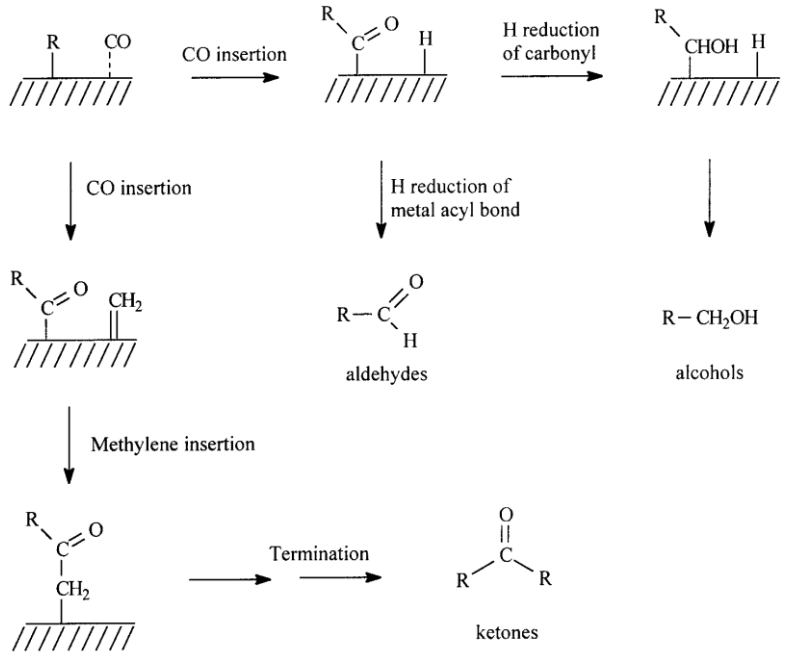

Figure 2.2: Postulated mechanisms for the formation of oxygenates in the Fischer–Tropsch reaction [27].

2.1.4. Product distribution

The product obtained in the Fischer-Tropsch synthesis is a complex mixture of many organic compounds. The selectivity towards liquid hydrocarbons (C_{5+}) is the primary important subject, as ultraclean liquid fuels are of industrial importance. Therefore, the chain growth probability, represented as p_g, is a good parameter to assess the C_{5+} selectivity. The chain growth probability is a function of the rate of desorption ($r_{d,n}$) and rate of chain growth ($r_{g,n}$) according to equation 2.2.

$$p_g = \frac{r_{g,n}}{r_{g,n}+r_{d,n}} \qquad (2.2)$$

A simplified schematic of the chain growth reactions over the catalyst surface and termination of the surface species is shown in Scheme 2.1. Only one sort of products is assumed to be formed in this simplified scheme.

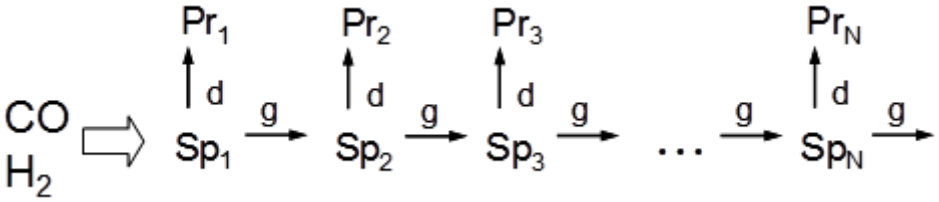

Scheme 2.1: Chain growth reactions over the surface and termination of the surface species [28]

After dissociation of the adsorbed CO and H_2, monomers and chain starters (C_1 surface species, Sp_1) are formed, which can either desorb to form a C_1 product molecule (Pr_1) or successively grow via insertion of C_1 monomers. If the rate of chain termination is much greater than the rate of adsorption, then the chain growth probability will be diminished and vice versa (*cf*. Equation 2.2). Therefore, higher hydrocarbons inevitably would be observed at higher chain growth probabilities as depicted in Figure 2.3. The wide hydrocarbon product (α-olefins and alkanes) distribution has been interpreted by the Anderson-Schulz-Flory (ASF) chain growth mechanism, and can be mathematically described assuming carbon-number is independent to the chain growth probability (ideal ASF- kinetics).

$$n/\sum n_i = (1 - p_g)\, p_g^{n-1} \qquad (2.3)$$

Where n is the number of carbon atoms in the product and p_g is called as ASF chain growth probability, which represents the overall chain growth probability. The chain growth probability can be obtained empirically from the product distribution (slope of the ASF plot).

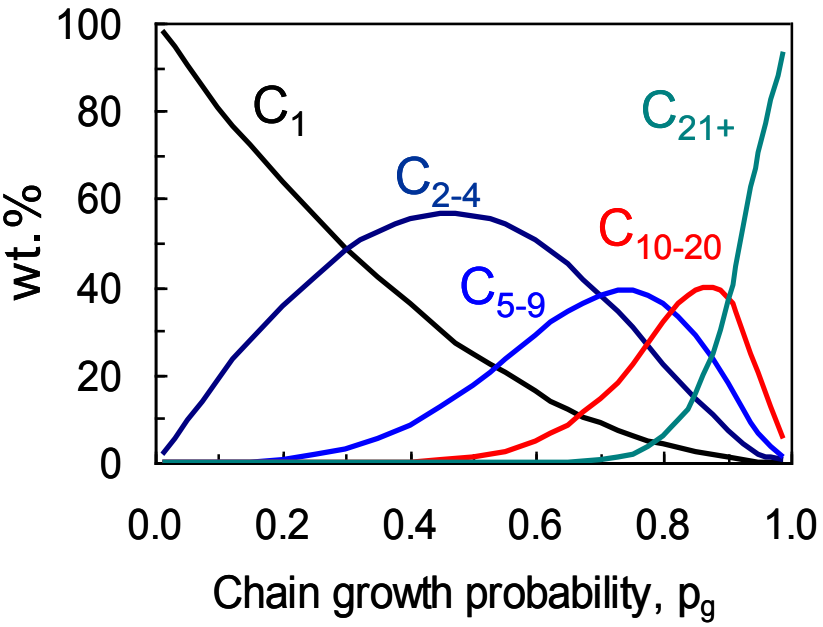

Figure 2.3: Product composition (wt.-%) as function of chain growth probability assuming ideal ASF kinetics [28].

Only methane and C_∞ can be produced with a selectivity of 100 wt.-%, i.e. at a chain growth probability of 0 ('methanation') and 1 respectively, with the assumption of ideal ASF kinetics [28]. The maximum middle distillate yield (carbon number range C_{10}-C_{20}) according to these kinetics is only around 40 wt.-% and can be obtained at $p_g \approx 0.85$. If higher overall yields of middle distillate are required, the FT process should be designed in a way that very high chain growth probabilities (high wax yields) are achieved. Mildly the products can be hydrocracked to middle distillate. In doing so a middle distillate selectivity of *ca*. 80 wt.% can, for example, be theoretically achieved when operating a Fischer-Tropsch process at a chain growth probability of 0.95 [28].

2.1.5. Selectivity

Methane selectivity is not a variable of commercial interest and should be therefore as low as possible. However, this is a multifaceted variable, which is governed by the probability that a surface carbon is transformed into a surface methyl group and the probability that the surface methyl group is hydrogenated yielding methane. Both probabilities increase with increasing hydrogen availability on the surface [29].

Product selectivity is influenced by reaction conditions, catalyst used and promoter employed. Cobalt-based catalysts are reported to have higher hydrogenation activity compared to iron-based catalysts. However, primary olefins selectivity is more pronounced for cobalt-based catalysts. Iglesia *et al*. [30-31] developed a model, in which they assumed diffusional limitations within the liquid-filled pores of a catalyst to slow down removal of long chain α-olefins (see Figure 2.4). Therefore, increasing their residence time and thus enhancing the extent of secondary conversion yields heavier and more paraffinic products [28]. This would justify the observed chain length dependencies in Fischer-Tropsch product.

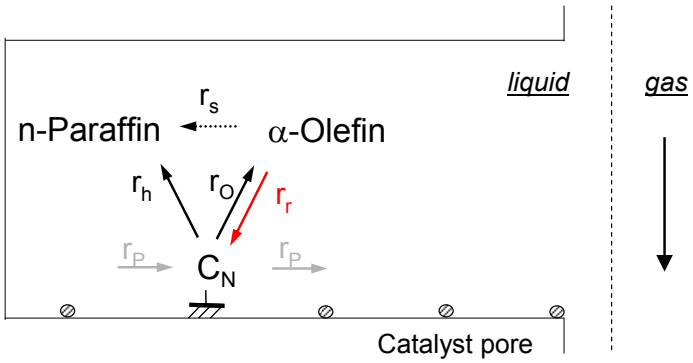

Figure 2.4: Diffusion enhanced olefin re-adsorption in liquid-filled catalyst pore [30-31].

Where r_p: rate of propagation, r_h: rate of hydrogenation, r_o: rate of olefin formation, r_r: rate of re-adsorption and r_s: rate of secondary reaction.

The high selectivity for linear olefins observed for iron-based catalysts can be explained based on the lower activity for secondary hydrogenation of the primarily formed α-olefins in comparison to cobalt-based catalysts [19].

The end products of the Fischer–Tropsch process are a mixture of higher alkanes and alkenes. The promoter elements could show, under Fischer–Tropsch conditions, some activities for hydrogenation or dehydrogenation reactions leading to a shift in the relative ratio of alkanes to alkenes.

2.2. Catalysts for the Fischer-Tropsch synthesis

2.2.1. The active metal

Transition metals such as Nickel (Ni), Ruthenium (Ru), Iron (Fe) and Cobalt (Co) have been observed to have significant activity for CO hydrogenation [19]. A common feature of these materials is their interaction with CO and their ability to dissociate adsorbed carbon monoxide [5]. It should be noted that the CO should not be too strongly nor too weakly adsorbed on the metals, since this will lead to methanation rather than chain growth [32] and low activity when strongly adsorbed. Under Fischer-Tropsch conditions Ni leads to methanation rather than chain growth [33]. On the other hand, Ru has been found to be less selective towards methane and more selective to C_{5+} hydrocarbon fraction than other Fischer-Tropsch active metals, but the scarcity and high cost of Ru make its use as an industrial catalyst unrealistic [34]. Therefore, iron and cobalt-based catalysts are the industrially preferred Fischer-Tropsch synthesis catalysts.

Iron-based catalysts are used for high temperature Fischer-Tropsch synthesis (HTFTS) which operates between 300-350°C [34]. High temperature Fischer-Tropsch synthesis is a process of choice for the production of gasoline and low molecular mass olefins [34]. On the other hand, low temperature Fischer-Tropsch synthesis (LTFTS) which operates between 200-250° uses either iron or cobalt-based catalyst and it produces high molecular mass mainly linear waxes [34]. The most commonly used catalysts for the low temperature Fischer-Tropsch synthesis are cobalt-based catalysts due to their selectivity for linear hydrocarbons. Furthermore, cobalt-based catalysts showed a higher productivity at lower relative space velocity and lower reactor pressures [35]. This was ascribed to the higher resistance of cobalt-based catalysts to higher water partial pressures [6]. This means that with cobalt-based catalysts at higher conversion per pass can be achieved thereby improving the economics of the overall Fischer-Tropsch process [6]. It has also been shown that cobalt catalyst show a low activity for the formation of CO_2

under Fischer-Tropsch conditions up to adequate levels of conversion [6] making it ideal for the conversion of synthesis gas with a feed ratio of H_2/CO of 2 [6], which can be obtained from natural gas.

2.2.2. The support

Fischer-Tropsch synthesis is a surface reaction. This implies that the catalytic activity is proportional to the surface area of the catalytically active phase in the catalyst. Therefore, large surface area per unit mass of the catalytically active phase in the catalyst is ideal to enhance the activity of the catalyst.

Small metallic cobalt crystallites (in a range of nanometers) are then expected to show a higher activity per unit mass of catalytically active material. Benzenzer et al. have shown that the intrinsic activity of cobalt per unit surface area increases with increasing diameter [36]. The dispersion decreases with increasing crystallite size. Hence, there exist an optimum in the crystallite size which yield the highest activity per unit mass of cobalt. (*cf*. Figure 2.5). However, small crystallite may sinter.

This is prompted by a strong dependency of the melting temperature of the active metal solid on its crystallite size. The melting temperature decreases strongly for crystallites with a size of less than 5 nm [37-38]. The decrease in melting temperature with decreasing crystallites size promotes mobility of the catalytically active material, subsequently agglomeration of particles. This represents a reduction of the surface area of the catalytically active phase.

The necessity for small crystallites for an enhanced activity means that the small crystallite sized material must be dispersed over a meso-porous metal oxide material which usually has a high surface area, a high thermal and chemical stability and a high mechanical strength. These materials include TiO_2, SiO_2 and Al_2O_3 [39]. This reduces the extent of sintering and exposes as many active metal atoms as possible to the gaseous reactants (H_2/CO) [40]. The number of catalytic active atoms on the surface (accessible to the gaseous reactants) relative to the number of atoms present in the material (known as dispersion) increases with decreasing crystallite size (*cf*. Figure 2.5). This suggests that highly dispersed cobalt species over the support enhances the activity of the catalyst.

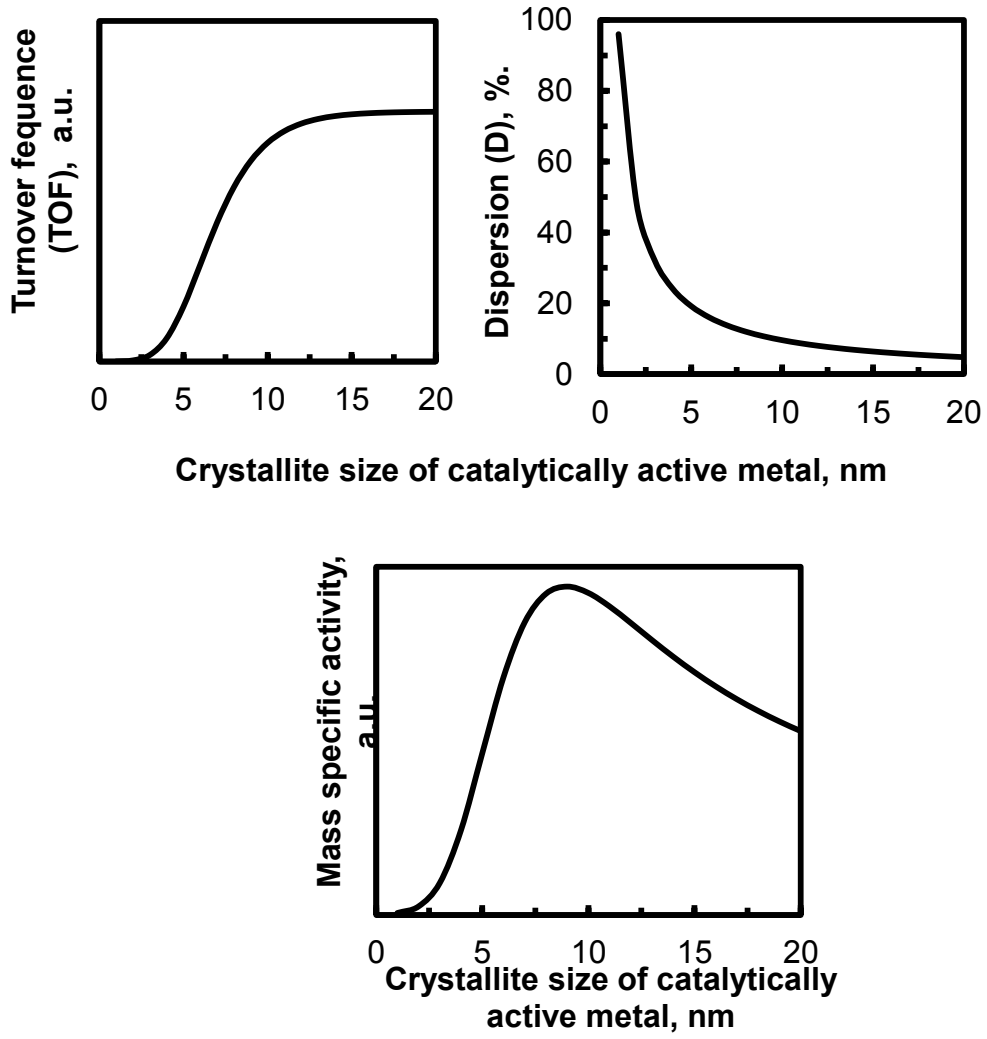

Figure 2.5: Top left: Turnover frequency as a function of crystallite size of the active material.

Top Right: Dispersion of the active material over a support with increasing active material crystallite size

Bottom: Mass specific activity of the catalyst with increasing crystallite size of the active material

Supported cobalt catalysts are typically prepared by impregnation [5] of a pre-calcined support with cobalt containing solution, typically cobalt nitrate or acetate [40]. Incipient wetness impregnation is a method of choice in many laboratories due to its simplicity, in which a metal salt usually dissolved in water, although sometimes in organic solvents are used [41-43], is added to the carrier in an amount equal to pore volume of the support. Methods such as precipitation and ion-exchange can also be used to deposit the metal precursor on the surface of the carrier.

The impregnated support is subsequently dried, typically at 60-120 °C. Cobalt is fixated on the support by calcination (typically in air, between 300-350 ^{0}C) to decompose the cobalt salt after which most of the cobalt is present as Co_3O_4 [40]. The latter can be reduced (so as to activate the catalyst for Fischer-Tropsch synthesis) in hydrogen. The reduction is thought to proceed via a two-step process, viz. $Co_3O_4 \rightarrow CoO$ and $CoO \rightarrow Co^0$ [44].

A considerable fraction of cobalt may remain in its oxide form, mainly divalent cobalt [34]. Divalent cobalt associated with the support is much harder to reduce [34]. Highly dispersed cobalt can also interact strongly with surface hydroxyl groups of the oxidic carrier leading to the formation of cobalt species which are difficult to reduce [4], such as cobalt silicates, cobalt aluminates or cobalt titanates. The irreducible cobalt species represents a loss of the catalytically active material since metallic cobalt is the catalytically active species for the Fischer-Tropsch synthesis. This leads to a diminished catalytic performance.

The reduction of the CoO associated with the support to metallic cobalt will require high temperatures which will increase the extent of reduction of the cobalt species. This would, however, favour crystallite growth (sintering) which will decrease the surface area of the Co particles (*cf.* Figure 2.6).

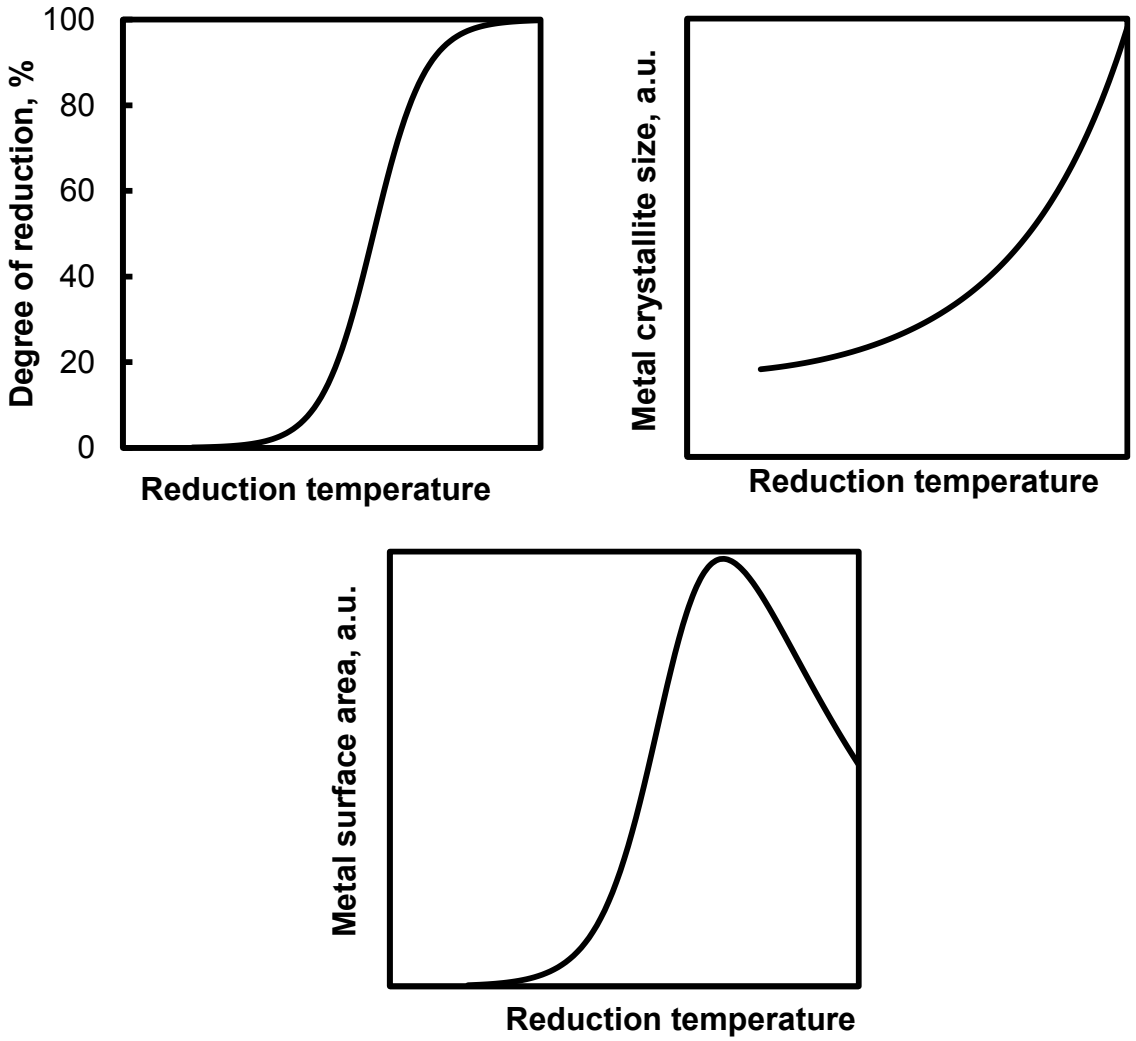

Figure 2.6: Top left: Degree of reduction as a function of temperature
Top Right: Metal crystallite size as a function of reduction temperature
Bottom: Typical behaviour of a metal surface area of the active material with increasing reduction temperature.

2.2.3. Promoters

Strategies to improve the catalyst performance have been reported in literature. This includes the addition of promoters on supported cobalt systems.

Promoters are doping agents added to catalyst materials with intent to improve activity, selectivity and stability of the catalyst. Although promoter elements or compounds are not considered to be catalytically active themselves, they may play a role under Fischer-Tropsch conditions [32].

Promoters induce beneficial effects in numerous approaches. These promoters can be classified according to their promoting effects into structural or structure promoters, electronic promoters, textural promoters, stabilizers and catalyst-poison-resistant promoters [33]. In practice these effects tend to overlap, making it difficult to define accurately the observed functioning of the promoter.

This study focuses on promoters that influence the reduction of oxidic cobalt species to metallic cobalt. A highly reduced cobalt catalyst results in an increased number of active cobalt metal surface and, therefore, in a high coverage by the reactants, and as a consequence an improved catalyst activity.

These promoters may lead to an enhanced catalyst activity and stability, but in principle do not affect the product selectivity since it only increases the number of active sites in a catalyst material. This increase in the number of active sites can be achieved by a stabilization of the catalyst and active cobalt phase due to the presence of the promoter element. The promoter can either retard the formation of metal-support compounds, or assist the reduction of the hard-to-reduce supported cobalt systems.

2.2.3.1. Oxide promoters

Oxide promoters include lanthanide and thorium oxide, ceria, zirconia, titania, vanadia, chromia and manganese oxides. Typically, these oxide promoters are added to supported cobalt systems to modify the catalyst texture and/or porosity. This reduces formation of hardly reducible cobalt mixed oxides, increases cobalt dispersion, reducibility, and fraction of different cobalt metal crystalline phases, enhances mechanical and attrition resistance of cobalt Fischer-Tropsch catalysts, and improves the chemical stability of the support.

MnO_2 promotion of supported cobalt catalyst may prevent the inclusion of the cobalt species into the structure lattice of the support by occupying the vacant site of the support, as shown in Figure 2.7 [45].

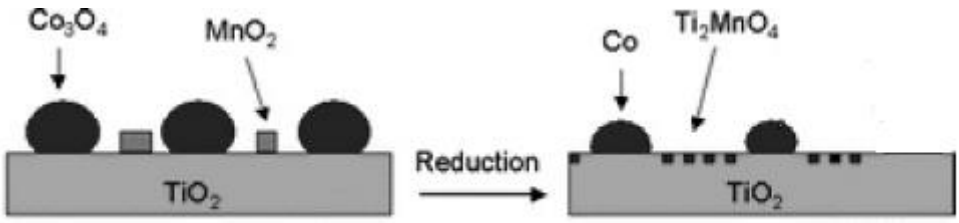

Figure 2.7: Incorporation of MnO_2 promoter, preventing the formation of cobalt titanate [45]

Jongsomjit et al. showed that addition of zirconia to alumina-supported cobalt catalysts resulted in stabilization of alumina support and prevention of cobalt surface "aluminate" formation [46]. Similar conclusions were drawn by Xiong et al. suggesting that addition of zirconia could impede $CoAl_2O_4$ formation [47].

2.2.3.2. Noble metal promoters

Addition of noble metals, such as Pt, Re, Ru, Au and Pd [11-18] to supported cobalt systems could result in an enhanced extent of reduction of the oxidic cobalt species, due to appearance of additional sites of hydrogen activation, [17] modified electronic properties of the oxidic cobalt and/or a lower likelihood for the formation of barely reducible mixed oxides.

Upon promotion with a noble metal, such as Rh, Pt and Ru, the reduction temperature for both steps ($Co_3O_4 \rightarrow$ CoO and CoO $\rightarrow$ Co^0) shifts to lower temperatures [40]. Re as a reduction promoter has been observed to only affect the second reduction step (CoO $\rightarrow$ Co^0) [34]. This was attributed to the fact that reduction of ReO_2 occurred above the reduction temperature of Co_3O_4 to CoO [34].

The proposed mechanisms for these promoting effects include hydrogen spillover and direct cobalt-noble metal interaction. Both promoting mechanisms have an effect on the reduction behaviour and subsequently, catalytic performance under Fischer-tropsch synthesis conditions. Due to this occurrence the reduction temperature of the oxidic cobalt is decreased in certain cases by 200-400 °C.

2.2.3.2.1. Hydrogen spillover

In heterogeneous catalysis, the term spillover is regarded as the transportation of a sorbed active species [48]. Spillover can also be understood as the formation of the

active species on one surface transported to another surface [48]. After activation, the species is subjected to a different surface phase, called an acceptor. The activating species is called an initiator. Once the activated species comes into contact with the acceptor, diffusion to the acceptor proceeds and several processes may take place on the surface.

The first direct evidence for this mechanism was observed by Khoobiar [49]. WO_3 has been reported to reduce above 200 °C yielding W_4O_{11} [50]. On the contrary, when pure H_2 is passed over a physical mixture of 0.5%Pt/Al_2O_3 + WO_3 at room temperature, reduction occurred. Notably, this effect was not observed on the physical mixture Al_2O_3 and WO_3. This observation was ascribed to the fact that platinum dissociates hydrogen gas into H^+ ions which migrate over Al_2O_3 onto WO_3 species thereby reduce it.

The same analogy has been extended for supported cobalt-based catalysts for Fischer-Tropsch synthesis. Hence, the promotional effect of platinum on supported cobalt-based catalyst for Fischer-Tropsch synthesis is thought to occur via hydrogen spillover [6], which can be defined as *the diffusion of atomic hydrogen over the support from the noble metal to the oxidic cobalt moieties thereby reducing them to metallic cobalt*. The diffusion of the adsorbed hydrogen on the surface of the support may involve breaking and reformation of OH equivalent bonds with similar neighbouring atoms on the noble metal surface as well as the support surface [6]. The formed hydroxyl groups act as *bucket "brigade"* [6] with which eventually the spillover hydrogen species interact weakly as they are transported over the surface, as illustrated in Figure 2.8.

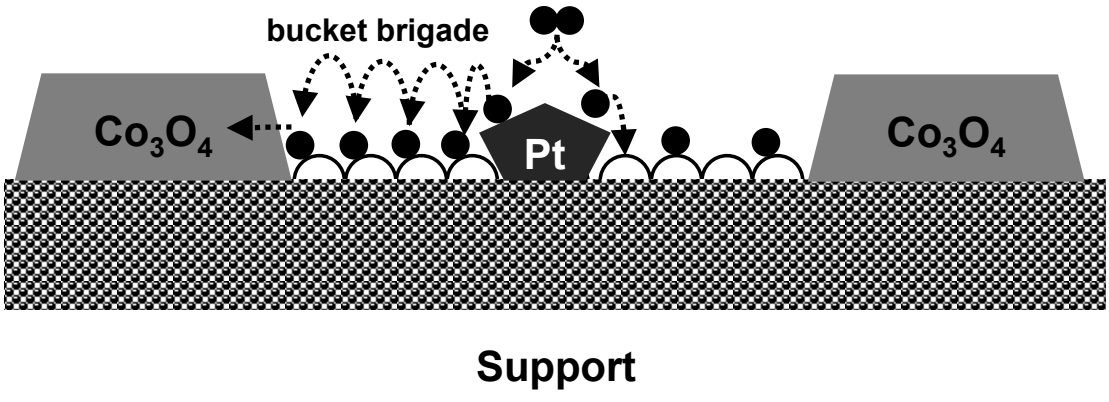

Figure 2.8: Hydrogen spillover transport via 'bucket brigade' [51].

The primary reason for hydrogen spillover is reported to be the difference in the energetic stability between the adsorbed hydrogen in the noble metal and the adsorbed hydrogen on the support [6]. Figure 2.9, shows a schematic representation of the required energy levels for the dissociation of the adsorbed H_2 on the noble metal promoter, followed by the diffusion of atomic hydrogen on to the support and consequently on to the reducible cobalt oxide. It should be noted, the true evidence for hydrogen spillover is only available for Re-promoted catalysts [5].

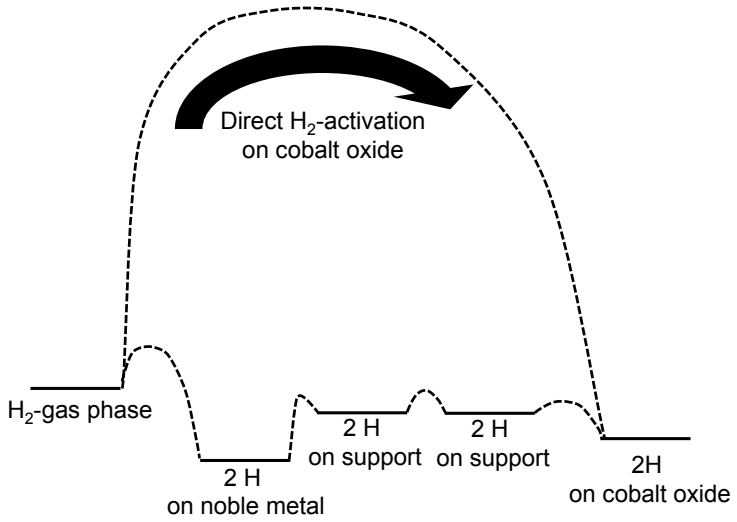

Figure 2.9: Energy diagram for H_2 dissociation on the noble metal promoter, followed by diffusion of the activated hydrogen over the support to oxidic cobalt species [6].

A direct-cobalt noble metal interaction is also possible for platinum promoted cobalt catalysts. Hence, association of platinum and the cobalt moiety cannot be ruled out.

2.2.3.2.2. Direct cobalt-noble metal interaction

The reduction behaviour of oxidic cobalt species can also be affected by direct cobalt-noble metal contact yielding more easily reducibly cobalt species, thereby lowering the reduction temperature. The interaction between the noble metal and cobalt could be better understood in terms of a ligand effect. The interaction between cobalt species and the noble metal induces an electron donation and/or withdrawal [45] between the involved species, thereby altering the chemical and reduction behaviour of the oxidic cobalt species.

The phenomenon of this synergism has been thought to be the mechanism for the change in the reduction behaviour of the supported oxidic cobalt species. This is probably the promoting mechanism for noble metals that has a lower chemisorption and adsorption energy for hydrogen, thereby ruling out hydrogen spillover as a possible mechanism.

According to Jalama et al. the reduction promotional effects brought about by Au could be ascribed to direct cobalt-gold interaction rather than H_2 spillover for its functioning as a promoter [18].

Beside the reduction promotional effects, direct cobalt-noble metal interaction promoting mechanism may also result in a decreased rate of deactivation by altering the adsorption/desorption properties of the reagents/reaction products [45]. The ligand effect could be responsible for an increased resistance of the supported cobalt nanoparticles to re-oxidation during Fischer-Tropsch conditions. This might involve transfer of electrons from the d-orbital of the noble metal to the anti-bonding orbital of the cobalt, thereby decreasing a bonding order between cobalt and oxygen atom. Decreasing cobalt-oxygen bond order in that way the bond between the cobalt and oxygen is weakened, facilitating the reduction.

2.2.3.3. Productivity on promoted cobalt systems

The influence of noble metal promoter on the intrinsic catalytic activity of supported cobalt catalysts has been studied extensively. Addition of a noble metal may result in an electronic modification of the catalyst which may result in the modification of adsorption characteristics of the surface of the catalyst [42]. Xu et al. showed that the carbon monoxide conversion increases upon promotion of Co/Al_2O_3 by platinum (Pt) [35]. Similar conclusions were drawn by Meng et al. when 0.1 wt% noble metals (Pt, Pd or Rh) to Co/Ce-Al-O catalyst were employed [52]. Due to an increased degree of reduction of cobalt species upon promotion, more catalytic active phase of cobalt is accessible to reaction gases, hence an increased activity [34].

Mo et al. observed that the addition of copper as a reduction promoter for Co/CuZnO decreases the activity for CO hydrogenation [53]. This was ascribed to the blockage of the active metallic cobalt surface with the promoter. Metallic copper surface enrichment could be probable if the promoter metal is associated with the cobalt

species. This is normally observed for promoter metals with lower surface energy than cobalt, especially at high loadings.

It is expected that when a higher degree of reduction is obtained the number of active cobalt sites would increase compared to the unpromoted catalyst. However, both the type and loading of the noble metal dictates whether or not, promoting effects will occur (observed on CO conversion). Hence a link between the degree of reduction of the oxidic cobalt and the activity as measured by carbon monoxide conversion cannot be established. Jalama et al. showed that at high loading of Au (≥ 1wt.-%) as a promoter, the carbon monoxide conversion decreases considerably [18], although the degree of reduction of oxidic cobalt is improved in comparison to the unpromoted catalyst. A similar behaviour was observed by Jacobs et al. At a 5.05wt.-% Au loading the catalyst performed poorly with a steep drop in productivity (from X_{CO} of 51.7% at 1.51wt.-%Au to an X_{CO} of 14.1% at 5.05wt.-% Au at space velocity (SV) of 4.2 NL/(g_{cat}·h)) [34]. This was ascribed to metallic cobalt surface enriched with promoter metal, might be due to lower surface energy of the promoter compared to the cobalt species. This might be ascribed to the presence of the promoter metal on the metallic cobalt. The decrease in X_{CO} would be enhanced at high loading. Contrary to this, the activity of Pt, Ru and Re promoted supported cobalt catalysts; is improved with increasing loading. Chu observed that CO conversion increases with increasing Pt loading [54]. This could be ascribed to an increased surface hydrogen subsequently improving hydrogenation activity when platinum is used as a reduction promoter [54].

2.2.3.4. Selectivity on promoted cobalt systems

The product selectivity is influenced by numerous factors. This includes reaction conditions and the composition of the catalyst used. Methane selectivity is also influenced by the CO-conversion ability of the catalyst. A recent kinetic study by Jacobs et al. showed that CH_4 selectivity changes with changing CO-conversion. At lower and higher CO-conversions show high CH_4 selectivity and at moderate CO-conversions is lower compared to lower and higher CO-conversions, see Figure 2.10, [34].

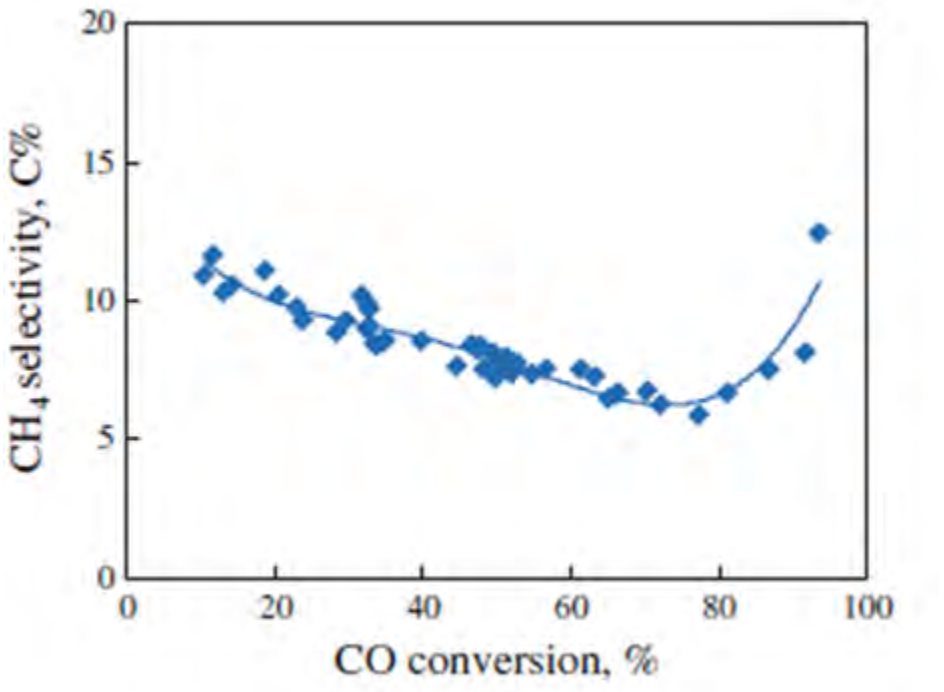

Figure 2.10: Changes in over 0.27%Ru-25%Co/Al_2O_3 catalyst (Reaction conditions: 220 °C, 1.5 MPa, H_2/CO = 2.1 and SV = 0.3–15 NL/g_{cat}h) [34].

As noted cobalt based catalysts contain small additives as promoter. In some promoted cobalt catalyst, the liquid hydrocarbon selectivity is improved relative to the unpromoted catalysts, but in some it is diminished. Ruthenium is catalytically active for the Fischer-Tropsch synthesis reaction and higher chain growth probability was measured in the hydrocarbon distribution [34]. Hence, lower methane and higher C_{5+} selectivity might be considered to be inevitable when Ru is used as a promoter for 0.26%Ru-25%Co/Al_2O_3 catalyst relative to the unpromoted catalyst [34]. Pt- and Pd-containing samples show high methane and suppressed C_{5+} selectivity compared to the unpromoted cobalt systems [15]. This is ascribed to a larger availability of surface activated hydrogen (supplied by hydrogen spillover) content for Pt-containing supported cobalt system. In the case of Pd promoted catalyst this could be attributed to the formation of highly dispersed Pd, which reduced CO adsorption on cobalt, taking into account that CO adsorption negatively impacts the hydrogenation of 1-olefins [15]. On the other hand Au showed slightly improved C_{5+} selectivity compared to the unpromoted supported catalysts. However, at higher Au loadings (5.05wt.-%) the selectivity towards C_{5+} hydrocarbons was diminished significantly, from 81.6% for the unpromoted catalyst to 60.1% for 5.05wt.-% Au promoted catalyst at constant

X_{CO} of ~28%). When copper is used as reduction promoter, at a lower promoter loading (0.49wt.-%), the methane selectivity is slightly increased, subsequently C_{5+} is slightly decreased [40]. Increasing the Cu promoter loading (1.67wt.-%) further leads to an excessive increase in methane selectivity (21.6% of 1.67wt.-% Cu compared to 9.2% of 0.49wt.-% Cu) and a steep drop in C_{5+} selectivity (47.7% of 1.67wt.-% Cu compared to 81.6% of 0.49wt.-% Cu) [34]. This was ascribed to the blockage of the active metallic cobalt surface with the promoter (Au or Cu) [5].

2.2.3.5. Alloy systems as reduction promoters

There are possible negative effects with regard to the activity and selectivity associated with the addition of the promoter metal [5]. However, addition of two alloyed noble metals may give additional physicochemical properties which are quite different than the expected for the individual noble metal component. It has already been established that the reduction of the unpromoted catalyst occurs at relative high temperatures compared to the pure noble and/or alloyed noble metal promoted catalysts. However, low reduction temperature does not necessarily mean an enhanced catalytic activity (as a measure of carbon monoxide conversion at same space velocity) as it is in the case of gold promoted cobalt catalyst at high loadings. It has also been noted that gold is inactive under Fisher-Tropsch conditions. Furthermore, it blocks the active sites of the catalyst [18], and consequently decreases the catalytic activity. Platinum is a well-known reduction promoter, but it has also been shown to be catalytically inert under Fischer-Tropsch conditions due to its strong competitive CO adsorption and the promotional effects are thought to be solely due to the increased reduction obtained in the presence of platinum. One of the main focuses on Fischer-Tropsch catalyst design is to obtain high selectivity towards C_{5+} hydrocarbons but for platinum promoted catalysts the large availability of surface hydrogen result in methane selectivity enhancement.

Platinum-gold alloys may possess a lower strength of CO adsorption which may lead to an improved selectivity towards C_{5+} relative to the unpromoted and pure Pt- and Au promoted catalysts. Therefore, the catalytic conversion of the alloy promoted supported cobalt catalyst might improve significantly compared to the unpromoted, pure platinum and gold promoted cobalt catalyst. Pt/Au alloy may also result in a dual promotional functioning on the reduction behaviour of the oxidic cobalt species,

i.e. H_2 spillover and direct Co-noble metal interaction. In the case of Au, Pt may modify the H_2 dissociative ability for Au such that it can promote via hydrogen spillover mechanism to some degree.

2.2.4. Nanoparticle synthesis

The noble promoter metal is usually deposited onto the supported catalyst in nanometric dimensions. Methods such as thermal decomposition of organometallic compounds and metal-surfactant complexes in the presence of stabilizing agent yield well-crystallised nanoparticles with a narrow size distribution. Nonetheless, purification of the nanoparticles is a challenge as it requires multiple purification steps. Other methods include formation of stable metal organosols that can be achieved by refluxing of α-alcohols (such as ethylene glycol) with a dual role as a solvent and a reducing agent [55]. This method is known as polyol-reduction method (developed by Hirai and Toshima [56-58]) and yields a wide variety of metal nanoparticles. Nonetheless, heating at high temperatures and the presence of other stabilizing and polymers such as poly(vinylpyrrolidone) (PVP) or poly(vinyl alcohol) (PVA) is generally required. Duff et al. proposed a new method for the synthesis of gold nanoparticles at room temperature, that involved the use of a tetrakis-(hydroxymethyl)-phosphonium chloride, $P(CH_2OH)_4Cl$, which is a low-chain compound with a reducing and ionic stabilizing twofold role in aqueous phase [59]. In this present study the noble metal nanoparticles is deposited on TiO_2 and Co_3O_4/TiO_2 catalyst precursor following the procedure proposed by Duff et. al [59] and Hueso et al. [55].

2.2.5. Project Overview

In this study *ca*. 2 nm Pt, Au and AuPt alloy nano-particles with narrow particle size distribution will be synthesized. These nano-particles are used to promote a cobalt-based Fischer-Tropsch catalyst. The dispersion of these nano-particles over the Co/TiO_2-catalyst will be controlled by adjustment of the pH of the suspension containing the Co/TiO_2 catalyst prior to the addition of tetrakis(hydromethyl) phosphonium chloride THPC and NaOH. The effect of Pt/Au alloys as a noble metal reduction promoter on the physical characteristics of a Co/TiO_2 catalyst and its reduction behaviour are investigated. Moreover, the catalytic activity (given by CO

conversion) during the Fischer-Tropsch synthesis and the product selectivity are evaluated. The mechanism, by which the reduction of the cobalt species is promoted, may depend on the ratio between Pt and Au. The objective of the study is to investigate the effect of Pt/Au ratio at a constant noble metal/cobalt ratio under Fischer-Tropsch synthesis conditions. The influence of each individual metal on Pt/Au alloy on the Fischer-Tropsch product distribution will be evaluated, with platinum promoted Co/TiO_2 and gold promoted Co/TiO_2 catalysts as basis for comparison.

Hypotheses

To provide an appraisal for the expected result outcome, it is postulated that:

- With increasing Pt/Au ratio the reduction temperature for the reduction of oxidic cobalt species to Co^0 would shift to lower temperatures
- With increasing Pt/Au ratio methane selectivity increases.

With the insight gain from previous studies, the promotional mechanism for platinum was ascribed to an increase in atomic surface hydrogen content, as hydrogen is the reduction species. This is linked to the product selectivity, as platinum dissociate diatomic hydrogen into atomic hydrogen. Subsequently an increased hydrogenation is anticipated, due to a larger availability of surface hydrogen. Hence, methane selectivity is predicted to increase.

The key questions that are addressed in this thesis include:

- Can Au/Pt alloys be used as reduction promoters for Co/TiO_2 catalysts for the Fischer-Tropsch synthesis?
- How does the Pt:Au ratio affect cobalt reduction behaviour, catalytic activity and C_{5+} selectivity?
- How does the method of depositing the nano-particles affect the catalyst performance under Fischer-Tropsch synthesis?

3 Experimental Procedure

3.1. Chemicals

Cobalt acetate ($C_4H_6CoO_4.4H_2O$, Sigma Aldrich) and cobalt nitrate ($Co(NO_3)_2.6H_2O$, Kimix), Tetrakis(hydroxymethyl) phosphonium chloride solution (THPC, 80 wt% Aldrich), Chloro-platinic acid hexahydrated ($H_2PtCl_6.6H_2O.6H_2O$, Alfa Aesar), Chloro-auric acid tetrahydrated ($HAuCl_4.4H_2O$, Aldrich), Sodium hydroxide (NaOH, Kimix) were all used. TiO_2 (P25, Evonik), was calcined in air at 350 °C for 6 hours.

3.1.1. Preparation of standard solution

Standard cobalt acetate and nitrate solutions (3.5 M) were prepared. The solutions were mixed to obtain a variety of acetate to nitrate plus acetate (Ac/(Ac +Nitrate) ratios of 0, 0.15, 0.3, 0.45, 0.6, 0.85 and 1. De-ionised water was used as a solvent.

3.2. Synthesis of standard Co/TiO_2 catalysts

A series of TiO_2 supported cobalt catalysts were prepared by slurry impregnation of TiO_2 (S_{BET} = 46.4 m^2/g; V_{pore} = 0.1 cm^3/g). The support was impregnated with the prepared standard solutions ($[Co^{2+}]$ = 3.5 M; $[Ac^-]/[NO_3^-]$ = 1, 0.15, 0.3, 0.45, 0.6, 0.85, 0) using approximately 2 mL of solution per gram of TiO_2. The solvent was dried off at 333K for 6 hours at atmospheric pressure. The catalyst precursor was subsequently calcined in a fluidised bed at 623 K for 6 hours using air (100 mL (NTP)/min). The obtained cobalt loadings were between 12wt.-% and 18 wt.-%.

3.3. Synthesis

3.3.1. Nano-sized Au/Pt alloys preparation

The synthesis of nano-sized particles involved addition of a sodium hydroxide solution (0.2M, 1.5 mL) into 45 mL of distilled water in a 100 mL of round-bottomed flask under stirring at 300 rpm. Subsequently, the reducing agent tetrakis(hydroxymethyl) phosphonium chloride (THPC) solution (1 mL of a solution of 1.2 mL of 80% aqueous solution diluted in 100 mL of distilled water). Metal solution precursors (0.4 mL) were added dropwise into the NaOH/THPC solution. Chloro-platinic acid, 8wt.% in water, and 4.8wt.-% chloro-auric acid metal solution were

used for the synthesis. A drop of 4.8wt.-% chloroauric metal solution was added to initiate nucleation of platinum nanoparticles. Two minutes was allowed between the addition of THPC and metal acid solution. A clear brown orange was obtained for pure gold hydrosol. Platinum and the alloy hydrosols were obtained as olive-grey hydrosol. The resulting hydrosol was wrapped in aluminium foil to prevent from photo-thermal decomposition. The product was kept in the refrigerator until further characterisation.

3.3.2. TiO_2 supported nano-particles

The deposition of Au and $Au_{30}Pt_{70}$ on TiO_2 support was preceded by calcination of TiO_2 (S_{BET} = 46.4 m^2/g; V_{pore} = 0.1 cm^3/g) in air (50 mL/min (NTP)) at 300 °C for 2 hours. The calcined TiO_2 was finely ground and 0.1g was suspended in 50 mL of 1M KCl in a sample bottle. The pH of the TiO_2 suspension was adjusted to 1.03 – 1.46 using concentrated HCl or 1M NaOH. Metal acid solution (150 μL) was added into the mixture. The mixture was ultra-sonicated for 5 minutes. For the synthesis of the $Au_{30}Pt_{70}$ alloy promoted TiO_2 support, 2 mL of 8wt.%chloro-platinic acid solution was mixed with 3.33 mL of 4.8wt.% chloro-auric acid solution before added to TiO_2 suspension.

Aside, 35 ml of distilled water was added in a three-necked round-bottomed flask followed by addition of 1.2 ml of 0.2M of NaOH, under a magnetic stirrer with a rotation speed of 300 rpm. Tetrakis (hydroxymethyl) phosphonium chloride solution (1 mL) (1.2 mL of 80% aqueous solution diluted in 100 mL of distilled water) was added into NaOH solution. Au-TiO_2 mixture was added dropwise to NaOH/THPC solution. Approximately, 2 minutes was allowed between the addition of THPC into NaOH solution and addition of Au-TiO_2 mixture into NaOH/THPC solution.

3.3.3. Promoted Co/TiO_2 catalyst preparation

A series of unpromoted and promoted Co/TiO_2 catalyst were prepared. TiO_2 supported cobalt catalyst prepared with [Co^{2+}] = 3.5 M; [Ac^-]/[NO_3= 0.6 was used for promotion. Gold, platinum and gold-platinum alloys were used as reduction promoter.

The synthesis of the gold-platinum alloys was based on the hydrosol method proposed by Duff *et al.* [55, 59] in the presence of the catalyst. The catalyst precursor, 18 wt.% Co/TiO_2, (between 0.4 and 2 g) was re-suspended in 10 ml distilled water. The pH of the solution was adjusted to 1-1.5 using a concentrated HCl-solution. A solution containing the appropriate amount of auric chloric acid and/or hexachloro-platinic acid was added to the slurry in a ratio of 1 mL of solution per 2.75 g of catalyst precursor (see Table 3.1). The resulting slurry was sonicated for 5 min. Aside, 35 mL of distilled water was added together with 3.6 mL of an aqueous NaOH-solution (0.2M) in a three-necked round-bottomed flask. A solution of 1.28 wt.-% tetrakis (hydroxymethyl) phosphonium chloride (THPC) solution in water (1 mL) was added under stirring (850 rpm). Approximately 2 minutes later, the suspension containing the catalyst precursor, 18 wt.-% Co/TiO_2, and the noble metal precursor was added drop-wise to the solution containing THPC. The reaction was allowed to proceed for *ca*. 16 hours. The reaction vessel was wrapped in aluminium-foil to avoid thermal photodecomposition. Subsequently, the water was removed using rotor evaporator at 333K and 343.15 K. Attempts to synthesize pure platinum nano-particles supported on Co/TiO_2 or TiO_2 using this method were unsuccessful; addition of a small amount of auric chloric acid to the synthesis solution (*cf*. Table 3.1) was necessary to force the formation of nano-particles in the allotted synthesis time.

As a control Co/TiO_2 catalyst was treated in a similar manner as when Au-Pt nanoparticles were deposited on Co/TiO_2. Catalyst precursor (Co/TiO_2, 2g) with the ratio of *ex* $[Ac^-]/[NO_3^-]$ = 0.6 was suspended in distilled water (50 mL). The pH of the suspension was adjusted to *ca*. 1.5 using concentrated HCl. The suspension was then added into a mixture of distilled water (45 mL), tetrakis(hydroxymethyl) phosphonium chloride solution (1 mL of a solution of 1.2 mL of 80% aqueous solution diluted in 100 mL of distilled water) and NaOH (0.2M, 1.5 mL) under stirring at 300 rpm. This sample was then referred to as THPC-Co/TiO_2.

Table 3.1: Synthesis of the various promoted Co/TiO_2 catalysts

	Au-Co/TiO_2	**$AuPt$-Co/TiO_2**	**$Au_{30}Pt_{70}$-Co/TiO_2**	**Pt-Co/TiO_2**
m_{Co/TiO_2}, g	0.41	2.0	0.41	0.50
pH	1.46	1.03	1.03	1.46
Au:Co[1], mg/g	97	61	49	3[2]
Pt:Co[1], mg/g	0	61	81	133

[1]Relative amount of gold/platinum to cobalt loading in the synthesis mixture

[2]Small amount of auric chloride was needed to initiate the formation of platinum nano-particles using the method applied in this study

3.4. Characterisation of catalysts

3.4.1. Inductively coupled plasma-optical emission spectroscopy (ICP-OES)

The elemental composition of the (promoted) Co/TiO_2 catalyst precursors were determined by inductively coupled plasma - optical emission spectroscopy (ICP-OES) using a Varian ICP 730-ES spectrophotometer. The samples were digested in a MARS-5 Microwave digester. The calcined samples (*ca.* 5 mg) of the promoted and unpromoted catalysts (*ca.* 50 mg) were placed in Xpress Teflon tubes. A mixture of 6mL concentrated HCl-solution, 2mL concentrated HF-solution and 2mL concentrated HNO_3-solution was used to digest the sample. Calibration curves are given in appendix Figure 1A.

3.4.2. Fourier Transform Infra-Red Spectroscopy (FTIR)

FTIR spectroscopy was used to observe the presence of THPC derivatives on the surface of the unreduced calcined unpromoted catalyst. The THPC free Co/TiO_2 catalyst was used as baseline. A total of 64 scans were taken in the range between

400 and 4000 cm^{-1} for each sample with a resolution of 16 cm^{-1}. A background scan is taken prior to every analysis.

3.4.3. BET-surface area

The specific surface areas of the TiO_2 support, the unpromoted and promoted (Pt, Au and AuPt alloy systems) Co/TiO_2 catalysts were determined according to the BET method using a Micromeritics ASAP 2000 analyser (Micromeritics Instruments Corp., USA) via N_2 adsorption/desorption.

3.4.4. Transmission electron microscope (TEM)

The morphology of the nano-particles in the Co/TiO_2 catalyst precursor were imaged using transmission electron microscope (TEM) using a TECHNIA 200II operating at 200kV. The samples were sonicated in distilled water for *ca.* 10 minutes. Subsequently, the suspension was loaded on a carbon copper coated grid for analysis. The particle size distribution and the average particle size of the nano-sized particles representing the noble metal nano-alloy was determined by measuring between 50 and 200 nanoparticles using ImageJ®.

3.4.5. X-ray diffraction analysis (XRD)

The average crystallite size of Co_3O_4 crystallite in the calcined catalysts was determined by line broadening analysis from the X-ray diffraction analysis of the unpromoted and promoted catalyst precursor on a Bruker D8 ADVANCE diffractometer (Co-K_α radiation, 35 kV, 40mA). The scan was taken from 2θ=10° to 130° and compared to the standard compounds reported in the JCPDS data file for phase composition. The structure of the titania support and the average size of the noble metal nano-alloys was determined as well by refinement of the XRD-pattern using TOPAS.

3.4.6. Temperature programmed reduction, TPR

The reduction behaviour of the promoted and unpromoted Co/TiO_2 was studied using temperature-programmed reduction (TPR) in a Micromeritics Autochem HP II 2950 Chemisorption Analyzer. The calcined sample of the promoted or unpromoted catalysts (*ca.* 300 mg) was placed in a U-shaped quartz tube. The reduction was

performed in a 5% H_2/Ar mixture. The gas flow rate was kept at 50 mL(NTP) /min for all the catalyst characterised in the present study. The heating rate was set at 10°C/min reaching a maximum temperature of 950 °C from room temperature. The hydrogen consumption was measured using thermal conductivity detector (TCD). Prior to reduction the catalyst samples were dried in pure N_2 for 5 minutes.

3.4.7. Thermo-gravimetric analysis (TGA)

The isothermal reduction behaviour of the calcined material was studied by thermal gravimetric analysis (TGA) using Mettler-Toledo TGA/SDTA851^e. Prior to the reduction of the oxidic cobalt supported catalyst in hydrogen, the catalysts were heated in nitrogen (10 mL(NTP)/min) from room temperature to 350 °C at a rate of 3 for and kept at 350 °C for 1 hour. The catalyst precursor was reduced isothermally at 350 °C in hydrogen (10 mL(NTP)/min) for 16 hours in the case of the unpromoted catalyst but only for 5 hours for the catalysts containing the reduction promoter. After the reduction step, the catalyst bed was purged isothermally at 350 °C with nitrogen (10 mL(NTP)/min) for 1 hour. In order to determine the degree of reduction, the catalysts were re-oxidised isothermally at 350^{o}C in air (10 mL(NTP)/min) for 2 hours.

3.4.8. H_2 Chemisorption

Number of active sites on the surface of the catalysts was determined by H_2 chemisorption analysis in a ASAP 2020 C unit. The sample weight was always ca. 100 mg. The catalyst was evacuated with helium (He) at 350 °C for 30 minutes. The sample was held at 350 °C under flowing hydrogen for 12 hours at atmospheric conditions. Followed by evacuation of the sample with He for *ca*. 165 minutes at 125 °C. H_2 chemisorption was performed at 125 ^{0}C.

The set-up consists of a vacuum line, a gas-dosing line and a line connected to the sample holder. The gas-dosing section and the sample holder are initially evacuated. The valve to the vacuum pump and to the sample holder is closed, and gas is added to the gas dosing system. The pressure of in the gas dosing system is controlled, and knowing the volume of the gas dosing system, the number of moles of gas in the gas dosing system is known (via e.g. ideal gas law). Opening the valve to the sample holder will reduce the pressure, since the volume occupied by the gas is now larger, and because gas is taken up by the solid (adsorption). Knowing the volume of the

gas-dosing system and the volume of the free space in the sample holder, the number of moles of gas adsorbed on the solid can be determined. The volume of the free-space can be determined by performing the adsorption experiment with a non-adsorbing gas (helium). The gas dosing is repeated till the change in pressure is within certain limits. The achievement of the equilibrium state is determined by looking at the pressure change over a given time interval.

In this method the determination of the pressure of the adsorbing species is directly measured. The determination of the amount adsorbed depends on the accuracy of the determination of the pressure, temperature, the volume of the gas dosing system, and the volume of the free space in the sample holder. The determination of the equilibrium state proceeds through a pressure measurement.

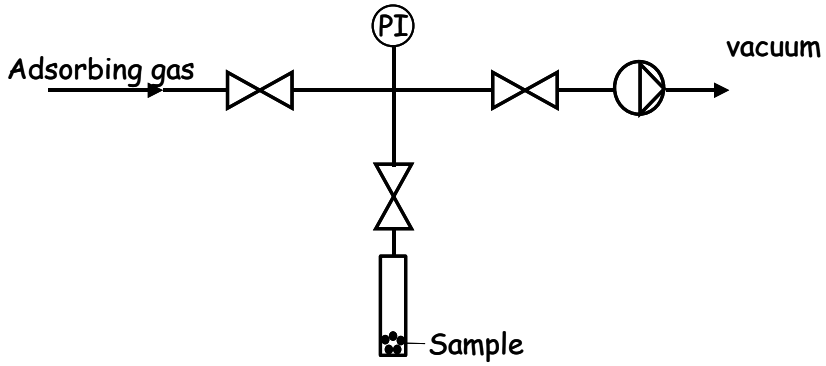

Figure 3.1: Principle of set-up for measuring adsorption isotherms using the static volumetric method. PI: Pressure indicator.

3.5. Fischer-Tropsch synthesis

The Fischer-Tropsch activity of the noble metal promoted and unpromoted Co/TiO_2 catalyst materials was tested in a fixed bed reactor at 220°C, 20 bar and a space velocity for CO, of 20 mL(NTP)/(min.g) for all catalyst, except for $Au_{50}Pt_{50}$-Co/TiO_2, which was tested at a space velocity for CO of 10 mL(NTP)/(min.g). A total of 0.5 grams (1 gram for $Au_{50}Pt_{50}$-Co/TiO_2) of catalyst was distributed over 6.5 grams of silicon carbide. A constant feed gas with a H_2 to CO ratio of 2 was passed over the catalyst and the catalyst was tested for a period of 4 days. Prior to FT analysis the catalysts were reduced *in-situ* in 200 ml (NTP)/min H_2 at 350 °C for 16 hours.

3.5.1. Reactor set-up

The gas streams were fitted with control valves. The control valves were connected to the mass flow controllers to control the flow rates of all the supplied gases (H_2, CO, Reference gas and Ar) received from the storage gas cylinder. The reference gas was used an internal standard for analysis, a mixture of 0.1 mol.-% cyclohexane in N_2.

The H_2 and CO streams were joined into one stream passing a four-way valve which was used to change the flow of the gases between bypass and the reactor. Argon was added after the reactor in a pressure controlled mode so as to control and maintain the total pressure of the system. To monitor the pressure of the system a pressure indicator was connected to the reactor. The total gas flow out of the reactor was controlled using two needle valves which were positioned after the wax trap. The reference gas is fed directly into the product stream using a flow controller before the ampoule sampler.

The gas flow rates were calibrated using bubble flow meter before the gases were vented off. To maintain constant temperature in the reactor during the reaction, the reactor was equipped with heating elements. The exit lines were maintained at 180^0C using heating wires. The wax trap was also maintained at 180^0C and insulated using quartz wool. The formed products from the reaction collect in the wax trap and removed using control valve.

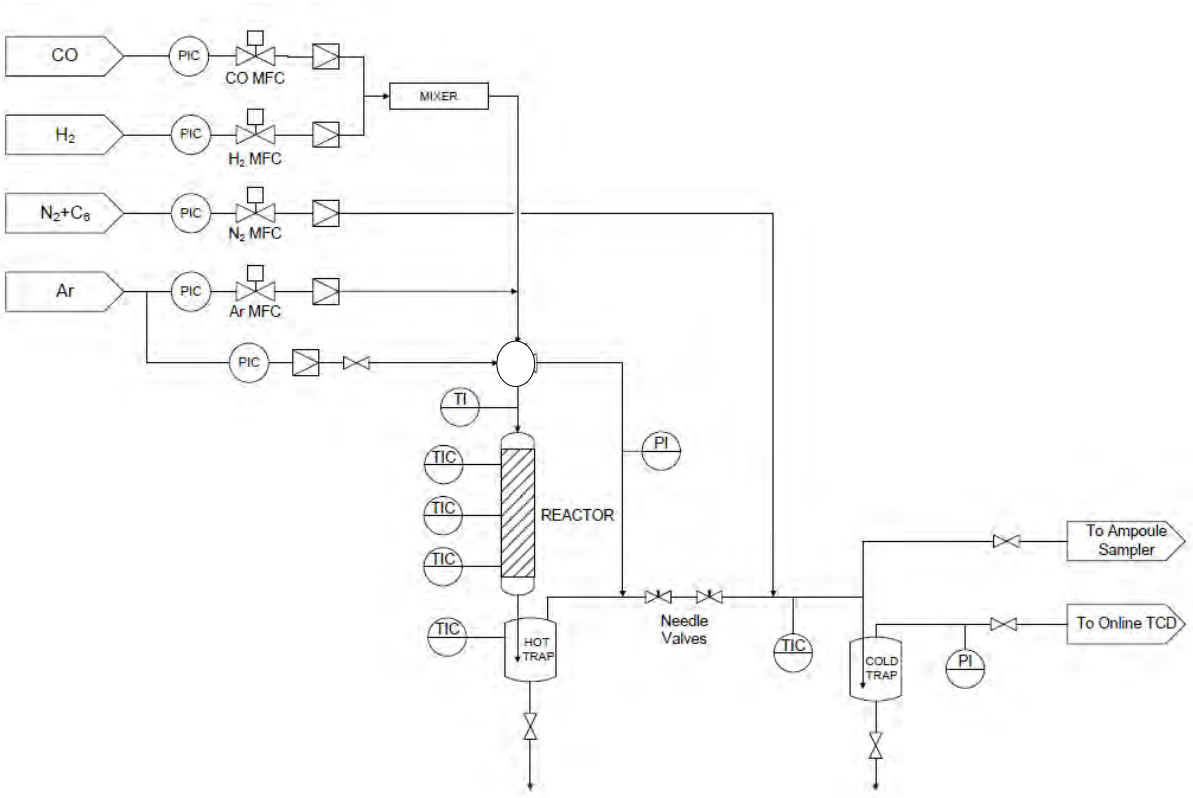

Figure 3.2: Setup for Fischer-Tropsch synthesis.PIC: flow control valves, MFC: Mass Flow Controller, PI: Pressure Indicator and TI: Temperature Indicator.

3.5.2. Reactor packing

The catalyst precursor (0.5 g) was physically mixed with SiC (6.5 g). The mixture was wetted with acetone, and mixed ensuring uniform distribution of the catalyst precursor. The catalyst bed was diluted to lower the amount of heat released per bed volume. SiC has a relative high thermal conductivity, enabling rapid heat transfer. The mixture was then loaded into the reactor based with a glass wool. The reactor is filled up with SiC, glass wool is used to separate the catalyst/ SiC mixture and SiC. Subsequently the reactor is fitted into the Fischer-Tropsch synthesis set-up.

3.5.3. Reaction procedure

Before the Fischer-Tropsch synthesis, the catalyst precursor had to be activated by reduction in flowing H_2 at atmospheric pressure. The reactor was pressurized overnight to ensure that there were no leaks. The four-way valve was turned to direct H_2 the reactor. The hydrogen flow was set to 40 mL(NTP)/min and was opened. The

bubble flow meter was used to ensure that there was gas flow. The heating element positioned in the reactor was programmed to increase the reactor temperature to 350 ^{0}C at a heating rate of 1 ^{0}C/min. The reduction proceeded isothermally at 350 ^{0}C for 16 hours in pure H_2. The system was the purged with Ar to ensure an inert environment while the H_2 valve was closed. The four-way valve was switched to bypass the reactor and the reactor temperature was dropped to 220 °C. Syngas was the allowed to flow over the bypass and the flow controllers of CO and H_2 were set to 10 mL(NTP)/min and 20 mL(NTP)/min respectively. The reference gas controller was set to 10 mL(NTP)/min. Using pressure controlled addition of Ar in conjunction with the needle valve the system was then pressurized to 20 bar.

After bypass sampling, the 4-way valve was switched to flow through the reactor and the Fischer-tropsch synthesis then was started.

The pressure gauge for CO, H_2 and N_2 were set to 25 bar to allow flow, while that of Ar was at 20 bar.

3.5.4. Sampling

Sampling was divided into two parts. The inorganic gases and methane were analysed using an on-line method while the organic compounds were analysed using an off-line method.

3.5.4.1. On-line GC-TCD

The Gas Chromatograph (GC) was fitted with a Thermal conductivity detector (TCD), which was used to analyse different gases. Argon was used as a carrier gas. The operating conditions and the gases detected in the column are given in Table 3.2.

Table 3.2: On-line TCD conditions for GC-TCD (Varian 4900) chromatographic analysis

	Conditions
Column Type	100/120 carbosieve SII
Column length	10ft x1/8
Compounds analysed	CO, N_2, CH_4, CO_2 and H_2
Column Temperature (^{0}C)	80
Carrier gas	Ar
Detector Temperature (^{0}C)	200
Injector Temperature (^{0}C)	200
Inlet Pressure (psi)	28.5
Sampling time (s)	900

Prior to the determination of the CO and H_2 conversions, the Gas Chromatograph (Varian 4900) equipped with Thermal Conductivity Detector system (GC-TCD) was calibrated using 45% H_2, 5% N_2, 25% CO, 5% CH_4, 15% Ar and 5% CO_2 gas mixture cylinder so as to determine the response factor ($Rf_{TCD,\ i}$), see Table 3.3, of each of the gases using N_2 as a reference gas.

$$\frac{\mathrm{ni}}{\mathrm{n_{N2}}} = \mathrm{Rf}_{TCD,i}\left(\frac{\mathrm{Ai}}{\mathrm{A_{N2}}}\right) \qquad (3.1)$$

Where n_i is a molar flow rate of component i, n_{N_2} is a molar flow rate of component N_2, A_i is the area representing component i in the gas chromatogram and A_{N_2} is the area representing N_2 in the gas chromatogram.

Table 3.3: Response Factors for various gases

Gas	**Calibration Factor**
H_2	0.10± 0.004
N_2	1
CO	0.99± 0.0047
CH_4	0.29± 0.0075
CO_2	1.01± 0.002

After GC-TCD was calibrated, the flow rates of CO and H_2, controlled by flow controllers and feed ratio, were confirmed by the online GC-TCD measurement. A total of 10 bypass samples were taken for each catalyst sample for the duration of the run.

3.5.4.2. Off-line sampling

The composition of the products obtained from Fischer-Tropsch synthesis were sampled in their gas phase using heated glass ampoule as described by Schulz and Nehren [60]. This technique involves insertion of the capillary end of an evacuated glass ampoule through the septum of a sampling device, into the effluent stream. The exposed end of the glass ampoule is slightly heated with a butane flame, after which the inserted capillary end was broken with the breaking fork. The gas phase products were drawn into the ampoule and the broken capillary was sealed with a butane flame (see Figure 3.2).

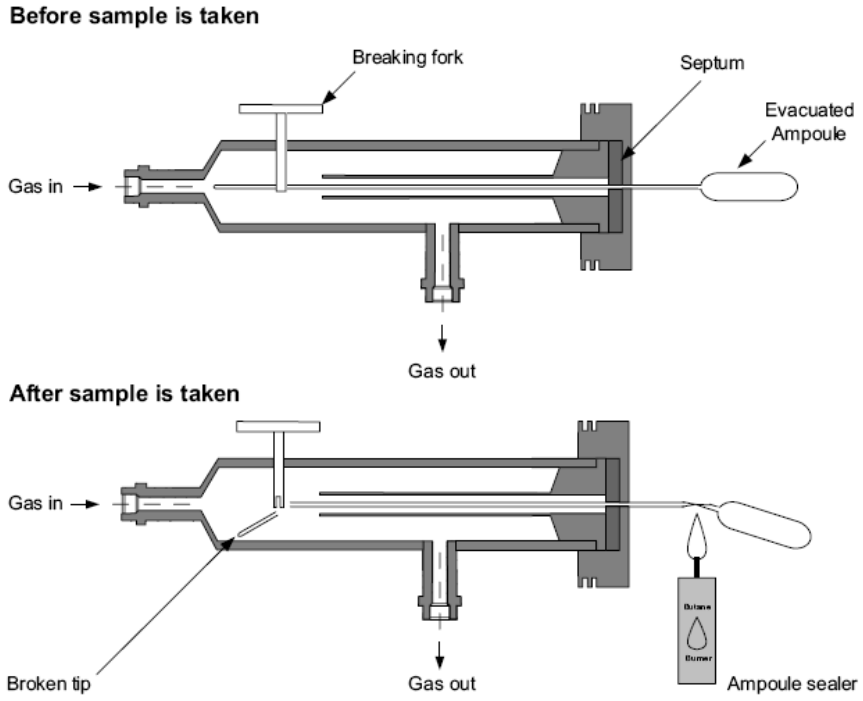

Figure 3.3: Ampoule sampling procedure [Adapted form 22, 60].

The sealed ampoules are crushed within an ampoule breaker device, as shown in Figure 3.3. The gas content was released into an off-line GC-FID for analysis.

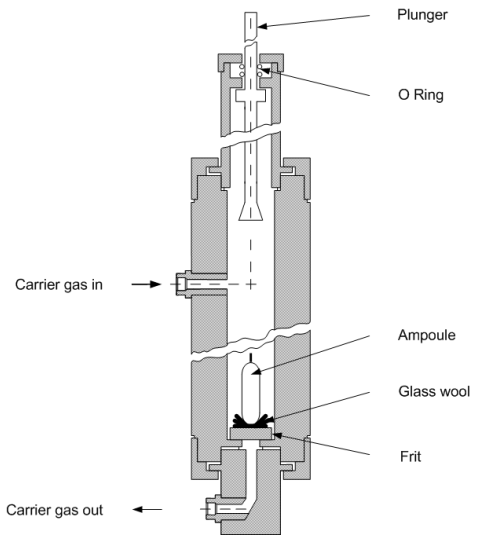

Figure 3.4: Ampoule breaking procedure [Adapted form 22, 60].

The organic products including methane were analysed in an off-line Gas chromatograph (Varian 3400) equipped with a flame ionisation detector (FID). The conditions for off-line GC-FID analysis are shown in Table 3.4. A mixture of cyclohexane and nitrogen was used as an internal standard for this analysis.

Table 3.4: Off-line GC-FID (Varian 3400) conditions for chromatographic analysis

Gas Chromatograph (Varian 3400)	
Detector	Flame Ionisation detector (FID), $T_{detector}$ = 250 $^{\circ}$C
Column	Column RT X-1(Restek) Fused Silica capillary column, 60m x 0.25 mm Stationary phase: 0.5μm dimethyl siloxane (cross-linked)
Carrier gas	H_2
Introduction gas	Nitrogen
Injector	Split injector, T =250 ^{0}C/ split ratio = 1:10
Column Head pressure	2.9 bar
Temperature programme	-55 °C, 1.5 min, Isothermal at 12 °C/min to 0°C, 0 min isothermal at 9 °C/min to 100°C, 0 min, isothermal at 7°C/min to 280°C, 30 min, isothermal at 20 °C/min to 150°C isothermal
Temperature	150 °C

3.5.5. Data evaluation

The conversion of CO and H_2 across the reactor was measured using N_2 as an internal standard. Valve 6 (which passes through the condenser before flowing to the GC-TCD) was opened during the online sampling. The bypassing sample readings taken prior Fischer-Tropsch synthesis were used to calculate the CO conversion (X_{CO}) according to equation 3.2.

$$X_{CO} = 1 - \frac{n_{CO,out}}{n_{CO,in}} = 1 - \frac{{(A_{CO})_{out}}/{A_{N_2}}}{{(A_{CO})_{in}}/{A_{N_2}}} \qquad (3.2)$$

The amount of product (P) formed is related to the amount of reactants fed to the reactor (yield). The molar yield of a product P is defined as:

$$Y_P = \frac{N_p}{N_{CO,in}} = \frac{{n_p}/{n_{N_2}}}{{n_{CO}}/{n_{N_2}}} \qquad (3.3)$$

The selectivity of a reaction (*i*) is defined as the amount of product formed relative to the amount of a reactant converted. In this study the selectivity of CH_4 and C_{5+} was determined.

$$S_i = \frac{Y_P}{X_{CO}} \qquad (3.4)$$

The integral rate of reaction was determined for each catalyst. Integral rate is defines as the amount of reactant (CO) convert per unit time relative to the mass of catalyst used.

$$-r_A = \frac{F_{CO,0} \cdot X_{CO}}{m_{catalyst}} \qquad (3.5)$$

The turnover frequency (TOF) describes the number of molecules of reactant converted per active site per unit time. It can be obtained from the intrinsic rate of reaction and the number of active sites per unit mass of catalyst ($N_{Active.\ sites}$).

$$TOF = -r_A . \frac{N_{Av}}{N_{active.sites}} \qquad (3.6)$$

4 Results

4.1. Synthesis of nanoparticles

Metallic Au, $Au_{50}Pt_{50}$ and Pt nanoparticles are synthesis from the reduction of $HAuCl_4$ and H_2PtCl_6 metal solutions in the presence of tetrakis(hydroxymethyl) phosphonium chloride (referred to as THPC hereafter) and NaOH at ambient conditions. The synthesis approach of these nanoparticle involves a two-step decomposition of THPC to (first step) formaldehyde and tris(hydrormethyl) phosphine **(II)** (referred to as THP hereafter) formation and (second step) to hydrogen gas and tris(hydroxymethyl)phosphine oxide **(III)** (referred to as THPO hereafter) in the presence of sodium hydroxide (*cf.* Scheme 4.1).

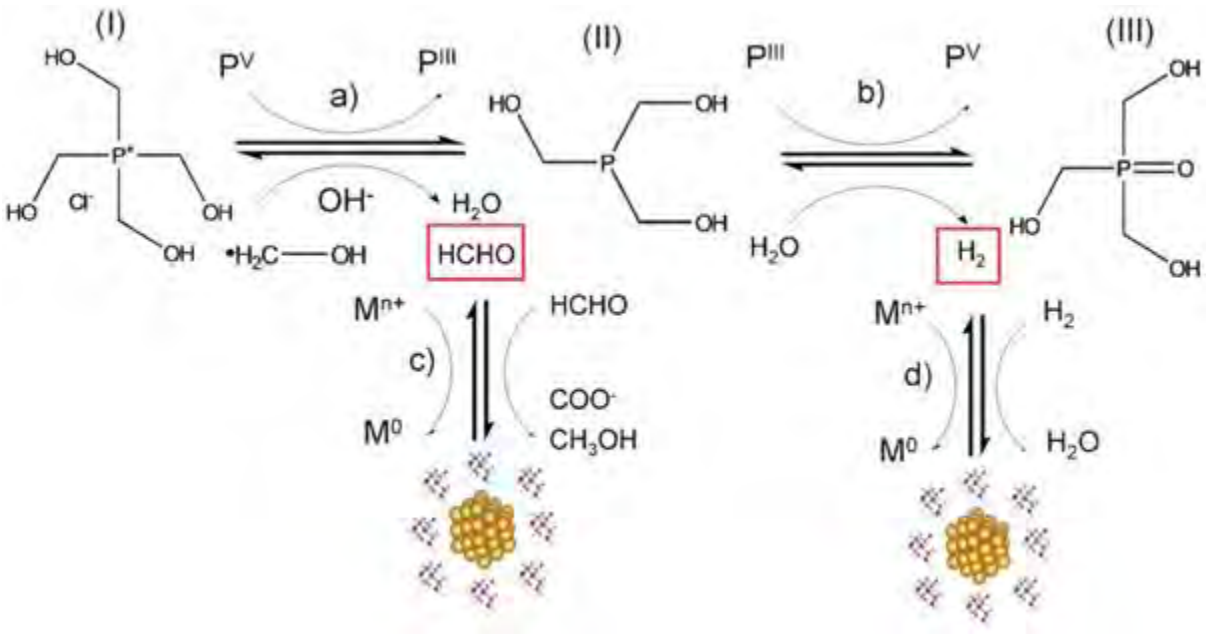

Scheme 4.1: Proposed reaction mechanism of metal nanoparticles, involving the conversion of THPC into THPO and the *in situ* generation of formaldehyde and H_2 as active reducing agents. [55].

A clear orange-brown hydrosol was obtained after 16 hours. A wax-like material was observed floating at the surface of the hydrosol at the end of the reaction. This could be oligomerized methoxy groups forming long chain organic material.

4.1.1. Particle morphology and size distribution

The synthesised Au, $Au_{50}Pt_{50}$ alloy and Pt nano-sized particles were viewed under transmission electron microscope (TEM) and the average particle size and the log-normal particle size distribution were determined for each sample. Figure 4.1 shows TEM images Au, $Au_{50}Pt_{50}$ and Pt, the particle size distribution and average size of Au and Pt nano-sized particles. The obtained average sizes of the nano-sized Au, $Au_{50}Pt_{50}$ and Pt, particles with the standard deviations were 1.4 ±0.3 nm, 2.1 ± 0.3 nm and 1.9 ±0.3 nm, respectively.

THPC acts as stabilizer preventing agglomeration and inter-particle growth of the nano-particles by providing steric hindrance around the nano-particles, resulting in well-dispersed particles in a nanometer range. Heuso *et al*. showed that inter-particle coalescence and wider size distribution is observed in the absence of THPC [55]. This was ascribed to steric hindrance offered by the hydroxymethyl groups of the THPC molecule preventing particle coalescence [55].

The difference in the average particle sizes of Au and Pt nanoparticles could be attributed to the reduction potential values for each of the metal precursors, which predicts the tendency of a chemical species to be reduced. High reduction potential values lead to kinetically favoured growth of metallic nuclei. The standard reduction potential values for Au and Pt at 25°C are shown in equation 4.1 and 4.2.

$$AuCl_4^-(aq) + 3e^- \rightarrow Au(s) + 4Cl^-(aq) \qquad E^0(Au^{3+}/Au) = +1\ V \qquad (4.1)$$

$$[PtCl_6]^{2-}(aq) + 2e^- \rightarrow Pt(s) + 4Cl^-(aq) \qquad E^0(Pt^{2+}/Pt) = +0.73\ V \qquad (4.2)$$

The reduction potential value for $Au^{3+} \rightarrow Au^0$ is more positive than $Pt^{2+} \rightarrow Pt^0$. This gives an indication that for a given reaction time the growth of Au metallic nuclei will be kinetically favoured compared to Pt, producing relatively larger metallic Au than Pt nanoparticles.

Synthesis of platinum nanoparticle required small addition of gold to initial nucleation. This was also attributed to the difference in the reduction potential values.

Notably, the standard deviation of the average size is comparable to that of pure platinum and gold, due to moderate difference between Pt and Au reduction potential

values. The precise distribution of Au and Pt atoms within the lattice structure of the $Au_{50}Pt_{50}$ alloy could not be analysed.

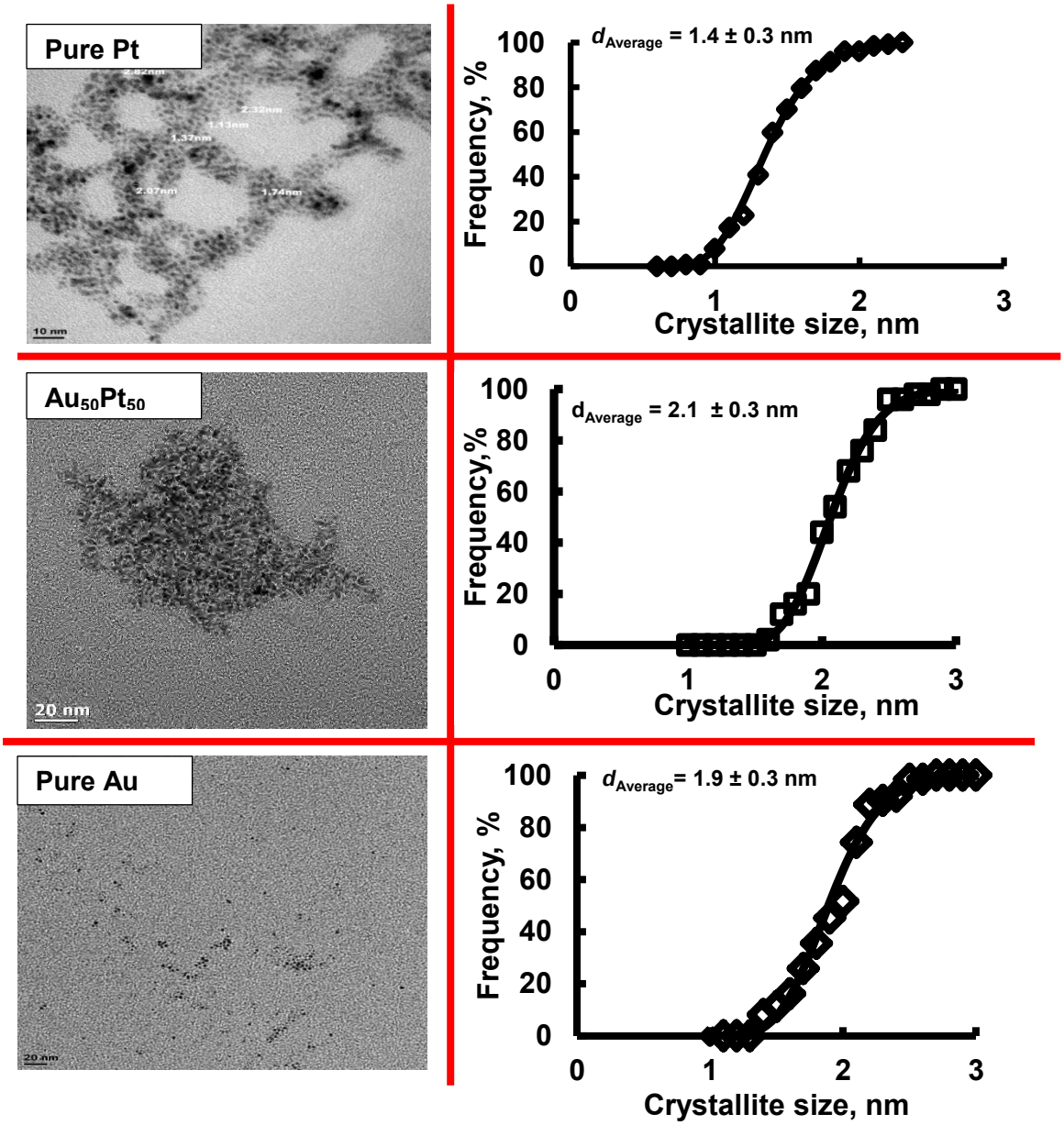

Figure 4.1: TEM-images and the log-normal distribution of the unsupported small nano-sized particles

Since nano-sized particles were obtained as a hydrosol, therefore further analysis of these unsupported particles using other characterisation techniques was impossible as the particles could not be recovered.

The nano-sized particles were deposited on TiO_2 (P25) obtaining well-dispersed nano-particles (cf. Figure 4.2).

The nano-particle size distributions and the average sizes of the TiO_2 supported nano-sized gold particles were modelled using a log-normal distribution, from which

the average crystallite size of the nano-particles and the standard deviations were determined. The average particle size of the Au supported nano-particles was 2.5 ±0.3 nm. The increase in the average particle size of the TiO_2 supported nano-particles compared to the unsupported nano-particles might be due to the interaction of the noble metal e.g. gold, and the hydroxyl groups of the support, providing nucleation site for the nanoparticles.

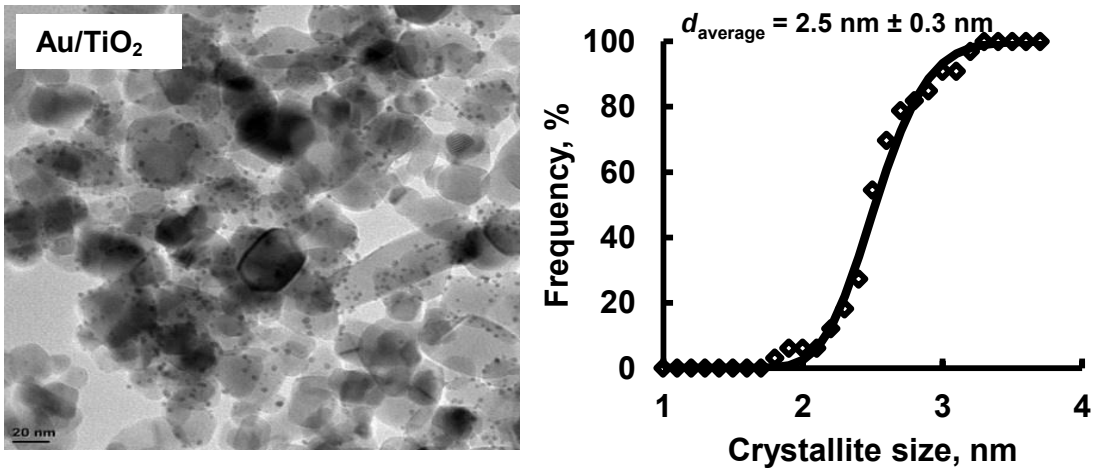

Figure 4.2: Transmission electron microscope (TEM) images of TiO_2 supported nano-particles (Au).

Unsupported nanoparticles were observed (as indicated by a red arrow in Figure 4.3). This would give result to a wide size distribution of the particles, as the environment varies from particle to particle.

The surface of the support consists of hydroxyl groups, this means that protonation and deprotonation (in an aqueous medium) of the surface of the oxide support may occur according to equation 4.3 and 4.4. Metal oxide support surfaces can be functionalised with hydrophilic functional groups such as hydroxyl (OH) and amino (NH_3) groups which are known to bind gold nano-particles [61].

Low pH: $-OH + H^+ \leftrightarrow OH_2{}^+$ (4.3)

High pH: $-OH \leftrightarrow O^- + H^+$ (4.4)

The surface chemistry of the metal oxide support is governed by the pH of the suspension. At low pH i.e. when the solution is acidic, the surface hydroxyl groups of the metal oxide are protonated forming a positively charged surface (see equation 4.3). At high pH values i.e. high basic environment, deprotonation of the surface hydroxyl groups is possible, subsequently a negatively charged surface is observed. Since the $[AuCl_4]^-$ and $[PtCl_6]^{2-}$ complexes are negatively charged, therefore the surface of amphoteric TiO_2 support was modified in such a way that protonation occurs leading to a positively charged surface. In doing so, the noble metal complexes can be stabilised by surface proton(s) through electrostatic interaction between the noble metal complex and the surface of the support.

The pH of TiO_2 suspension was then adjusted to *ca*.1.5 using concentrated HCl. The resulting suspension of nanoparticle deposited onto the surface modified TiO_2 support was viewed under TEM after reduction using THPC and NaOH. Well-distributed nanoparticles were observed over the support (see Figure 4.3). Notably, no unsupported nanoparticles were observed in this case.

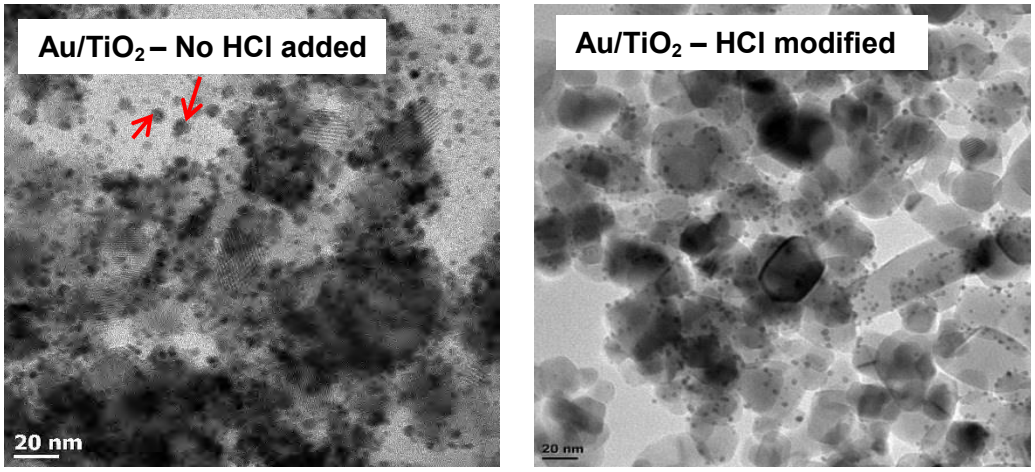

Figure 4.3: Transmission Electron Microscope images highlighting the effect of modifying the surface of the TiO_2 support with concentrated HCl on the deposition of the Au noble metal nano-particles.

4.1.2. X-ray diffraction

The XRD analysis of TiO_2 supported Au was done to identify the phase composition of the nanoparticles in the samples, see Figure 4.4. Rutile, anatase and gold X-ray diffraction patterns are included for comparison in Figure 4.4 with only most intense

peaks of these components are shown. Titania, P25, is a well crystallized material showing the expected diffraction peaks due to the anatase and rutile phase.

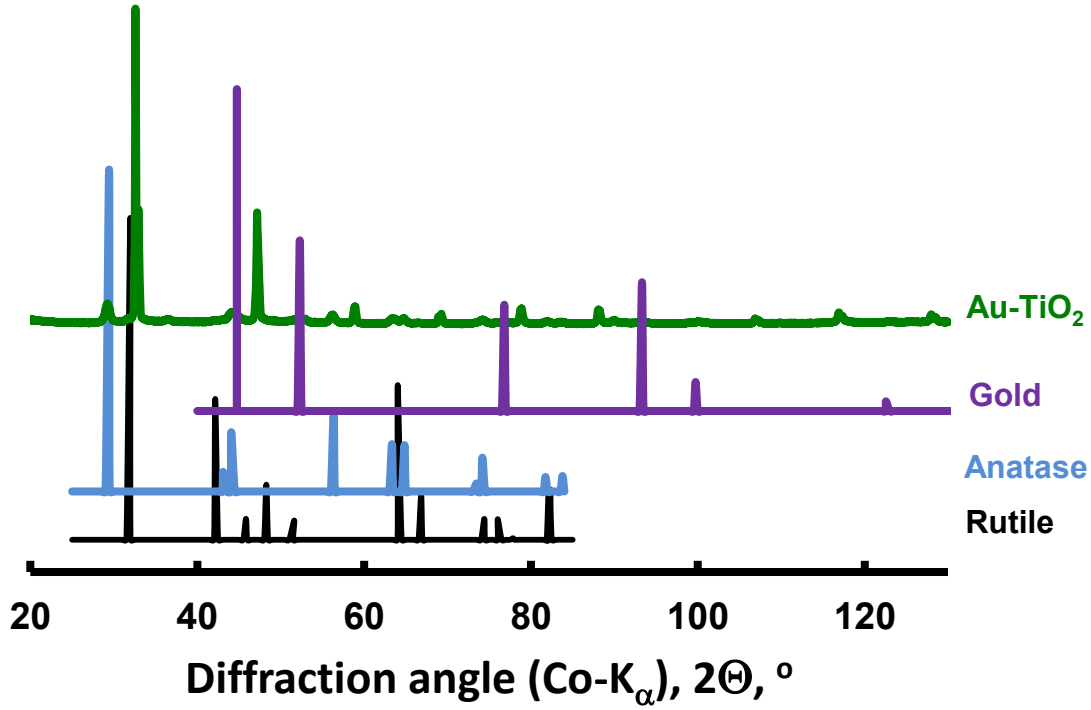

Figure 4.4: XRD-pattern of the TiO_2 supported Au sample.

The XRD-patterns of the Au-TiO_2 show very broad diffraction peaks at $2\theta \sim 44.8°$ and 52.3°, which are characteristic for the most intense diffraction lines of fcc-Au (corresponding to (hkl) of (111) and (200) respectively). Hence, it might be concluded that gold is present as metallic fcc-Au in Au-TiO_2. This further verifies the THPC decomposition assisted reduction of $Au^{3+} \rightarrow Au^0$ and $Pt^{2+} \rightarrow Pt^0$ method. The broadness of the peaks could be due the nano- size of gold particles.

Two additional intense peaks were observed at 32.6° and 32.9°, as shown in Figure 4.5. These peaks could be ascribed to the formation of crystalline salt that might be formed during the reduction of the noble metal solution to metallic gold.

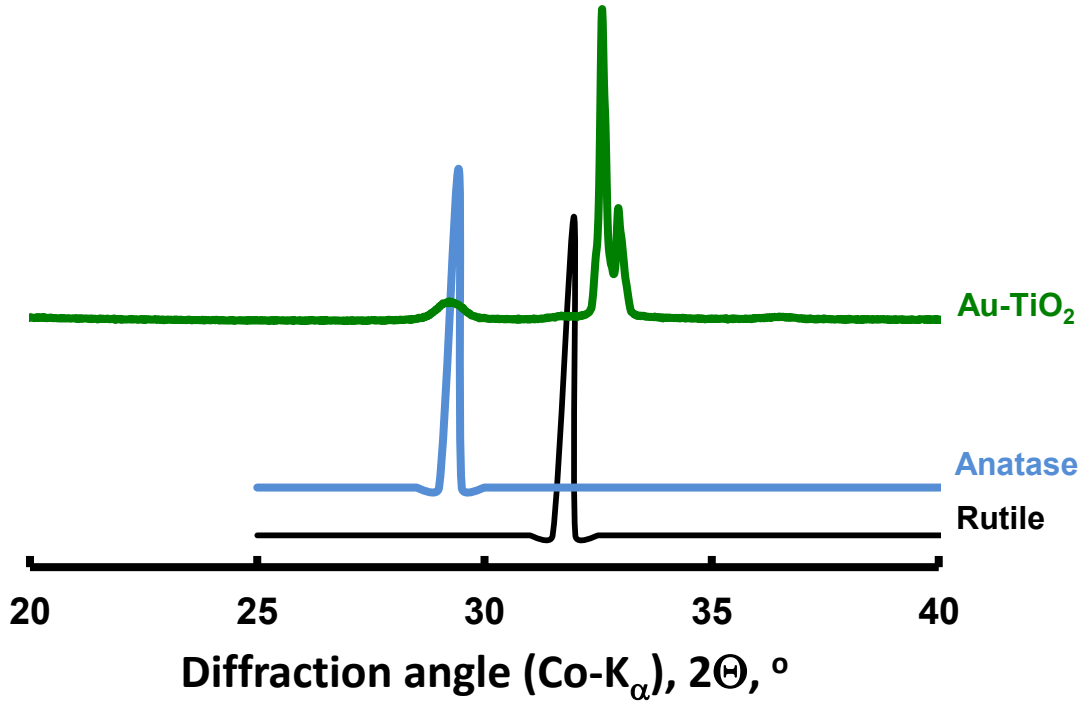

Figure 4.5: XRD-pattern of the TiO_2 supported Au sample, highlighting an additional diffraction peak.

4.2. Supported cobalt catalyst precursors

Different cobalt metal salts have a notable effect on the reducibility of the catalyst [31]. A range of supported cobalt catalyst were synthesised via slurry wetness impregnation of calcined TiO_2 with cobalt acetate and cobalt nitrate solutions with varying ratios of cobalt acetate/ nitrate + acetate mixture.

4.2.1. Catalyst composition

The cobalt loading of Co_3O_4 of the synthesised catalyst precursors was analysed using inductively coupled plasma-optical emission spectroscopy (ICP-OES). Table 4.1 show a summary of the loadings of the synthesised cobalt catalysts. The cobalt loading was determined using Co/Ti ratio.

Table 4.1: Elemental analysis of the unpromoted catalysts with varying $[Ac^-]/[NO_3^-]$ ratios.

Catalyst	$\frac{\text{Acetate}}{\text{Acetate + Nitrate}}$	Co (wt.-%)	$d_{Co_3O_4}$ (nm)*
Cat 1	0	16.9	22 ± 1.2
Cat 2	0.15	13.3	20± 0.9
Cat 3	0.3	14.6	19± 2.1
Cat 4	0.45	18.6	21± 0.7
Cat 5	0.6	18.0	16± 1.3
Cat 6	0.85	17.5	22± 0.6
Cat 7	1	7.8	23± 0.9

*Determined by Debye-Scherrer.

After drying a ring of precipitated cobalt acetate salt was observed hence **Cat 7** showed the lowest cobalt loading.

4.2.2. X-ray diffraction (XRD)

XRD patterns for the calcined Co/TiO_2 catalysts are shown in Figure 4.6. TiO_2 and Co_3O_4 XRD patterns are used for reference purpose. The diffraction peaks at 22.1°, 36.5°, 43.1°, 52.5°, 65.6°, 70.2° and 77.5° corresponding to Co_3O_4 (111), Co_3O_4 (220), Co_3O_4 (311), Co_3O_4 (400), Co_3O_4 (422), Co_3O_4 (511) and Co_3O_4 (440) crystal plane were observed. The cobalt oxide moieties exist as Co_3O_4 species in these samples. No diffraction peaks corresponding to the cobalt(II)oxide species were observed in all the catalyst precursor samples.

The average crystallite size of Co_3O_4 was determined (as given in Table 4.1) from the most intense and well resolved Co_3O_4 XRD peaks (2θ = 22.2°, 36.5° and 52.7°) using Debye-Scherrer's equation and the average crystallite size of Co_3O_4 in the catalyst precursors is comparable between 19 nm and 23 nm. The average crystallite size of Co_3O_4 for **Cat 5** was 16 nm. No obvious effect of acetate to nitrate ratio can be observed although **Cat 5** yield smaller particles.

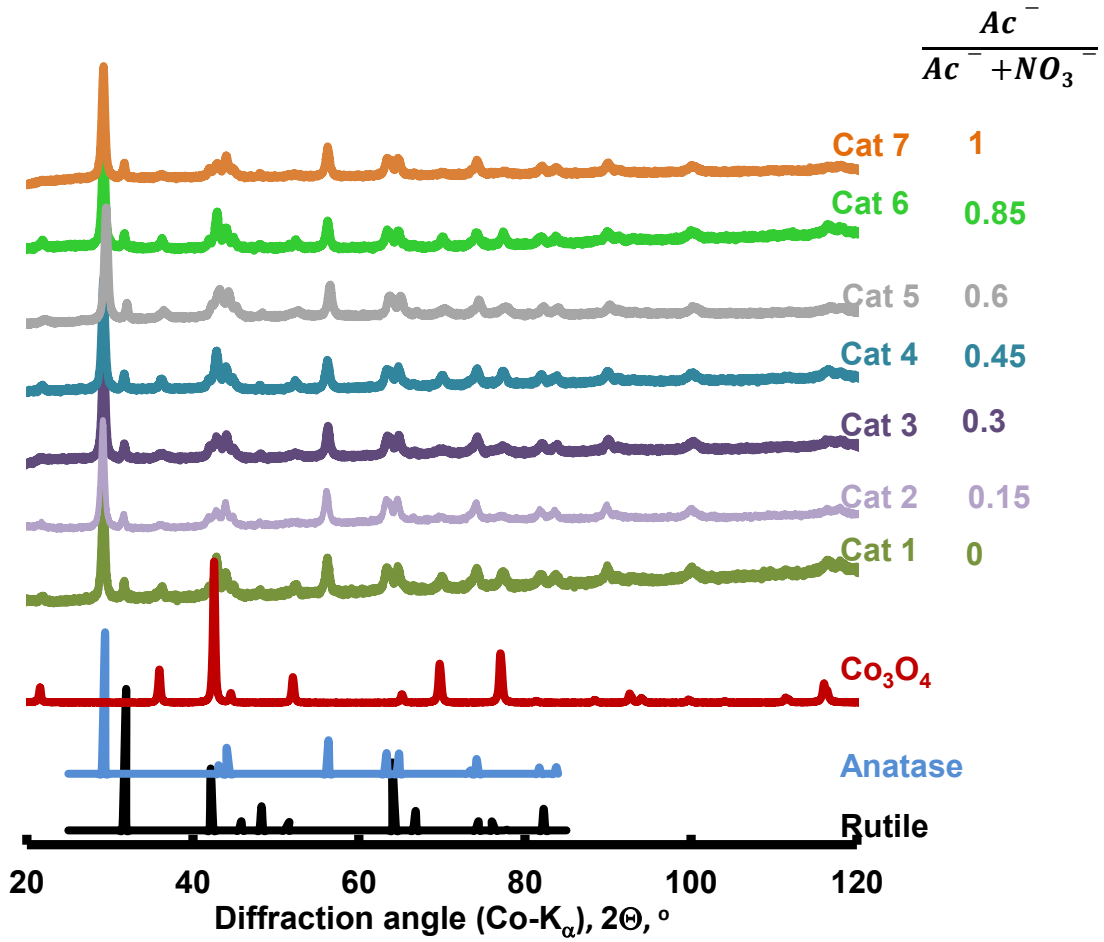

Figure 4.6: XRD-pattern of the calcined, catalyst samples with varying [Ac^-]/[NO_3^-] ratios.

4.2.3. Temperature Programmed Reduction (TPR) analysis

The reduction behaviour of the ex-[Ac^-]/[NO_3^-] Co/TiO_2 catalyst precursors (with varying [Ac^-]: [NO_3^-] ratios) was determined using Temperature reduction programme (TPR). Each catalyst was reduced in 5%H_2/Ar at atmospheric pressure.

The TPR profile of the impregnated pre-calcined TiO_2 with cobalt nitrate and/or acetate (**Cat 1**-**Cat 7**) consists of two main distinct peak maxima. The reduction of the catalyst is proposed to occur in two steps resulting in crystalline phase change according to equation 4.4 and 4.5 [44].

$$Co_3O_4 + H_2 \leftrightarrow 3CoO + H_2O \qquad (4.4)$$

$$CoO + H_2 \leftrightarrow Co + H_2O \qquad (4.5)$$

The TPR spectrum of each catalyst precursor is comprised of low-temperature peak with a maximum occurring at *ca*. 280 °C and high temperature peaks occurring at *ca*. 496 °C. According to Jalama *et al.* the first reduction peak signifies the reduction of Co_3O_4 to CoO [18]. The second peak denotes the reduction of CoO to metallic cobalt [19]. This is in agreement with previous reports [18].

The observed shoulder peak in between the two distinct maxima was thought to be due to the reduction of CoO to Co^0 that is relatively less interacting with TiO_2. The shoulder peak between the two main reduction peaks was also observed by Li *et al*. [62] in a Co/TiO_2-catalyst *ex* cobalt nitrate. In this study, the shoulder peak is observed to all the catalysts with different $[Ac^-]/[NO_3^-]$ ratios including pure *ex* cobalt acetate catalyst, hence the shoulder peak cannot be ascribed to a specific cobalt precursor. The shoulder peak is more pronounced at higher $[Ac^-]/[NO_3^-]$ ratios (**Cat 6**). The TPR spectrum of **Cat 6** consists of broad diffuse hydrogen consumption between the first peak and the second maxima. According to van Steen *et al*. broad peaks indicate the existence of several species reducing at approximately similar temperature [40]. The shoulder reduction peak may represent the reduction of divalent cobalt with minimal interaction with the support, whereas the main reduction peak with a maximum around *ca*. 445^oC represents divalent cobalt species with relatively stronger interaction with titania. There is no specific trend observed associated with the $[Ac^-]/[NO_3^-]$ ratio. This could mean the reduction behaviour of ex acetate and nitrate cobalt catalyst is independent of the metal precursor for TiO_2 supported cobalt catalysts. The observed shoulder reduction peak could suggest that the interaction of the ex-acetate and nitrate cobalt Co_3O_4 with the surface of the support is comparable, as the shoulder peak was observed in all the TPR spectra.

In this study no high temperature peaks are observed that represent the reduction of oxidic cobalt interacting strongly with the TiO_2 support (*cf.* Figure 4.7).

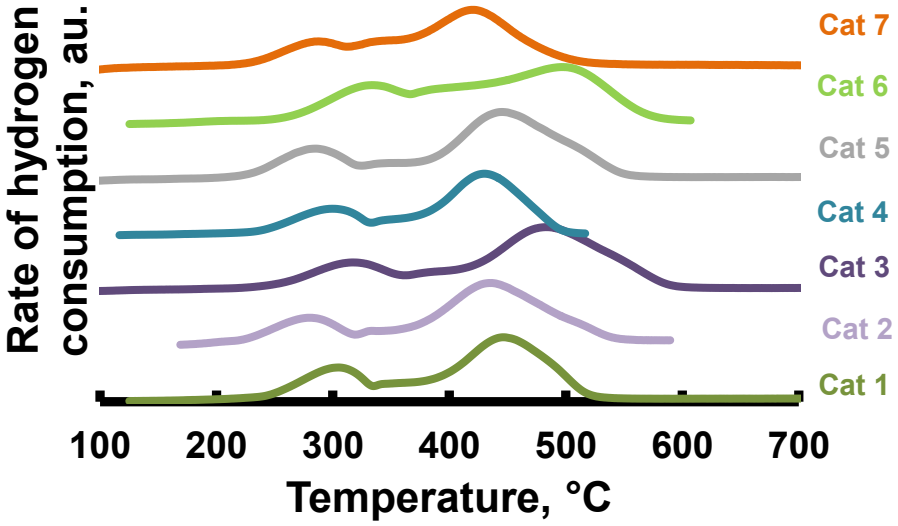

Figure 4.7: TPR-profiles of the calcined Co/TiO_2 catalyst precursors with varying $[Ac^-]/ [NO_3^-]$ ratios.

If the stoichiometric of reduction is well-established, the H_2/Co ratio can be used for peak identification [39]. Typically, the first reduction maximum at relatively low temperatures is ascribed to the reduction of cobalt(III, II) oxide spinel to cobalt(II) oxide when the amount H_2 of consumed of the first reduction peak is one third of the H_2 consumed for the second reduction peak. Table 4.2 shows the amount of H_2 consumption. Thus, the low temperature and high temperature reduction maxima observed for all the catalyst precursor can be ascribed to the reduction of the cobalt(III, II) oxide spinel to cobalt(II) oxide species and cobalt(II)oxide to metallic cobalt respectively.

Table 4.2: Quantitative analysis of the unpromoted and promoted Co/TiO_2 catalyst precursors

Catalyst Precursor	H_2 Consumption, a.u.				
	A_{1st}	A_{2nd}	A_{1st}/A_{2nd}	$T_{1st,}$ °C	$T_{2nd,}$ °C
Cat 1	0.43	1.25	0.35		447
Cat 2	0.23	0.82	0.27	280	437
Cat 3	0.45	1.51	0.3	317	483
Cat 4	0.51	1.4	0.36	300	430
Cat 5	0.41	1.5	0.27	286	446
Cat 6	0.52	1.3	0.4	334	496
Cat 7	0.16	0.57	0.28	288	421

4.3. Promotion of Co/TiO_2 catalyst for Fischer-Tropsch synthesis

The average particle size was the determining factor in choosing the catalyst to be tested for Fischer-Tropsch synthesis and to be promoted with Au, $Au_{30}Pt_{70}$ $Au_{50}Pt_{50}$ and Pt nano-sized particles. Small crystallite size yields an increased surface area subsequently an enhanced catalyst activity [4]. Therefore, **Cat 5** with a lowest Co_3O_4 average crystallite size of 16 nm was the catalyst precursor of choice.

4.3.1. *Catalyst composition*

The Co/TiO_2 sample (**Cat 5**) was suspended in distilled water. The pH of the suspension was adjusted to *ca*. 1.5 using HCl so as to positively charge the surface of the catalyst inducing an electrostatic interaction between the Co/TiO_2 catalyst precursor and the deposited noble metal. After deposition of the noble metal(s) onto Co/TiO_2 catalyst precursor in the presence of THPC, the promoted catalyst precursor was not calcined as it was thought that calcination would result in agglomeration of the nano-size particles. For fair comparison between the promoted and the unpromoted Co/TiO_2 catalyst precursors, the unpromoted catalyst was also stirred with a mixture of THPC and NaOH in equal ratios as the mixture used for the promoted catalysts. The resulting catalyst precursor was referred to as THPC-Co/TiO_2. A wax-like material was observed at the end of the synthesis for the promoted and the THPC-Co/TiO_2 catalyst precursors.

Loading of 0.5wt.% of the promoter on 18wt.%Co/TiO_2 was attempted. At these small loadings, the nano-sized particles could not be seen under transmission

electron microscope (TEM), and thus the particle size could not be determined. Therefore 1wt.% loading of noble metal (Au+Pt) was targeted in this study. The promoter loading is used here is thus much higher than an industrial catalysts [21] and the catalysts considered in this study can only be considered as a model for the industrial catalyst.

Atomic adsorption (AA) analysis was performed to verify the elemental composition of the catalyst precursors (*cf*. Table 4.3). The variation in the cobalt loading obtained after the addition of the noble metal gives some indication on the accuracy of the cobalt loading. The gold to cobalt loading in the calcined catalyst precursors is lower than the gold to cobalt ratio in the synthesis mixture (*cf*. Table 4.3) indicating that in the applied synthesis method only *ca*. 60% of gold has been deposited. This amount seems to be independent of the composition of the alloy. The platinum to cobalt ratio in the calcined catalyst precursor is also lower than that in the synthesis mixture. The actual amount of platinum deposited as nano-particle is however dependent on the final average composition; the fraction of platinum deposited decreases with decreasing Au/(Au+Pt)-ratio. This implies that platinum can be readily incorporated into gold–rich systems, but the platinum nano-particle formation using this method is not facile.

4.3.2. Surface properties

The BET-surface area of the promoted, calcined Co/TiO_2 catalyst precursor is lower than that of the starting titania (46.4 m^2/g). Cobalt(II,III) oxide has a higher density than titania. A pure, physical mixture of titania and Co_3O_4 would therefore also yield a decrease in the surface area even if the average crystallite size of Co_3O_4 is smaller than that of titania. The obtained surface areas of the catalyst precursors containing the noble metal reduction promoter are significantly smaller than that of the calcined, unpromoted catalyst precursor. This may be caused by the presence of the wax-like material noted after the synthesis of the promoted Co/TiO_2 catalyst precursor in the presence of THPC.

Table 4.3: Elemental analysis of promoted, calcined Co/TiO_2 catalyst precursors

	Composition (wt.-%)				S_{BET}, m^2/g	V_{pore}, cm^3/g
	Co	Au	Pt	Au/(Au+Pt)		
Co/TiO_2	18.0	0	0	0	41.5	0.11
THPC-Co/TiO_2	18.3	0	0	0	-	-
Au-Co/TiO_2	17.5	0.99	0	1.0	31.04	0.17
$Au_{50}Pt_{50}$-Co/TiO_2	16.3	0.62	0.60	0.50	31.4	0.1
$Au_{30}Pt_{70}$-Co/TiO_2	17.3	0.50	0.83	0.39	26.1	0.09
Pt-Co/TiO_2	20.2	1.03	2.079	0.25	27.2	0.09

4.3.3. Particle morphology

A dome shaped peak was observed between 20° and 60° for the promoted catalyst precursors, possibly ascribed to an amorphous material in the samples. The amorphous material was thought to be the wax-like material noted upon promotion of the Co_3O_4/TiO_2 catalyst precursor with noble metal(s) in the presence of THPC. After calcination of the promoted catalyst at 300°C in air in a static oven the amorphous phase was not detected by the XRD (*cf*. Figure 4.8). Thus, indicating that the material can be removed by thermal decomposition.

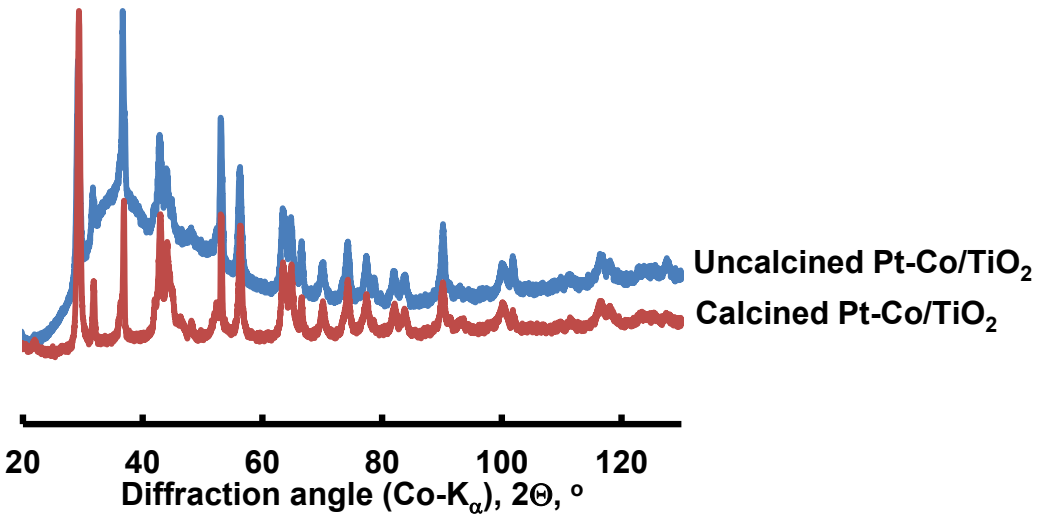

Figure 4.8: XRD-pattern of the calcined and uncalcined $Pt-Co/TiO_2$ catalyst promoter, highlighting the absence of the amorphous phase upon calcination.

However, it should be noted that the catalyst precursor used for Fischer-Tropsch synthesis were not calcined as it was thought that during reduction of the Co_3O_4/TiO_2 at 350 °C would be sufficient to remove this material.

The XRD patterns for the calcined, unpromoted 18wt.-% Co/TiO_2 catalyst precursor and its noble metal promoted catalyst derivatives are shown in Figure 4.9. Rutile and anatase phases remain clearly visible in the unpromoted and promoted catalyst precursors. Cobalt is XRD-visible in these materials as Co_3O_4 showing clearly the diffraction peaks at 2θ = 22.1°, 36.5° and 43.1° corresponding to Co_3O_4(111), Co_3O_4(210), and Co_3O_4(311). The average crystallite size of Co_3O_4 as determined using the Debye-Scherrer equation is *ca*. 16 nm for the unpromoted Co/TiO_2 (*cf*. Table 4.2). Despite the low amount of the noble metal promoter, some reflections due to the presence of gold, platinum and/or gold-platinum alloys are visible. The XRD-patterns of the Au-Co/TiO_2 show diffraction lines at $2\theta \sim$ 44.8°, 52.3°, 76.8° and 93.3°, which are characteristic for the most intense diffraction lines of fcc-Au (corresponding to (hkl) of (111), (200), (220) and (311), respectively). Hence, it can be concluded that gold is present as fcc-Au in Au-Co/TiO_2. Diffraction peaks corresponding to fcc-Pt are observed at $2\theta \sim$45.7°, 53.3° and 78.8° in Pt-Co/TiO_2. These diffraction peaks can be assigned to diffraction lines of Pt (111), Pt (200) and Pt (220) plane respectively.

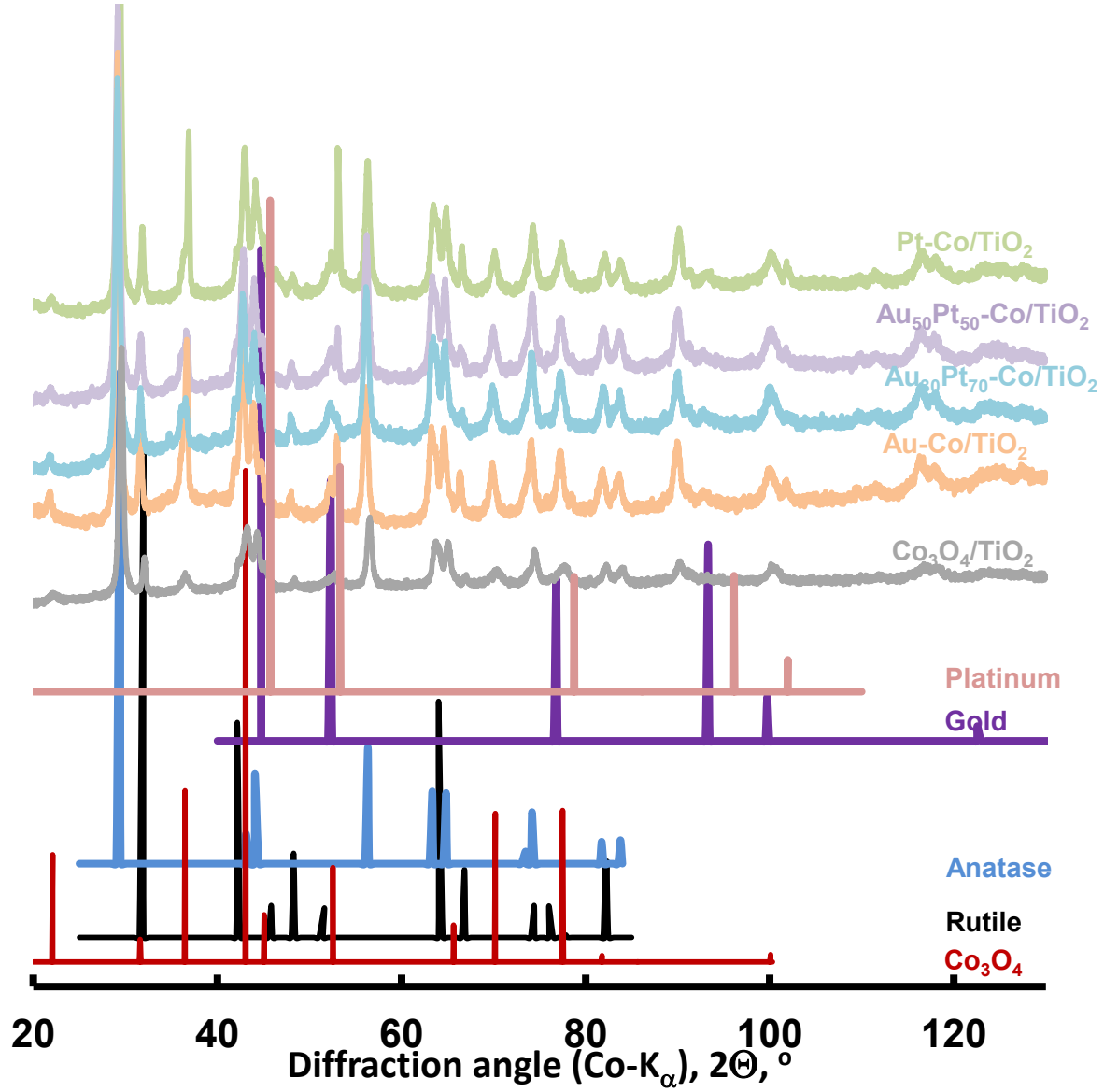

Figure 4.9: XRD-pattern of the calcined, catalyst samples (unpromoted and promoted with Au, $Au_{30}Pt_{70}$-alloy and Pt).

An additional diffraction peak at 2θ ~36.9° in noble metal containing Co/TiO_2 is observed, overlapping with a diffraction peak at 36.5° corresponding to Co_3O_4(210), shown in Figure 4.10. Similar peak was observed on an XRD pattern of Au-TiO_2. This could be ascribed to some material that forms when THPC in the presence of NaOH is used, as the peak is not observed for the unpromoted Co_3O_4/TiO_2.

.

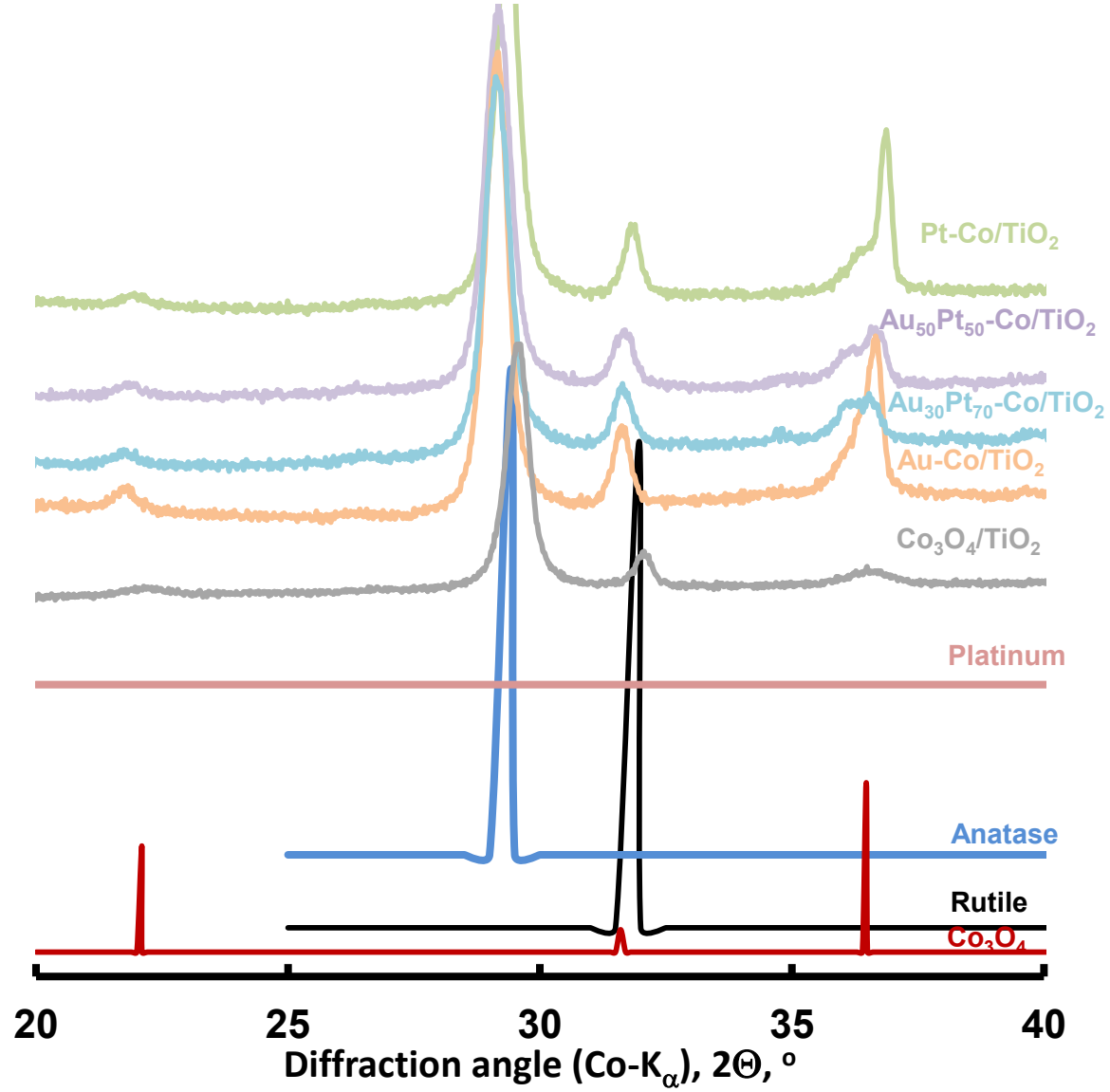

Figure 4.10: XRD-pattern of the calcined, catalyst samples (unpromoted and promoted with Au, $Au_{30}Pt_{70}$-alloy and Pt), Highlighting the additional diffraction peak observed on promoted catalyst precursors.

A more detailed analysis, such transmission electron microscope (TEM), is required to obtain the average particle size of the gold containing crystallites in $Au_{30}Pt_{70}$-Co/TiO_2, since the overlapping peaks make the assignment of the peak maximum (an essential aspect for the expected alloy formation) a non-trivial exercise. Furthermore, an exact determination of the average crystallite size of the noble metal promoter using the Debye-Scherrer was therefore not feasible.

A poor contrast between Co_3O_4 and TiO_2 did not allow for an accurate determination of the crystallite size distribution of Co_3O_4 in these samples using TEM (*cf.* Figure 4.11).

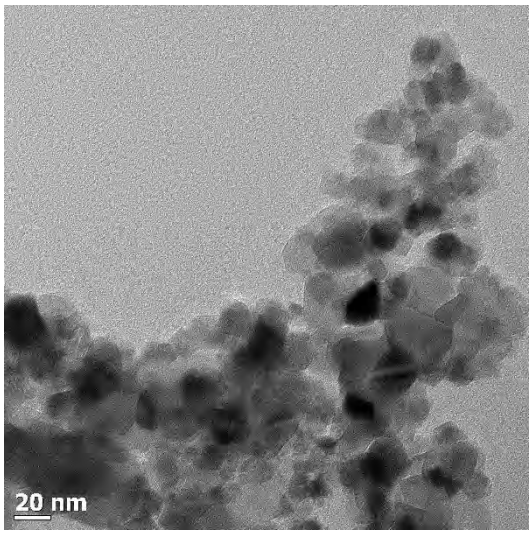

Figure 4.11: TEM-images of the calcined Co/TiO_2 emphasizing poor contrast between Co_3O_4 and TiO_2 support in the catalyst

The resulting promoted catalyst precursors were further imaged using electron microscopy (*cf.* Figure 4.12). The particle size distribution of the nano-sized materials visible in the noble metal promoted samples, which is attributed to the presence of the noble metal, were modelled using a log-normal distribution, from which the average crystallite size of the nano-particles and the standard deviation were determined. The obtained crystallite sizes of the nano-sized particles are in the range between 1.5-3.5 nm.

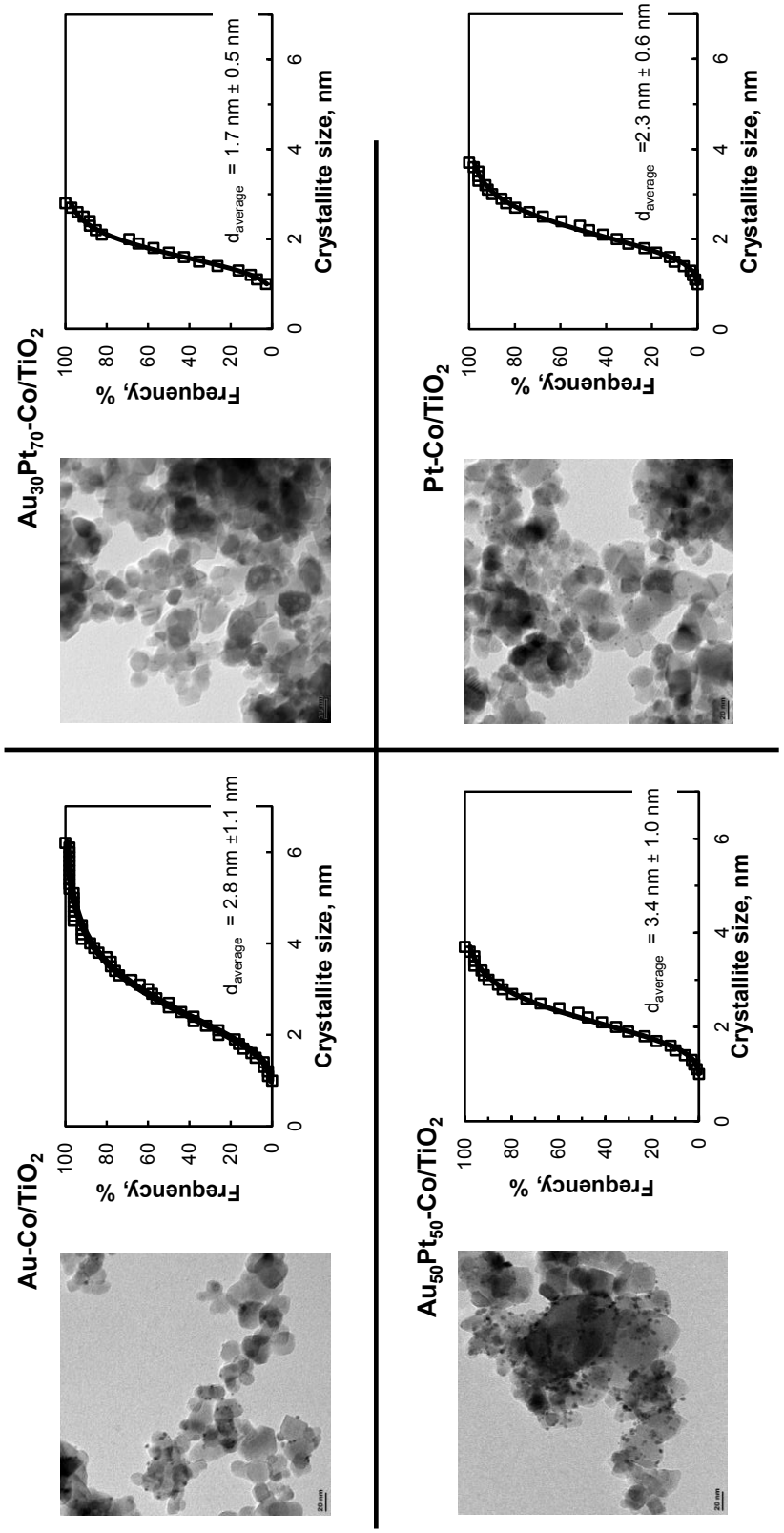

Figure 4.12: TEM-images of the calcined, promoted catalyst samples emphasizing the random deposition of small nano-sized particles on the calcined Co/TiO_2-catalyst.

The Au-Co/TiO_2-catalyst precursor has quite a wide distribution of nano-particles. The width of the distribution was measure to be 1.1 nm, while the width distribution for Au /TiO_2 was 0.3 nm. This is in contrast to the size distribution obtained when the gold nano-particles were synthesized in the presence of titania (as shown in Figure 4.2) rather than Co/TiO_2. It may be argued that cobalt in these samples act as initiation sites for the formation of larger gold nanoparticles. The width of the distribution is significantly smaller when platinum is introduced in the sample (again showing the facile incorporation of platinum in these structures using the applied synthesis method). The distribution obtained when synthesizing the platinum containing nano-particles in the presence of the calcined Co/TiO_2 is similar to the distribution obtained when synthesizing these particles in the presence of TiO_2. This might indicate that the platinum containing nano-particles are not interacting with the solid in the synthesis mixture at all or mainly interacting with the titania surface rather than with Co_3O_4 in the catalyst.

4.3.4. Fourier Transform Infra-Red, FTIR

Fourier Transform Infrared (FTIR) analysis of the samples Co/TiO_2 and THPC-Co/TiO_2, i.e. a sample which was exposed to the synthesis mixture of the noble metal supported catalysts but without the addition of the noble metal salt solution was performed (*cf*. Figure 4.13).

The sample THPC-Co/TiO_2 show strong absorption band at 517 cm^{-1} (478 cm^{-1}) and 656 cm^{-1}, which are absent in the sample Co/TiO_2. The observed absorption bands for THPC-Co/TiO_2 could be ascribed to P-Cl and P-C (aliphatic) respectively [63]. A wax-like material was observed when calcined Co/TiO_2 was exposed to THPC/NaOH mixture. The wax-like material was observed during the synthesis of noble metal promoted Co/TiO_2 catalyst precursors. THPC-Co/TiO_2 was not calcined after being recovered from THPC/NaOH solution. The material was thought to be due to residuals of the decomposed THPC and/or oligomerized methoxy groups forming a ling chain organic material. Therefore, the observed absorption bands were ascribed to the THPC derivatives on THPC-Co/TiO_2 since they were not observed for Co/TiO_2.

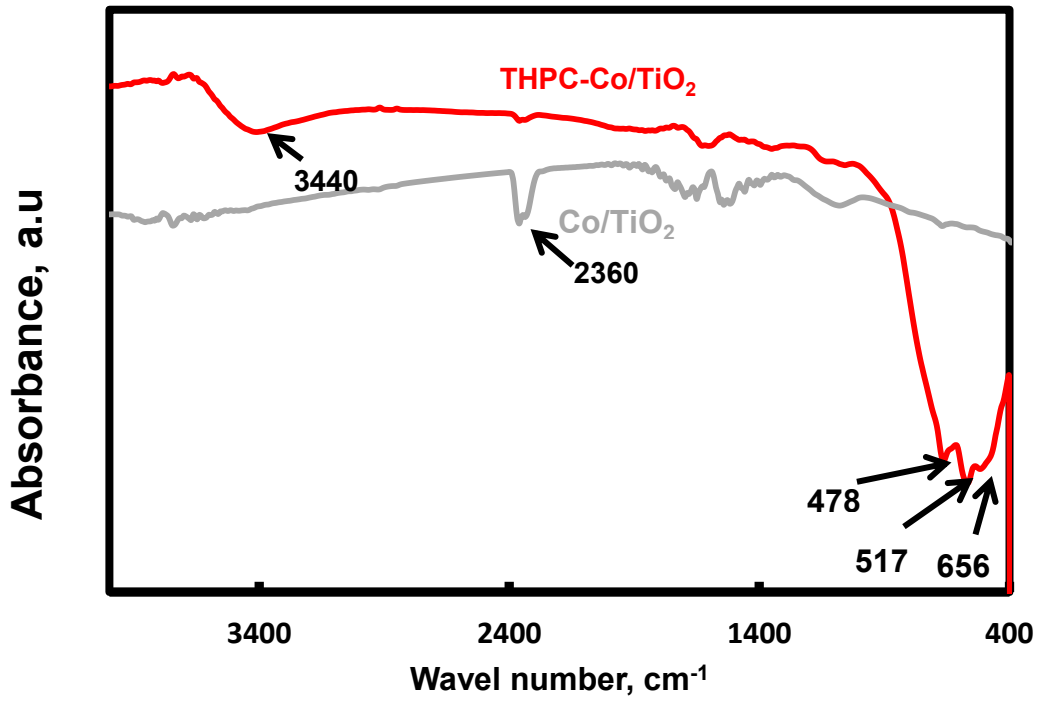

Figure 4.13: Infrared spectra of uncalcined THPC-Co/TiO_2 and calcined Co/TiO_2.

A strong absorption bands for Co/TiO_2 occurring at *ca*. 2360 cm^{-1} depict the asymmetric vibration of CO_2 from the atmosphere [63]. This band is not as pronounced for THPC-Co/TiO_2 as it is for Co/TiO_2 sample. THPC-Co/TiO_2 show absorption bands at 3440 cm^{-1}, due to the stretching of hydroxyl groups (-OH) [64-65], usually associated with the presence of water.

4.3.5. Temperature Programmed Reduction (TPR) analysis

The reduction behaviour of the unpromoted and the promoted catalysts was studied using temperature programmed temperature reduction (TPR). Figure 4.14 shows the TPR-profiles for unpromoted Co/TiO_2 and the noble metal promoted Co/TiO_2.

The TPR profile of the unpromoted catalyst precursors constitutes the base case for comparison and shows two reduction peaks with a shoulder visible between the first and the second reduction peak. The first peak with a maximum at *ca*. 285°C is typically ascribed to the reduction of trivalent cobalt present in the spinel to divalent cobalt, Co(II)O, and the second peak at *ca*. 445°C is typically ascribed to the reduction of Co(II)O to metallic cobalt [18, 62]. The peaks can be ascribed to a stepwise reduction of oxidic cobalt via $Co^{3+} \rightarrow Co^{2+} \rightarrow Co^{0}$.

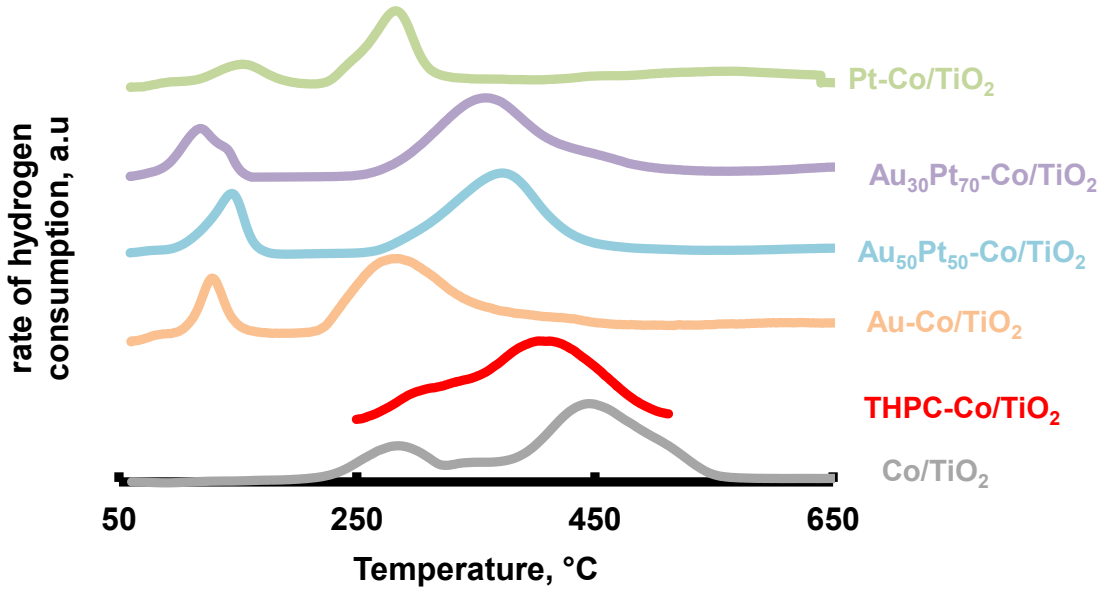

Figure 4.14: TPR-profiles of the calcined Co/TiO_2 and promoted catalysts samples

The shoulder between the two main reduction peaks was also observed by Li et al. [68] in a Co/TiO_2 catalyst *ex* cobalt nitrate. This shoulder may represent the reduction of divalent cobalt with minimal interaction with the support, whereas the main reduction peak with a maximum at *ca*. 445°C represents divalent cobalt species with a stronger interaction with titania. Quantitative analysis of H_2 consumption for each reduction peak shows a peak area ratio ($A_1^{st}{}_{peak}/A_2^{nd}{}_{peak}$) of *ca*. 3 (*cf.* Table 4.4) which is consistent with the theoretical calculation.

4.3.5.1. Reduction behaviour of THPC-Co/TiO₂

The reduction temperature peak of THPC-Co/TiO_2 occurring between *ca*. 315 °C and 512 °C was evaluated as one single area due to bad peak separation, although this broad peak consists of at least two peaks.

The reduction behaviour of the THPC-Co/TiO_2 compared to Co/TiO_2 could be ascribed to the presence of THPC and NaOH, which were used for the reduction of the $HAuCl_4$ and H_2PtCl_6 to metallic Au and Pt respectively. It is proposed that the observed slight shift in the reduction temperature peaks is attributed to the reduction role of THPC in the presence of NaOH. Upon decomposition of THPC in the presence of NaOH *in-situ* formaldehyde is formed (the reducing agent precursor) facilitated the reduction of Co^{3+} ions in the cobalt(III, II) oxide spinel according to

Figure 4.15 [66]. This behaviour is not observed for the promoted Co/TiO_2 this could be due to the difference in activation energies for the reduction of noble metal precursor to noble metals. The activation energy for the reduction of noble metal precursor solution to noble metal is thought to be lower than the reduction of cobalt(III, II) oxide spinel to cobalt(II)oxide. Moreover, the *in-situ* generated formaldehyde is thought to be the limiting reactant.

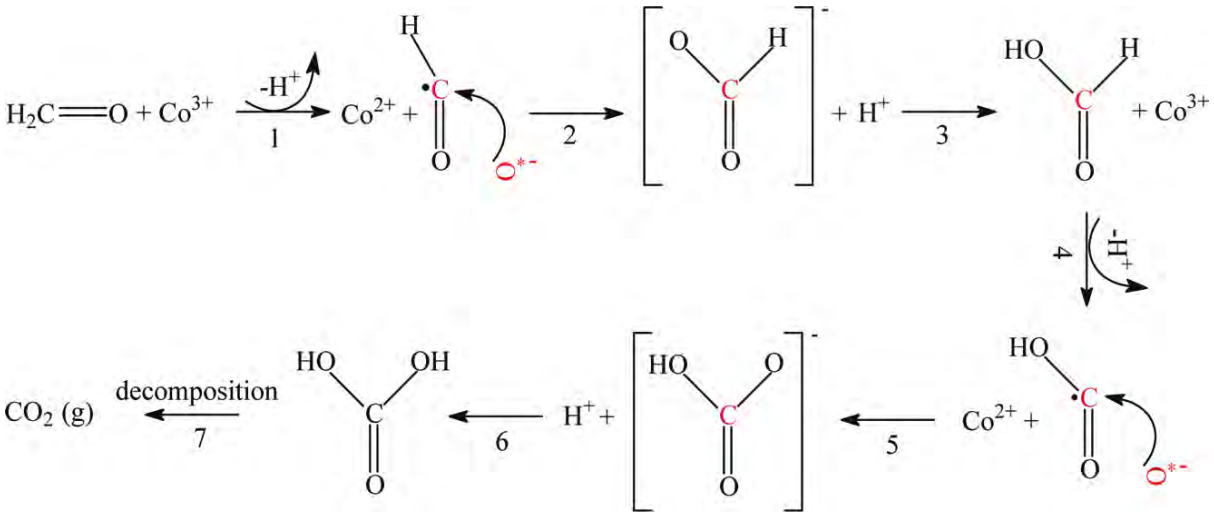

Figure 4.15: Formaldehyde oxidation over Co_3O_4 at 25 °C. Red highlighted atoms adsorbed on the surface [66].

The *in-situ* generated formaldehyde (after THPC decomposition in the presence of NaOH base) is adsorbed on the surface of Co_3O_4, which further undergoes 1,2-nucleophilic addition forming adsorbed formate species (step 1-3). The generated formiate is oxidised, while reducing Co_3O_4 to CoO (step 4), generating bicarbonate (HCO_3^-) species (step 5), and bicarbonate (HCO_3^-) species is protonated forming carbonic acid (step 6). Finally, the bound carbonic acid species decomposes into CO_2 (step 7) [66]. At the end of the reaction the cobalt oxide species exists as CoO. Hence compared to the unpromoted Co/TiO_2, the first reduction peak corresponding to the reduction of Co^{3+} ions in the cobalt(III, II) oxide spinel is not observed for THPC-Co/TiO_2 sample. Therefore, the peak occurring at 315 °C is proposed to be the shoulder peak observed in TPR spectra of the unpromoted Co/TiO_2 catalysts precursors which was thought to be due to the reduction of CoO to metallic cobalt

that is not strongly interacting with the surface of the support. The peak maximum occurring at 512 °C was ascribed to the reduction of the bulk cobalt(II) oxide.

The reduction of the peak ascribed to reduction of Co_3O_4 to CoO temperature peak could further confirms that the first reduction temperature peak represents the conversion of cobalt(III, III) oxide spinel to cobalt(II)oxide.

4.3.5.2. Reduction behaviour of promoted Co/TiO_2 systems

The TPR-profiles of the samples containing the noble metal promoters are characterized by a strong shift of both reduction peaks to lower temperatures compared to Co/TiO_2. Interestingly, the shift in the reduction peaks for the gold-platinum systems is less than for the pure gold or the pure platinum system. Platinum particles may act as a reduction promoter via the hydrogen spill-over mechanism, for which these particles need not to be associated with the cobalt(II,III) oxide particles [5]. The platinum-gold particles are expected to be less effective for hydrogen spill-over mechanism, since the surface of these particles is expected to be enriched with gold in absence of a strongly adsorbing species [67] resulting in a reduced ability to activate hydrogen. The low heat of adsorption for hydrogen on the gold enriched surface (as deduced from the behaviour of pure gold [68]); will impede the H_2 spill-over mechanism over these materials. Hence, the extent to which the reduction of cobalt is facilitated due to the presence of gold-platinum particles is expected to be less in comparison to platinum (as is observed). The behaviour of the gold promoted catalysts observed is surprising (i.e. a stronger enhancement of the reducibility as for the platinum-gold particles). It might be speculated that these gold crystallites are in contact with cobalt and enhance the reduction process via an electronic interaction.

The strong shift of both reduction peaks to lower temperatures for noble metal promoted catalyst precursors may imply that the presence of the noble metal promoter increases in the rate of reduction of both trivalent cobalt and divalent cobalt. Since the reduction of cobalt(III, II) oxide spinel is a consecutive process ($Co^{3+} \rightarrow Co^{2+} \rightarrow Co^0$) could also mean that the acceleration of the first reduction step may automatically lead to a shift in the second reduction peak since after the first reduction the CoO is present.

Table 4.4: Quantitative analysis of the unpromoted and promoted Co/TiO_2 catalyst precursors

Catalyst Precursor	H_2 Consumption, a.u.			$T_{1st\ peak}$, °C	$T_{2nd\ Peak}$, °C
	$A_{1st\ Peak}$	$A_{2nd\ Peak}$	$A_{1st\ peak}/A_{2nd\ peak}$		
Co/TiO_2	0.41	1.5	0.27	286	446
THPC-Co/TiO_2	-	0.38	-	-	402
Au-Co/TiO_2	0.603	2.99	0.202	128	284
$Au_{30}Pt_{70}$-Co/TiO_2	0.51	1.4	0.22	119	358
$Au_{50}Pt_{50}$-Co/TiO_2	0.41	1.5	0.27	145	372
Pt-Co/TiO_2	0.52	1.3	0.4	153	282

4.3.6. Isothermal reduction behaviour

The isothermal reduction behaviour of the noble metal(s) promoted and unpromoted Co/TiO_2 was investigated.

Prior to isothermal reduction of the catalyst precursor samples (promoted and unpromoted), the samples were dried under flowing nitrogen at 350 °C for 1 hour Nitrogen was passed over the catalyst for drying. This led to a reduction of the mass of the sample. This could be due to the removal of the wax-like material and/or water from the sample. The catalysts precursors were reduced under H_2 (10 mL(NTP)/min) at 350 ^{0}C. The mass of the catalyst was further reduced, until the curve describing the method behaved asymptotically. The mass reduction was ascribed to the removal of oxygen atoms as water. When the curve plateaued it was the concluded that the cobalt species was present as metallic cobalt. After isothermal reduction, N_2 was used to flush out H_2 followed by oxygen titration (10 mL(NTP)/min), see Figure 4.16.

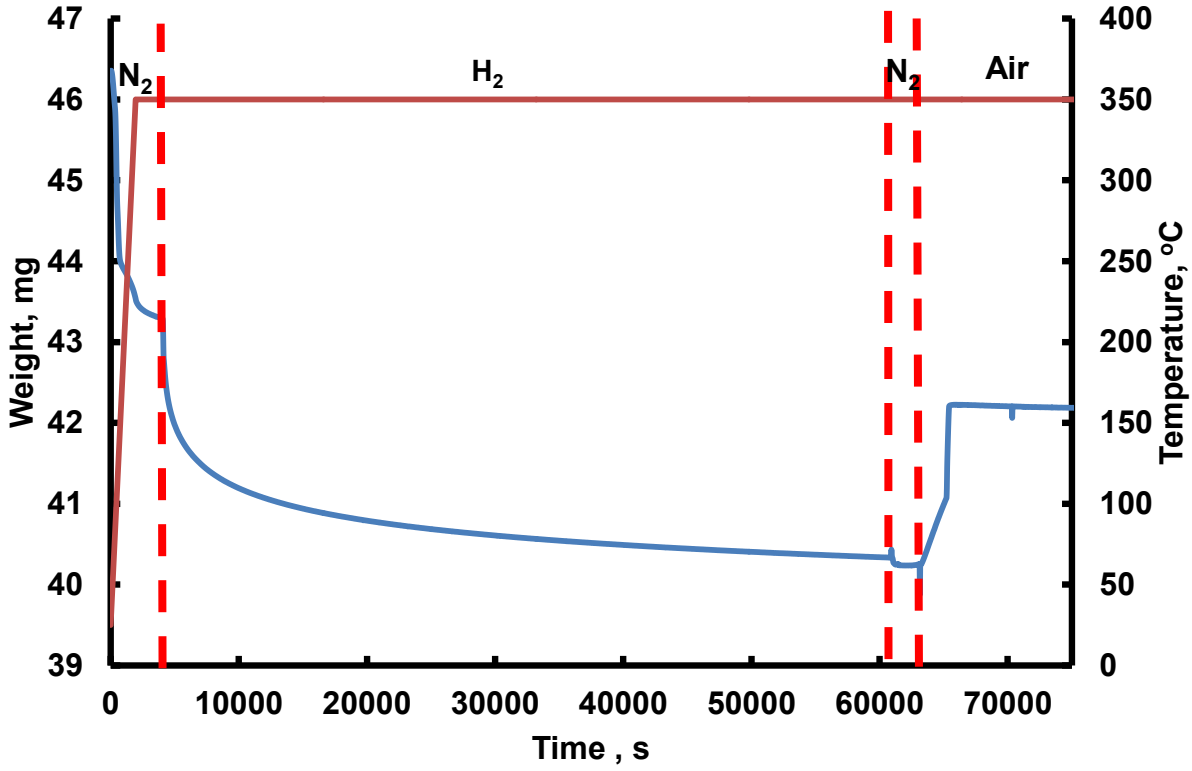

Figure 4.16: Thermal gravimetric analysis profile of Pt-Co/TiO_2 catalyst precursor

4.3.6.1. Isothermal reduction

The isothermal reduction profiles shown in Figure 4.17 depict the relative mass loss per mass of catalyst as a function of the reduction time on a semi-logarithmic scale. For the unpromoted catalyst, the rate of mass loss during the isothermal reduction process then slows down, before going through a second auto-catalytic reduction step. The rate of reduction for the noble metal promoted catalysts show only a single process.

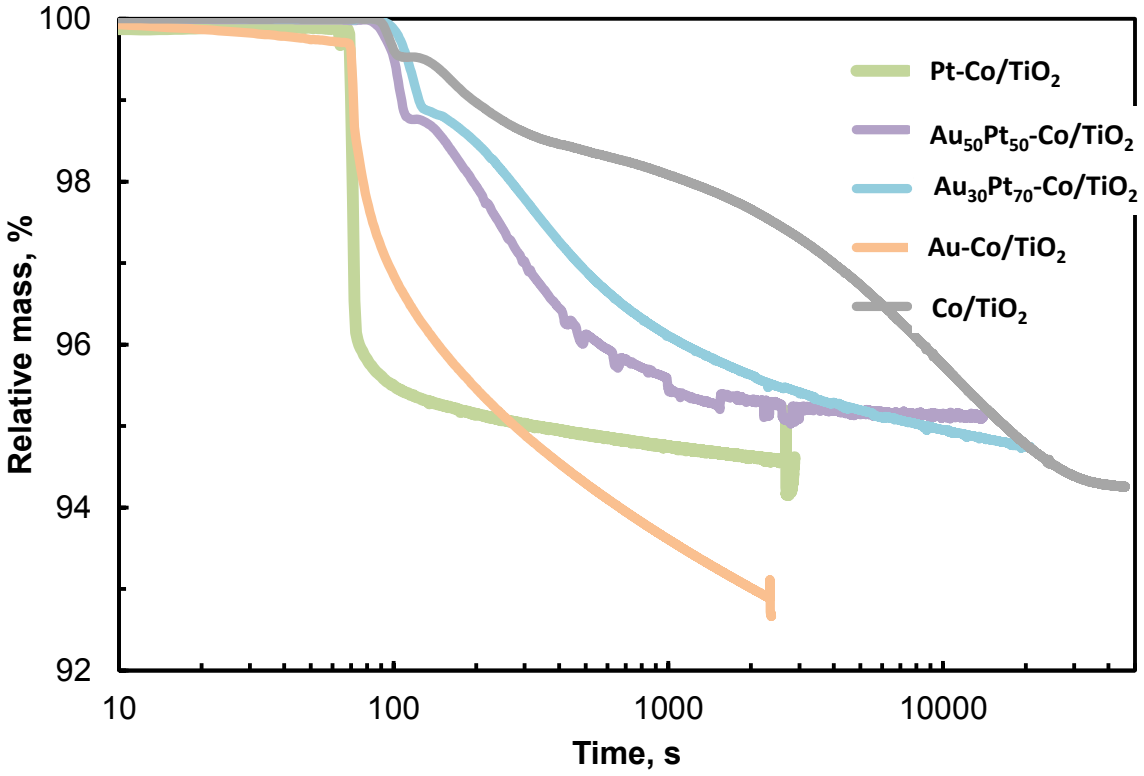

Figure 4.17: Relative mass loss during the isothermal reduction of the promoted and unpromoted Co/TiO_2 in hydrogen at 350°C

The two different reduction steps, which were evident in the temperature programmed reduction (TPR) profiles, are no longer clearly visible in the isothermal reduction at 350°C (although the slowing down of the reduction of the unpromoted cobalt catalyst after *ca.* 200 s may be related to the sequential reduction process of $Co_3O_4 \rightarrow CoO \rightarrow Co^0$). It can be further noted that initially the rate of reduction for the unpromoted and the noble nano-alloy promoted catalysts are very similar implying that the noble metal promoter does not affect the initial reduction at 350 °C, or otherwise stated at this temperature the pathway provided by noble metal promoter to enhance the reduction process is kinetically irrelevant in comparison to the direct initial reduction process. $Pt\text{-}Co/TiO_2$ catalysts precursor shows a relatively fast rate of reduction this could be due to a larger availability of activated H^+ ion. This could be attributed to the H_2-spillover mechanism.

The TPR experiments were done in $5\%H_2/Ar$ mixtures, whereas the catalysts were reduced in pure hydrogen for catalytic measurements. It has been shown that

hydrogen partial pressure can affect the extent of cobalt reduction [69]. Greater cobalt reduction is usually obtained in pure hydrogen. Thus, TPR measurements provide only qualitative information on cobalt reducibility and cannot be used for quantitative evaluation of the fraction of cobalt metal phase in catalysts reduced in pure hydrogen.

4.3.6.2. Degree of reduction

The final degree of reduction (350°C in pure H_2 (10 mL (NTP)/min titrated with air (10 mL (NTP)/min) of the catalysts was determined by oxidation of the reduced catalyst in air at 350 °C. Assuming that all metallic cobalt oxidises to Co_3O_4 under these conditions, the degree of reduction was found to be 88% for the unpromoted Co/TiO_2 after a reduction time of 16 hrs, whereas it was 85% and 82% for $Au_{30}Pt_{70}$-Co/TiO_2 catalyst and $Au_{50}Pt_{50}$-Co/TiO_2 catalyst, respectively, after 5 hours of reduction. Hence, it was possible to obtain similar degree of reductions within a much short time period, due to promotion of the catalyst with the noble metal. Au- and Pt-promoted Co/TiO_2 were exposed in H_2 for 5 hours prior to re-oxidation. The degree of reduction for Au- and Pt -Co/TiO_2 was found to be 95% and 73 % respectively. An increased degree of reduction of the oxidic cobalt might have been expected for Pt-promoted catalysts precursor instead a significant lower value is obtained. The implication is this observation is unclear. However, this could be due to some error during reduction.

4.3.7. Hydrogen chemisorption

The number of active sites on the surface of the promoted and unpromoted (THPC-Co/TiO_2 and Co/TiO_2) catalyst precursor was determined using H_2 chemisorption analysis.

H_2 chemisorption isotherms were obtained as shown in Figure 4.18. Co/TiO_2 THPC-Co/TiO_2 are used as a standard for comparison using static volumetric method. The obtained isotherm was modelled and fitted in a Langmuir isotherm according to equation 4.6.

$$V_{ads} = \frac{V_1 \cdot K_1 {p_{H_2}}^{1/2}}{1 + K_1 {p_{H_2}}^{1/2}} + K_2 {p_{H_2}}^{1/2} \qquad (4.6)$$

With adsorption constants K_1 and K_2, which give an indication of the strength of adsorption of hydrogen on cobalt and titania (TiO_2) surface respectively, varied significantly.

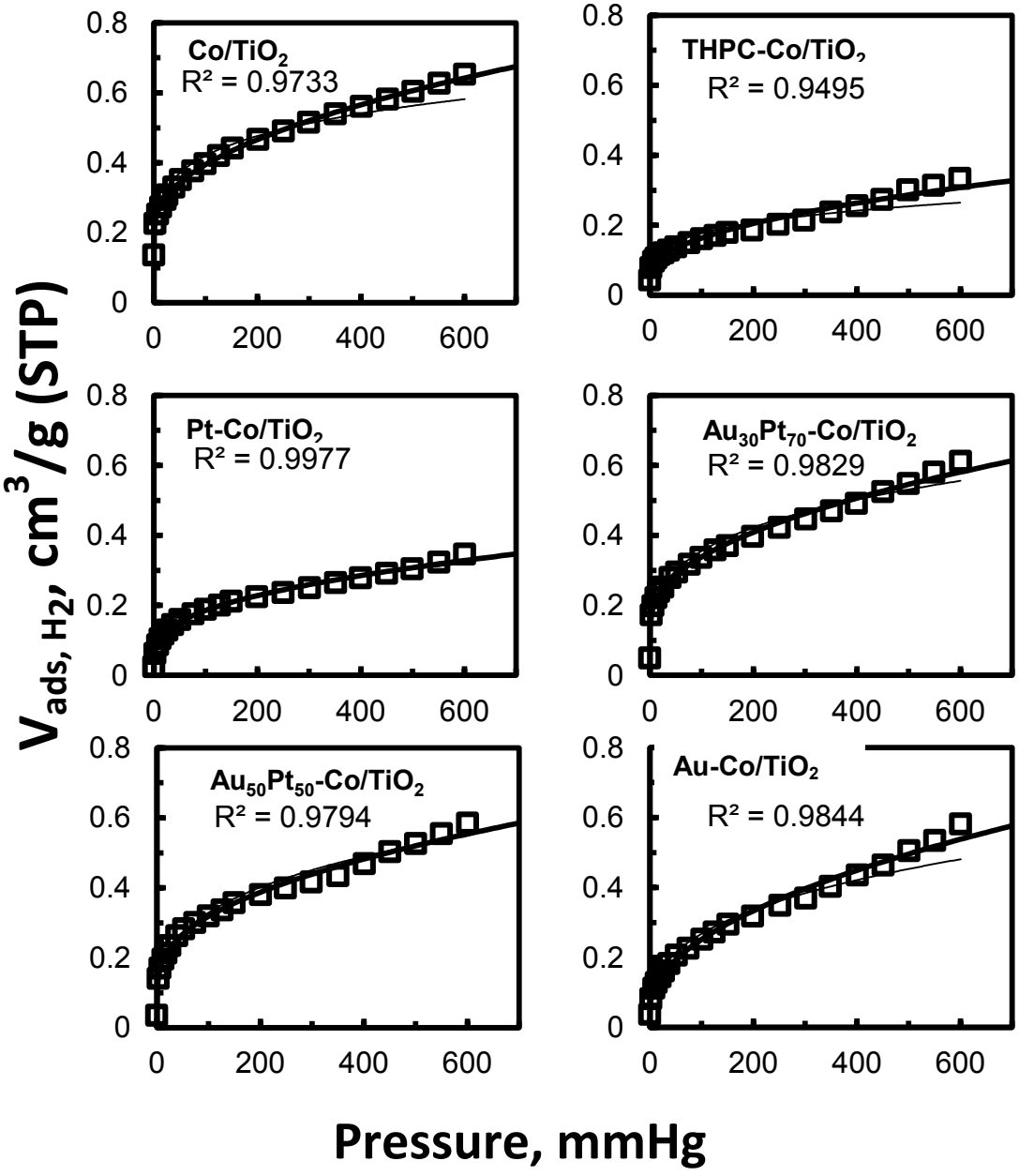

Figure 4.18: H_2 chemisorption on Co/TiO_2, THPC-Co/TiO_2 and noble metal(s) promoted Co/TiO_2

The number of active site on the surface (accessible active sites) of catalyst were determined using H_2-chemisorption the volume of hydrogen adsorbed ($V_{ads,\ H_2}$) on the surface of the Co/TiO_2 and THPC-Co/TiO_2 were measured to be *ca.* 0.23 and 0.14 cm^3/g respectively. This might indicate that addition of THPC/NaOH poisons the

catalyst by decreasing the surface area of the catalyst by a factor of *ca*. 2, (cf and Table 4.5). The measurements of the volume of hydrogen adsorbed on the surface of the catalyst precursors were repeated. The measured values for THPC-Co/TiO_2 and noble metal(s) promoted catalyst precursors varied significantly (*cf*. Table 4.5). This could imply that THPC-Co/TiO_2 and noble promoted catalyst precursor is not homogenously poisoned. Notably, the volume of adsorbed H_2 for THPC-Co/TiO_2 and Pt-Co/TiO_2 is comparable, while for Au-containing Co/TiO_2 catalyst precursors are also comparable but vary from the THPC-Co/TiO_2 and Pt-Co/TiO_2.

Table 4.5: Volume of H_2 adsorbed on the surface of the unpromoted and promoted Co/TiO_2 and their adsorption constants.

	Co/TiO_2	THPC-Co/TiO_2	Pt-Co/TiO_2	$Pt_{70}Au_{30}$-Co/TiO_2	$Pt_{50}Au_{50}$-Co/TiO_2	Au-Co/TiO_2
V_{ads},	0.232	0.136	0.108	0.185	0.177	0.056
$cm^3(STP)/g$	0.231	0.157	0.085	0.099	0.097	0.035
K_1	4.007	7.096	0.598	1.859	1.085	4.599
	4.755	4.443	0.707	2.374	1.428	5.929
K_2	0.017	0.015	0.009	0.016	0.016	0.020
	0.011	0.010	0.009	0.012	0.009	0.016

Expectedly, K_1 is significantly larger than K_2. Hydrogen is expected to be strongly adsorbed on the surface of cobalt (Fischer-Tropsch synthesis active metal) compared to titania, the support.

The strength of adsorption of hydrogen onto the surface of titania is comparable for the unpromoted and promoted catalysts. This could imply that the strength of adsorption of hydrogen on the surface of titania support is independent of catalyst composition. On the contrary, the strength of hydrogen adsorption onto the cobalt surface seems be influenced by the composition of the catalyst. Moreover, the hydrogen adsorption strength on the surface of the unpromoted (THPC-Co/TiO_2 and Co/TiO_2) and noble metal promoted Co/TiO_2 catalysts vary significantly.

4.4. Catalyst Evaluation- Fischer- Tropsch synthesis

The catalyst performance of the promoted and unpromoted catalysts was evaluated in a fixed-bed reactor at 220 °C and 20 bar using constant feed gas with a H_2 to CO ratio of 2 was used. The space velocity of CO was 20 mL/g_{cat}·min.

4.4.1. CO-conversion: The effect of THPC/NaOH

The CO conversion of the catalyst precursors as a function of time on stream is shown in Figure 4.19. The first hour the Co/TiO_2 catalysts precursor on stream shows 100% CO conversion. This could be due to the diffusion of the gas through the reactor filled with SiC, therefore CO could not be detected by the TCD hence the counterfeit 100% CO conversion. After 1 hour, CO was detected by the TDC hence the decrease in CO conversion until steady-state is stablished.

The low CO conversion of 1.4% for the THPC-Co/TiO_2 catalyst compared to 27% CO conversion of the unpromoted Co/TiO_2 may suggest decreased number of active sites when THPC/NaOH is added. This could possible imply catalyst poisoning by THPC derivatives, which is not removed during reduction.

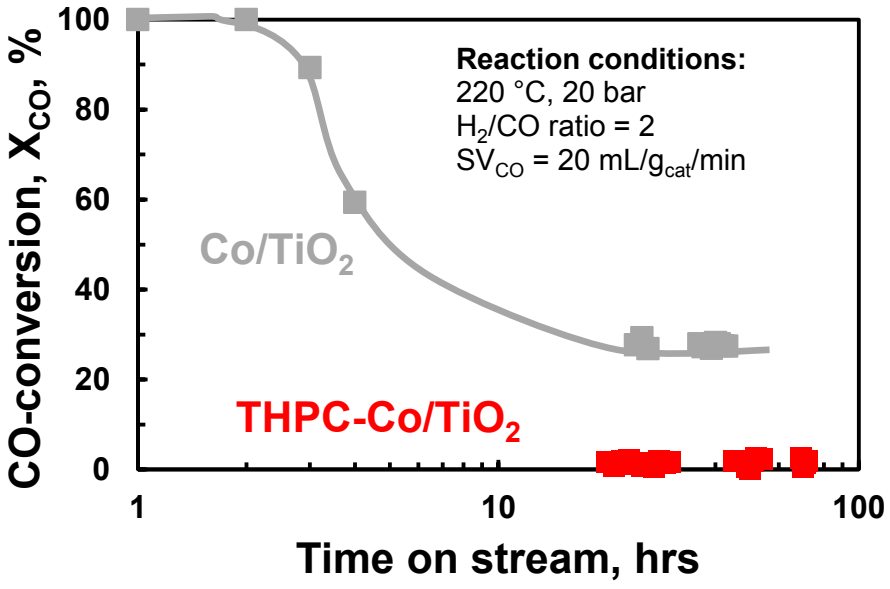

Figure 4.19: CO-conversion of Co/TiO_2 and THPC modified Co/TiO_2 catalyst in the Fischer-Tropsch synthesis at 220 °C, 20 bar, $F_{CO,0}$/W = 20 mL/(min.g_{cat}) represented after reduction in H_2 (40 mL (NTP)/min) at 350 °C for 16 hours.

4.4.2. CO-conversion: The effect of Pt/Au alloy

Figure 4.20 shows CO conversion of the promoted and THPC-Co/TiO_2 catalyst precursor. The low conversions of the promoted Co/TiO_2 could also be due to the poisoning of the catalyst by THPC/NaOH. Moreover, the low catalytic activity of Au-containing Co/TiO_2 could also be attributed by active site blockage by gold. Low surface energy of Au favours surface enrichment of cobalt species by Au. Jalama *et. al*. reported a slight decrease in CO conversion at high loading of Au ≥ 1 wt.% attributed by site blockage by gold promoter [18].

A direct comparison of the catalytic activity of the gold containing noble metal (Au and AuPt alloy) promoted and THPC-Co/TiO_2 catalyst precursors show an enhanced CO-conversion upon noble metal promotion. The AuPt alloy is proposed to be associated with the support (based on surface energies). Therefore, it is proposed that active site blockage is might not be possible as it would require a direct contact with the active metal. Furthermore, Au in alloy systems might have been chemically modified such that to some degree H_2-spillover can occur, consequently increasing the amount of surface hydrogen which would enhance CO hydrogenation. The significant increase in Pt–Co/TiO_2 catalyst could be ascribed to an increased hydrogenation brought about a larger availability of activated hydrogen through H_2-spillover mechanism. Au-promoted catalysts show better activity compared to the unpromoted Co/TiO_2 catalyst, but the CO conversion of the alloy promoted Co/TiO_2 are higher than the Au promoted and the unpromoted Co/TiO_2. The activity of the promoted catalyst increases with increasing platinum content of the promoter. This might attributed by increased surface hydrogen (contributed by H_2-spillover mechanism prompted by platinum promoter) facilitating CO hydrogenation.

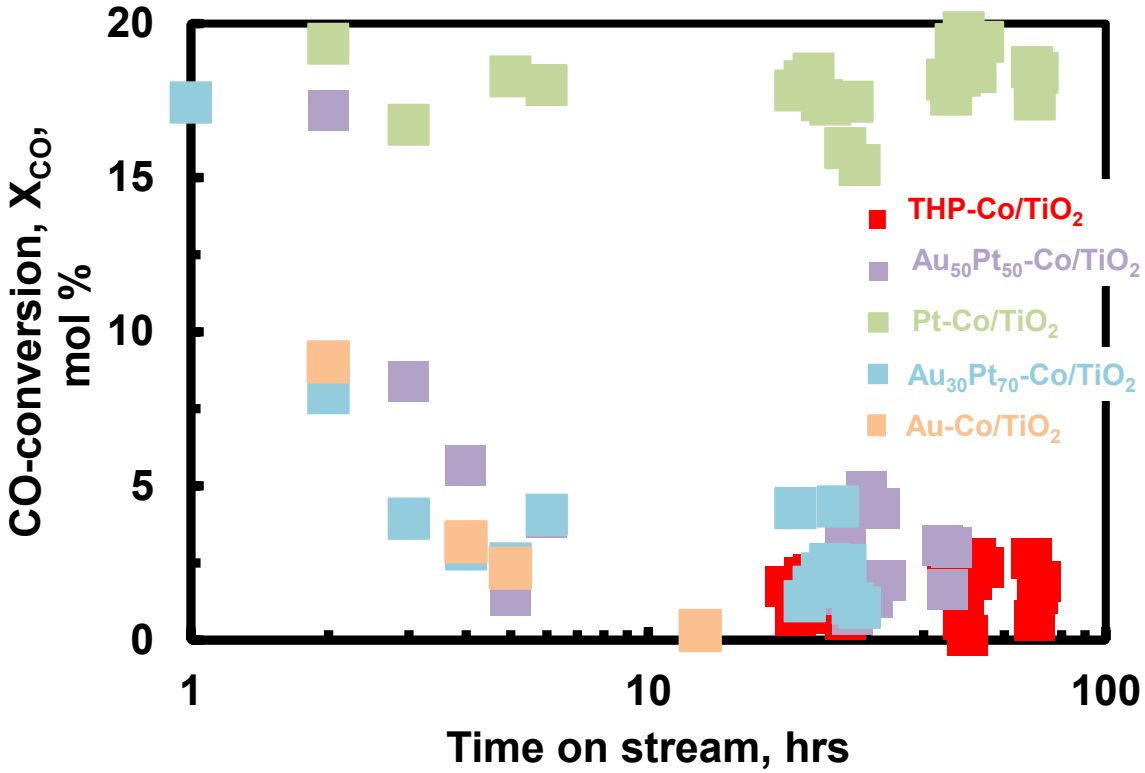

Figure 4.20: CO-conversion of promoted and unpromoted catalysts in the Fischer-Tropsch synthesis at 220 °C, 20 bar, $F_{CO,0}/W$ = 20 mL/(min.g_{cat}) represented after reduction in H_2 (40 mL (NTP)/min) at 350 °C for 16 hours.

4.4.3. Selectivity

The effect of the promoter on the product distribution and selectivity was evaluated. Physiochemical properties brought about the promoter could be evaluated based the product selectivity of the catalyst. Comparison of catalysts' product selectivity is strongly dependent on catalytic activity in (terms CO conversion) of the catalyst [34]. Therefore, product selectivity of the catalysts could be compared at similar CO conversions.

The catalyst precursors (unpromoted and promoted Co/TiO_2) showed low CO-conversions due to catalyst poisoning. This made quantification of product selectivity rather a challenge, as the GC-FID product signals were very small making it difficult to quantify the GC-FID profile of the catalyst precursors.

4.4.3.1. C_1 selectivity

Methane is the least desired organic product in Fischer-Tropsch synthesis; however it is the most thermodynamically favoured product under Fischer-Tropsch synthesis. Methane formation involves hydrogenation of surface methyl species (by surface hydrogen) consequently leading to desorption, forming methane. This means that methane selectivity is influence by the probability that the surface carbon is hydrogenated such that it forms surface methyl species and the probability that the surface methyl species is hydrogenated and desorbed to form methane. Both probabilities increase with increasing surface hydrogen. Furthermore, Jacobs *et al*. showed that methane selectivity is affected by the activity of the catalyst, especially at relatively lower and higher CO conversions [40]. This makes methane selectivity rather a complex variable.

$Au_{30}Pt_{70}$-Co/TiO_2 has been observed to have higher C_1 selectivity compared to $Au_{50}Pt_{50}$-Co/TiO_2. However, since both catalysts showed low CO conversion the C_1 selectivity may vary significantly. On the other hand the high C_1 selectivity of $Au_{30}Pt_{70}$-Co/TiO_2 may also be influenced by increased surface hydrogen, leading to desorption of the surface methyl species. Based on this, C_1 selectivity cannot be compared as it is not clear whether the difference in C_1 selectivity could be because of an increased Pt content of the alloy or it also be due to the difference in CO conversion of the two catalysts. At low CO-conversions, a slight difference in CO-conversion could result in significant difference in C_1 selectivity. This argument can be extended to all the catalysts. Table 4.6 shows the summary of the product selectivity.

Table 4.6: Summary of product selectivity and CO conversion of the promoted and unpromoted Co/TiO_2.

Catalyst	α	X_{CO}	Selectivity, C-%				
			C_1	C_2	C_3	C_4	C_{5+}
THPC-Co/TiO_2	0.35	1.4	44	15	4	2	35
Au-Co/TiO_2	0.35	1.9	80	15	3	1	1
$Au_{50}Pt_{50}$-Co/TiO_2	0.36	2.5	29	39	11	6	15
$Au_{30}Pt_{70}$-Co/TiO_2	0.52	2.6	52	13	7	13	15

Pt-Co/TiO_2	0.86	18.4	26	5	5	5	59

A significant increase in C_1 selectivity for the Pt-Co/TiO_2 might have been expected, due to increased surface hydrogen, however it has been obvious to have the lowest methane selectivity of *ca.* 26 C-%. This could be due to an increase CO conversion for Pt-Co/TiO_2 catalyst relative to other promoted and THPC-Co/TiO_2 catalysts.

4.4.3.2. C_{5+} selectivity

C_{5+} selectivity is determined by chain growth probability, which gives an indication of desorption and chain growth of surface of organic products. High chain growth probability represents long chain hydrocarbon formation. Unexpectedly, Pt-Co/TiO_2 catalyst showed highest chain growth probability with C_{5+} equals to *ca.*59 C-%. This could influence by the difference in CO conversion of the catalysts. This is unexpected as it is thought Pt increases surface hydrogen which favours desorption of surface products leading to a decrease in chain growth probability.

Notably, chain growth probability decreases with increasing Pt- content, may be due to increasing availability of surface hydrogen. This further means that the liquid hydrocarbon selectivity is decreasing with increasing Pt-content of the catalyst, as it is observed.

4.4.3.3. Olefin selectivity

The olefin selectivity was determined in comparison to formed paraffins, i.e. oxygenates were excluded.

Olefin selectivity may give an indication about the hydrogenation ability. Olefin content in the fraction of linear hydrocarbons was observed to decreasing with increasing platinum content for the promoted with the unpromoted catalyst precursor sample (THPC-Co/TiO_2) showing the highest olefin selectivity. This could suggest an increasing availability of activated surface hydrogen with increasing platinum content. This could result in an increased hydrogenation activity subsequently in a decrease in olefin fraction in linear hydrocarbons. (*cf*. Table 4.7).

$Au_{30}Pt_{70}$-Co/TiO_2 and $Au_{50}Pt_{50}$-Co/TiO_2 showed highest α-olefin selectivity in olefin fraction. Overall, there is no specific trend observed associated with Au/Pt ratio in

Co/TiO_2 and α-olefin selectivity in olefin fraction. This could be attributed by varying CO-conversions; hence the product selectivity could not be compared. However, at similar CO-conversion, α-olefin content is expected to decrease with increasing Pt-content, due to larger availability of surface hydrogen. This might be impelled by re-adsorption of α-olefin (and secondary reactions) which is enhanced with increasing surface hydrogen. Once the α-olefin is re-adsorbed, the larger availability of hydrogen would favour the formation of paraffins and thus have a negative effect on chain growth and the total α-olefin content.

Table 4.7: Product distribution of the promoted and unpromoted THPC-Co/TiO_2.

	Selectivity, C%			
Catalyst	**Paraffin**	**Olefin**	**α-Olefin**	**Oxygenates**
THPC-Co/TiO_2	76	24	97	4
Au-Co/TiO_2	81	23	91	13
$Au_{50}Pt_{50}$-Co/TiO_2	78	22	99	11
$Au_{30}Pt_{70}$-Co/TiO_2	92	8	98	7
Pt-Co/TiO_2	95	6	93	5

4.4.3.4. Oxygenate selectivity

The oxygenate content in hydrocarbon fraction decreases with increasing platinum content. This is expected as increasing platinum content increases surface hydrogen. Increasing hydrogen availability decreases OH concentration since the formation of water will be thermodynamically more favoured and thus the oxygenate content will decrease. Again, the selectivity is dependent on the CO-conversion. The oxygenate selectivity of THPC-Co/TiO_2 and Pt-Co/TiO_2 are comparable, However this could be due to the difference in CO-conversion (*cf*. Table 4.7).

The C_2 fraction is typically observed to be lower compared to the C_3 content in Anderson-Schulz-Flory plot. This may be attributed to re-adsorption of ethenee for secondary reactions. However, due to poor activity of the catalyst for Au-Co/TiO_2 the anticipated behaviour is not observed, rather a continuous decrease with carbon number is observed (see appendix Figure A2 and A3) The Anderson-Schulz-Flory plots typically has the C_2 content relatively smaller than the C_3 content.

5 Conclusions

Platinum, gold-platinum alloys and gold nanoparticle were synthesised using tetrakis(hydroxymethyl) phosphonium chloride solution in the presence of sodium hydroxide. A narrow size distribution of *ca*. 2 nm was obtained. The synthesis of platinum nanoparticles required gold as seed to initiate nucleation for a given reaction temperature. This has been attributed a stronger electron affinity of gold compared to platinum, hence gold is easily reduced forming metallic phase of gold. The average size of the Au nanoparticles increases upon the addition of the support. This might be attributed to the interaction of the nanoparticles with the surface hydroxyl groups of the support. Noble metal nanoparticles were deposited onto the support via electrostatic interaction. The surface of the amphoteric TiO_2 support was modified with concentrated HCl allowing electrostatic deposition of the noble metal nanoparticles onto the support.

Different metal salts have a noted to have an effect on the reducibility of the catalyst [31]. A range of supported catalyst were synthesised via slurry wetness impregnation of calcined TiO_2 with cobalt acetate and cobalt nitrate solutions with varying ratios of cobalt acetate/ (nitrate + acetate mixture). The XRD patterns of the synthesised Co/TiO_2 catalyst precursor show that cobalt oxide species are present as Co_3O_4. Due to poor contrast between TiO_2 and the cobalt species, the average particle size of the cobalt species could not be determined using transmission electron microscope (TEM). Therefore, the average crystallite size of Co_3O_4 was determined using the Debye-Scherrers equation.

Reduction behaviour

Two reduction peaks were observed in the TPR spectrum of the Co/TiO_2 catalyst precursors. The first maxima of all the catalyst precursor was thought to be attributed to the reduction of Co^{3+} ion in Co_3O_4 spinel and the second reduction peak was ascribed to the reduction of CoO to metallic cobalt. A shoulder peak was observed and was ascribed to the reduction of divalent cobalt weakly interacting with TiO_2 support. No obvious trend was observed associated with $[Ac^-]/[NO_3^-]$ ratios.

The mass specific catalytic activity of the unpromoted catalyst is known to increase with decreased crystallite size as the surface area is increased. The average crystallite size of **Cat 5** (*ex*-cobalt nitrate: acetate= 60%) was determined to be 16 nm, which was the smallest crystallite size compared to the synthesis Co/TiO_2 samples. Therefore, **Cat 5** was promoted with Au, $Au_{30}Pt_{70}$-Co/TiO_2, $Au_{50}Pt_{50}$-Co/TiO_2 and Pt nanoparticles. The catalyst precursor was suspended in water and concentrated hydrochloric acid was added to modify the surface charge of the TiO_2 supported catalyst. The noble metal promoter was then electrostatically deposited on Co/TiO_2 catalyst precursor. The average particle size of the noble metal promoter was determined and the particle size distribution was fitted in log-normal distribution model. Co/TiO_2 was exposed in a mixture tetrakis(hydroxymethyl) phosphonium chloride and NaOH solution (without noble metal precursor solution) for fair comparison between the promoted catalyst precursors (referred to as THPC-Co/TiO_2). The catalyst precursor was then referred to as THPC-Co/TiO_2. THPC-Co/TiO_2 catalyst precursor showed a broad reduction peak in the TPR spectrum at reduction temperature of *ca*. 402°C. The behaviour was ascribed to the oxidation of the *in-situ* generated formaldehyde during the decomposition of THPC by NaOH.

The reduction behaviour of the unpromoted and promoted catalyst precursors were investigated using temperature programmed reduction (TPR). Au, Au/Pt alloy and Pt noble metal promoters shift the reduction peaks of cobalt(III, II) oxide spinel to metallic cobalt to relatively lower temperature compared to the unpromoted Co/TiO_2. This was ascribed to an increased amount of activated hydrogen provided by H_2-spillover mechanism proposed to occur in the presence of Pt as a promoter. In the case of Au-Co/TiO_2, the shift in the reduction temperature peak could be due to electronic effects. Pure platinum and gold promoted Co/TiO_2 catalyst precursors showed significant shift in the reduction temperature for the two-step reduction Co_3O_4 to metallic cobalt compared to AuPt alloy promoted Co/TiO_2 samples. This observation was thought to be due to the decrease in H_2-spillover mechanism as the surface of the alloy is thought to be enriched gold due to lower surface energy of gold compared to platinum. The difference in reduction behaviour between pure noble metal (platinum and gold) and AuPt alloy was further thought to be due to diminished electronic effects as the alloy promoter is thought to be associated with the support rather than the cobalt species.

Hence, there is no contact between the alloy promoter and the cobalt species prompting electronic effects.

H_2 chemisorption measurements showed that the amount of H_2 adsorbed on the surface of THPC-Co/TiO_2 and noble metal promoted Co/TiO_2 is less than that of Co/TiO_2 catalyst precursor by a factor of *ca*. 2. This was proposed to imply catalyst poisoning. The H_2 chemisorption measurements were repeated and the measurements varied, suggesting THPC-Co/TiO_2 and noble metal promoted Co/TiO_2 were not homogenously poisoned. Infrared spectrum of THPC-Co/TiO_2 showed strong absorption band at 517 cm^{-1} (478 cm^{-1}) and 656 cm^{-1}, which are absent in the sample Co/TiO_2. The observed absorption bands for THPC-Co/TiO_2 could be ascribed to P-Cl and P-C (aliphatic) respectively. Furthermore, a wax-like material was observed which was thought to be an organic material that formed during the reduction of noble metal precursor solution to noble metal nanoparticles. The presence of the organic material was verified by an XRD pattern, as an amorphous material on promoted Co/TiO_2 catalyst precursors.

Fischer-Tropsch synthesis: Catalyst Evaluation

Carbon monoxide conversion of THPC-Co was compared to Co/TiO_2 at comparable space velocity. A strong decline in CO conversion for THPC-Co/TiO_2 (1.4%) was ascribed to catalyst poisoning by THPC/NaOH mixture. It was then established that the presence of THPC has an effect on the catalytic activity.

The CO conversion of the promoted catalyst precursor was investigated using THPC-Co/TiO_2 as a basis for comparison. Promoted Co/TiO_2 showed better CO conversion compared to THPC-Co/TiO_2. As much as CO conversion for promoted Co/TiO_2 was significantly less than Co/TiO_2, however the CO conversion was improved with increasing Pt content. This was ascribed to a larger availability of activated hydrogen, facilitating the hydrogenation process. Notably, the volume of adsorbed hydrogen for Pt- promoted and THPC-Co/TiO_2 are comparable, However, the Pt-Co/TiO_2 showed better CO conversion (*ca.* 18%) than THPC-Co/TiO_2. This was ascribed to an increased availability of surface activated hydrogen for Pt-Co/TiO_2. The CO conversion of Au-containing was expected to be less than the CO conversion of Co/TiO_2.

Selectivity

Due to low catalytic activity, the product selectivity of the unpromoted (THPC-Co/TiO_2) and promoted catalysts precursor remained as a challenge. The GC-FID trace of the promoted and unpromoted catalyst (THPC-Co/TiO_2) showed small peaks making it difficult to adequately quantify the product distribution.

$Au_{30}Pt_{70}$-Co/TiO_2 has been observed to have higher C_1 selectivity compared to $Au_{50}Pt_{50}$-Co/TiO_2. If the CO-conversion of the two catalysts was comparable then the observed selectivity would be due to an increased surface hydrogen which favours desorption of surface species. However, these results are not conclusive as the CO-conversion of the catalyst precursors varied. Unexpectedly, Pt-Co/TiO_2 showed highest chain growth probability, subsequently highest C_{5+} selectivity in linear hydrocarbon fraction. This could be due to the significant difference in CO-conversion between the Au-containing and THPC-Co/TiO_2 catalysts.

Take note, Pt is known to be catalytically inert under Fischer-tropsch synthesis due to CO poisoning. Therefore, the enhanced C_1 selectivity with increasing platinum content could be due to the fact that platinum is promoting the reduction of very small crystallite which may enhance methane during Fischer-Tropsch synthesis.

Olefin content in the fraction of linear hydrocarbons was observed to decreasing with increasing platinum content for the promoted with the unpromoted catalyst precursor sample (THPC-Co/TiO_2) showing the highest olefin selectivity. This was attributed to an increased availability of activated surface hydrogen with increasing platinum content. $Au_{30}Pt_{70}$-Co/TiO_2 and $Au_{50}Pt_{50}$-Co/TiO_2 showed highest α-olefin selectivity in olefin fraction. However, it was expected that the α-olefin content in olefin fraction would decrease with increasing platinum content, due to a larger availability of surface hydrogen which would favour re-adsorption (subsequently secondary reactions), thus lower α-olefin selectivity.

The oxygenate content in hydrocarbon fraction decreases with increasing platinum content. This was attributed to the decreasing OH concentration, with increasing surface hydrogen. The selectivity results neither disprove nor prove the hypothesis made, as the CO conversion varied significantly.

6 Recommendations

The use of tetrakis(hydroxymethyl) phosphonium chloride solution in the presence of NaOH was observed to decrease the catalytic activity of Co/TiO_2 under Fischer-Tropsch conditions. Therefore, other methods such as refluxing of α-alcohol (ethylene glycol) could be used to deposit the noble metal nanoparticles or instead a cleaning step of the calcined particles is necessary.

The interaction (location) of the promoter with either cobalt species or support material could be probe by X-ray adsorption spectroscopy at the Au, Pt and Co edge. Alternatively, EDX mapping (scanning TEM mode) of the promoted catalyst could be used to assist the location of the promoter on the catalyst sample.

Appendix

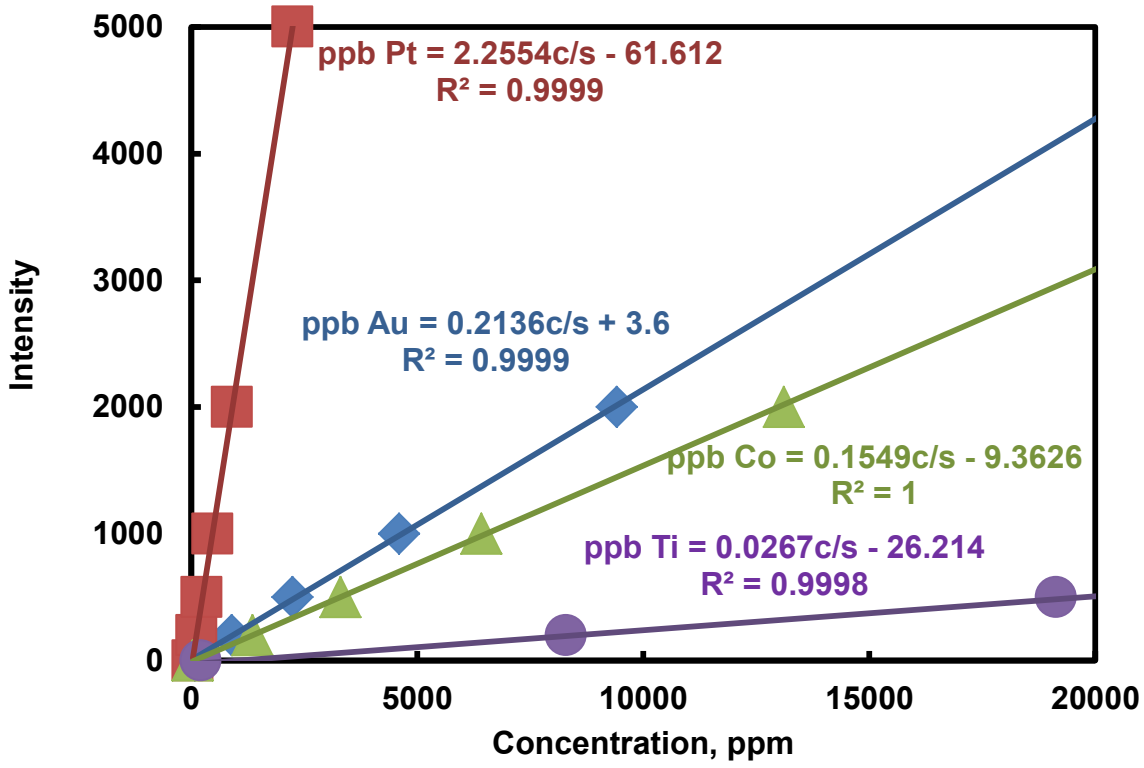

Figure A1: ICP calibration curves.

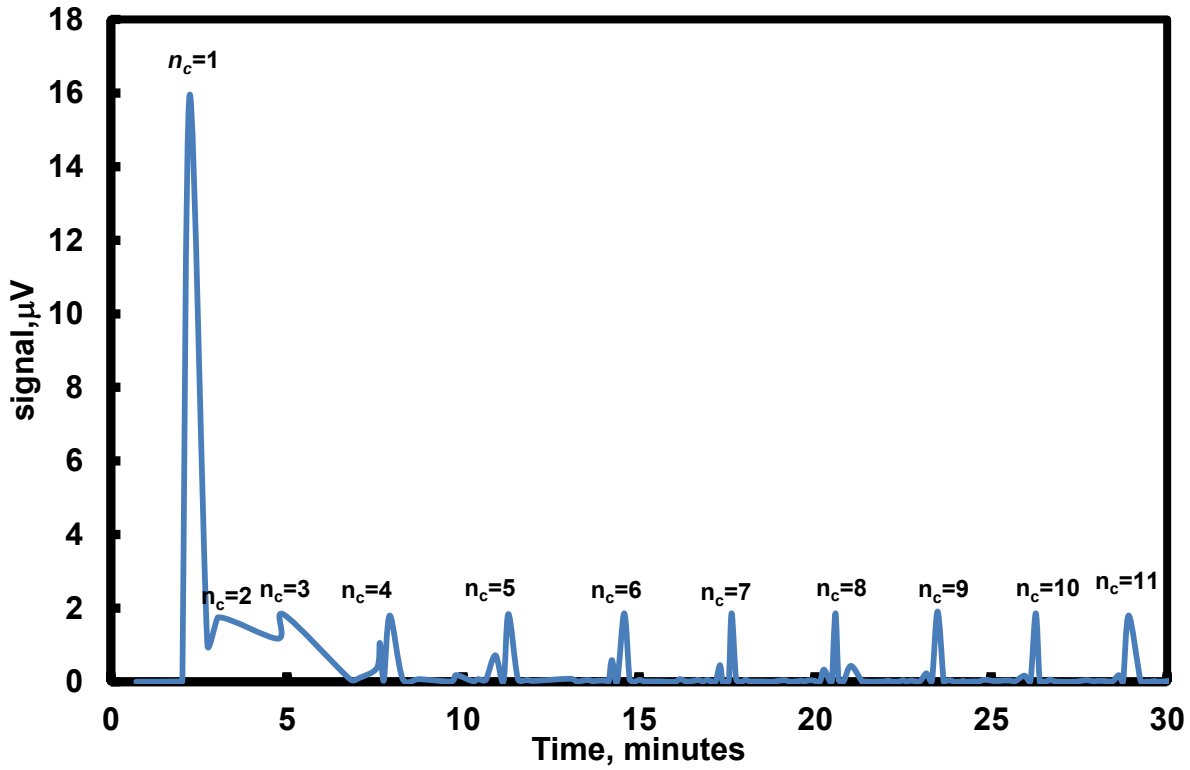

Figure A2: GC-FID chromatogram for Fischer-Tropsch runs with THP-Co/TiO_2.

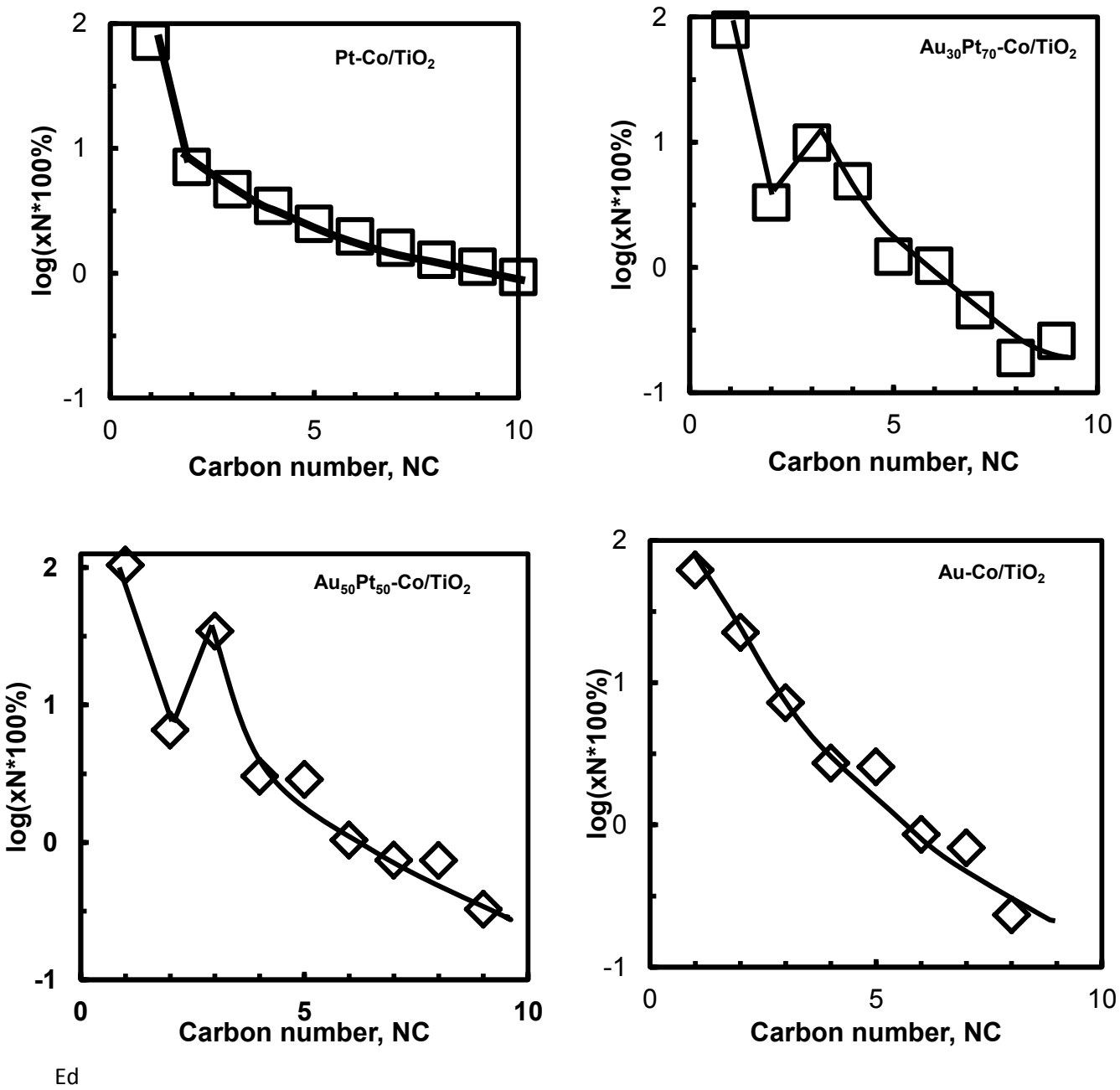

Ed

Figure A3: Anderson-Schulz-Flory plots, constructed from the GC-FID data from the Fischer-Tropsch runs of the promoted Co/TiO_2 catalysts.

7 Bibliography

[1] T. Krause, J. Kopasz, C. Rossignol, J. D. Carter and M. Krumpelt, *Fuel Chemistry Division Preprints,* **47** (2002), 542.

[2] A. J. Minchener, *Fuel*, **84**, (2005), 2222.

[3] C. Bouchy, G. Hastoy, E. Guillon and J.A. Martens, *Oil & Gas Science and Technology,* **64** (2009), 91.

[4] E. Iglesia, *Applied Catalysis A: General*, **161** (1997), 59.

[5] E. van Steen and M. Claeys, *Chemical Engineering & Technology*, **31** (2008), 655.

[6] M. de Beer, A. Kunene, D. Nabaho, M. Claeys and E. van Steen, *Journal of the South African Institute of Mining and Metallurgy*, **114** (2014), 157.

[7] G.L. Bezemer, J.H. Bitter, H.P.C.E. Kuipers, H. Oosterbeek, J.E. Holewijn, X. Xu, F. Kapteijn, J. van Dillen and K.P. de Jong, *Journal of the American Chemical Society*, **128** (2006), 3956.

[8] M. Rotan, E. Rytter, M.-A. Einarsrud and T. Grande, *Journal of the European Ceramic Society,* **33** (2013), 1.

[9] A. Martínez and G. Prieto, *Journal of Catalysis,* **245** (2007), 470.

[10] J. G. Choi, H. K. Choi, M. K. Jung, *Journal of Industrial and Engineering Chemistry*, 3 (**1997**), 235.

[11] S. Vada, A. Hoff, E. Ådnanes and D. Schanke, A. Holmen, *Topics in Catalysis*, **2** (1995), 155.

[12] A. Kogelbauer, J.G. Goodwin Jr. and R. Oukaci, *Journal of Catalysis*, **160** (1996), 125.

[13] G. Jacobs, T.K. Das, Y. Zhang,J. Li, G. Racoillet and B.H. Davis, *Applied Catalysis A: General*, **233** (2002), 263.

[14] H. Zhang, W. Chu, C. Zou, Z. Huang, Z. Ye and L. Zhu, *Catalysis Letters*, **141** (2011), 438.

[15] W. Ma, G. Jacobs, R.A. Keogh, D.B. Bukurv and B.H. Davis, *Applied Catalysis A: General*, **437– 438** (2012), 1.

[16] K.M. Cook, S. Poudyal, J. Miller, C.H. Bartholomew and W.C. Hecker, *Applied Catalysis A: General*, **449** (2012), 69.

[17] G. Jacobs, J.A. Chaney, P.M. Patterson, T.K. Das and B.H. Davis, *Applied Catalysis A: General*, **264** (2004), 203.

[18] K. Jalama, N.J. Coville, D. Hildebrandt, D. Glasser, L.L. Jewell, J.A. Anderson, S. Taylor, D. Enache and G.J. Hutchings, *Topics in Catalysis*, **44** (2007), 129.

[19] F. Morales and B. M. Weckhuysen, *Catalysis*, **19** (2006), 1.

[20] F. Fischer and H. Tropsch, *Brennstoff - Chemie,* **7** (1926), 97.

[21] F. Diehl and A.Y. Khodakov, *Oil & Gas Science and Technology,* **64** (2009), 12.

[22] E.I. Mabaso, Ph.D. thesis, University of Cape Town, Chemical Engineering (2005).
[23] R. C. Brady and R. Pettit, *Journal of American Chemical Society*, **102** (1980), 6181.
[24] R. C. Brady and R. Pettit, *Journal of American Chemical Society*, **103** (1981), 1287.
[25] A. B. Fontenelle Jr. and F. A. N. Fernandes, *Chemical Engineering and Technology*, **34** (2011), 963.
[26] J. Eilers, S.A. Posthuma, and S.T. Sie, *Catalysis Letters,* **7** (1990), 253.
[27] M. J. Overett, R. O. Hill and J. R. Moss, *Coordination Chemistry Review*, **581** (2000), 206.
[28] Claeys M., E. van Steen, In: A. Steynburg, M. Dry, (eds.): "*Fischer-Tropsch Technology, Studies in Surface Science and Catalysis* Elsevier, Amsterdam, Chapter.8, **152** (2004), 601.
[29] M.E. Dry, *Catalysis Today*, **71** (2002), 227.
[30] E. Iglesia, S.C. Reyes, R.J. Madon, and S.L. Soled, *Advances in Catalysis*, **39** (1993) 221.
[31] E. Iglesia, S.C. Reyes, and R.J. Madon, *Journal of Catalysis*, **129** (1991) 238.
[32] B. C. Enger and A. Holmen, *Catalysis Reviews: Science and Engineering*, **54** (2012), 437.
[33] A. Y. Khodakov, W. Chu and P. Fongarland, *Chemical Reviews*, **107** (2007), 1692.
[34] G. Jacobs, W. Ma and B. H. Davis, *Catalysts* **4** (2014), 49.
[35] Xu, D., Li, W., Duan, H., Ge, Q. and Hengyong Xu, H. 2005, *Catalysis Letters*. **102** (2005), 229.
[36] G. L. Bezemer, J. H. Bitter, H. P. C. E. Kuipers, H. Oosterbeek, J. E. Holewijn, X. Xu, F. Kapteijn, A. J. van Dillen, and K. P. de Jong, *Journal of the American Chemical Society*, **128** (2006), 3956.
[37] P. Buffat and J-P. Borelm *Physical Review A*, **13** (1976), 2287.
[38] J. C. W. Swart, PhD thesis, University of Cape Town (2008).
[39] A. M. Saib, M. Claeys and E. van Steen, *Catalysis Today*, **71** (2002), 395.
[40] E. van Steen, G.S. Sewell, R.A. Makhote, C. Micklethwaite, H. Manstein, M. de Lange and C.T. O'Connor, *Journal of Catalysis*, **162** (1996), 220.
[41] R. C. Reuel, and C.H. Bartholomew, *Journal of Catalysis*, **85** (1984), 63.
[42] K. H. Babb and M. G. White, *Journal of Catalysis*, **98** (1986), 343.
[43] K. H. Babb and M. G. White, *Journal of Catalysis,* **102** (1986), 252.
[44] H-Y Lin and Y-W Chen, *Materials Chemistry and Physics*, **85** (2004) 171.
[45] F. Morales, D. Grandjean, F. M. F. De Groot, O. Stephan and B. M. Weckhuysen, *Physical Chemistry Chemical Physics* **7** (2005), 568.
[46] B. Jongsomjit, J. Panpranot and J. G. Goodwin Jr., *Journal of Catalysis,* **215** (2003), 66.
[47] H. Xiong, Y. Zhang, K. Liew and J. Li, *Journal of Molecular Catalysis A: Chemical* **231** (2005), 145.
[48] V V Rozanov and O V Krylov, *Russian Chemical Reviews,* **66** (1997), 107.

[49] J Khoobiar, *Journal of Physical Chemistry* **68** (1964) 411.
[50] W. Curtis Conner Jr and J. L. Falconer, *Chemical Reviews*, **95** (1995), 759.
[51] J.-Y. Luo and W.S. Epling, *Applied Catalysis B, Environmental*, **97** (2010), 236.
[52] M. Meng, Y. Zha, J. Luo, T. Hu, Y. Xie and T. Liu, *Applied catalysis A: General*, **301** (2006), 145.
[53] X. Mo, Y-T. Tsai, J. Gao, D. Mao and J. G. Goodwin Jr., *Journal of Catalysis*, **285** (2012), 208.
[54] W. Chu, P.A. Chernavskii, L. Gengembre, A. Galina, G. A. Pankina, P. Fongarland, and A. Y. Khodakov, *Journal of Catalysis.* **252** (2007), 215.
[55] J. L. Hueso, V. Sebastian, A. Mayoral, L. Uson, M. Arruebo and J. Santamarıa, *RSC Advances*, **3** (2013), 10427.
[56] N. Toshima and T. Yonezawa, *New Journal of Chemistry*, **22** (1998), 1179.
[57] H. Hirai, Y. Nakao and N. Toshima, *Journal of Macromolecular Science-Chemistry*, **A13** (1979), 727.
[58] N. Toshima, K. Kushihashi, T. Yonezawa and H. Hirai, *Chemistry Letters*, **18** (1989), 1769.
[59] D. G. Duff, A. Baiker and P. P. Edwards, *Langmuir*, **9** (1993), 2301.
[60] H. Schulz, and S. Nehren*, Erdöl und Kohle - Erdgas - Petrochemie* **39** (1986), 93.
[61] S.L. Westcott, S.J. Oldenburg, T.R. Lee and N.J. Halas, *Langmuir*, **14** (1998), 5396.
[62] J. Li, G. Jacobs. T. Das and B.H. Davis, *Applied Catalysis A: General* **233** (2002), 255.
[63] L. W. Daasch and D. C. Smith, *Analytical chemistry*, **23** (1951) 853.
[64] D. Walters, *Thermochimica Acta*, **445** (2006), 195.
[65] E. Darezereshki, *Materials Letters* **65** (2011,) 642.
[66] C. Ma, D. Wang, W. Xue, B. Dou, H. Wang, and Z. Hao, *Environmental Science Technology*, **45** (2011), 3628.
[67] D. Schanke, S. Vada, E.A. Blekkan, A.M. Hilmen, A. Hoff and A. Holmen, *Journal of Catalysis*, **156** (1995), 85.
[68] B. Hammer and J.K Nørskøv, *Nature*, **376** (1995), 238.
[69] S.A. Hosseini, A. Taeb and F. Feyzi, *Catalysis. Communications*, **6** (2005), 233.